Functional Analysis of Class II Phosphoinositide 3-Kinases PI3KC2α and PI3KC2β in Neurotransmission

Inaugural-Dissertation

to obtain the academic degree

Doctor rerum naturalium (Dr. rer. nat.)

submitted to the Department of Biology, Chemistry, Pharmacy

Freie Universität Berlin

by

Albert Ian Mackintosh

from Norfolk, United Kingdom

2020

Period of doctorate studies: January 2016 to July 2020

Supervisor: Prof. Dr. Volker Haucke

Institute: Leibniz-Forschungsinstitut für molekulare Pharmakologie (FMP), Berlin

1st Reviewer: Prof. Dr. Volker Haucke

2nd Reviewer: Prof. Dr. Britta Eickholt

Date of defense: 10.02.2021

Affidavit

I declare that my PhD thesis at hand has been written independently and with no other sources and aids than quoted.

Berlin, August 20th , 2020

Acknowledgments

First, I would like to thank my PhD supervisor Prof. Dr. Volker Haucke, for his teaching, scientific discussions, and the opportunities he has provided me. He was able to push me to be better and was vital to completing the project.

I owe deep gratitude to Dr. Natalie Kaempf, for her guidance and training in my first years of the PhD, and her compassion and patience towards me. Equally, Dr. Gaga Kochlamazashvili was most supportive in the latter years, with both superb training in electrophysiology and his contributions to the project. To both I am extremely thankful.

I would like to thank Dr. Tanja Maritzen for all her project support, particularly project guidance, animal management and help with the seizure experiments, her support is greatly appreciated. I would also like to thank Dr. Martin Lehmann for his fantastic help and training in fluorescent microscopy, Dr. Dmytro Puchkov for providing electron microscopy images and converting me to the “Church of Stereology”! Thanks also go to Dr. Christopher Schmied for support in image analysis and training in automated analysis. Thank you also to Prof. Dr. Michael Krauß for both his personal support and detailed discussions in lab meetings.

Special thanks go to the groups of Dr. Tommaso Pippucci and Prof. Dr. Emilio Hirsch for their strong collaboration, particularly Dr. Sara Baldassari, Dr. Miriam Martini and Luca Gozzelino for their enthusiasm for the project. Furthermore, I would like to thank the Hirsch group for hosting me in Turin, Italy for 3 months, and particularly Dr. Maria Chiara De Santis for being so supportive while I was there.

I am grateful for the funding from the European Union’s Horizon 2020 Research and Innovation Programme under the Marie Skłodowska-Curie grant agreement (No 675392). Within this funding I am grateful to the PI3K-PhD training network and particularly Laia Muixi Ponsa for her tireless efforts, and all the PhD fellows for making it such a success.

I am grateful to the technicians of the lab, who have managed to keep experiments running smoothly. Delia Löwe and Sabine Hahn were immensely helpful with their preparation of neuron cultures. Silke Zillmann gave perfusion advice, organised the lab and orderings. Jenny Eichhorst was always willing to help troubleshoot microscopy issues with me. I would also like to thank Claudia Schmidt, Uwe Fink, Maria Mühlbauer and Sophia Greise for additional support. I owe a large thanks to Dr. Natali Wisbrun, Jenny Lendeckel, Eva Lojek, Sina Scholz and Jeannette Unnasch from the FMP animal facility for excellent animal welfare and management. I would also like to thank the lab secretaries, Alexandra Chylla and Juliane Langer for their care and support.

I would like to thank all the members of AG Haucke, AG Maritzen, AG Krauß, and AG Lehmann for making my time in Berlin so special. Both in and out of the lab there was always someone willing to help, console or celebrate with, with either a coffee or a beer as the situation required! Particularly my office with Dr. Marijn Kuijpers, Dr. Tolga Soykan, Dr. Domenico Azarnia Tehran, Dr. Wonyul Jang, Dr. Dorien Roosen, Dr. Agata Witkowska and Paula Samsó Ferre for always contributing ideas and making me laugh in equal measures. To all of you, thank you: Marietta Bergmann, Svenja Bolz, Caroline Bruns, Gabrielle Capin, Gala Claßen, Michael Ebner, Marine Gil, Hannes Gonschior, Manuel Hessenberger, Lennart Hoffmann, Burkhard Jakob, Maria Jäpel, Katarina Ketel, Philipp Koch, Natalia Kononenko, Guan-Ting Liu, Wen-Ting Lo, Tania Lopez Hernandez, Fabian Lukas, Marta Maglione, Charles Malek, Andrea Marat, Kristine Oevel, Christoph Ott, Filiz Sila Rizalar, Giulia Russo, Kyungyuen Song, Tolga Soykan, Dennis Vollweiter, Alexander Wallroth, Haibin Wang, Anna Wawrzyniak and Mirjana Weimershaus.

A special thank you to all my previous supervisors and mentors who have supported me and taught me throughout my academic career. From the NIMR Prof. Robin Lovell-Badge, Dr. Charlotte Scott-Cobb and Clare Wise. At the ICH Prof. Juan Pedro Martinez-Barbera and Dr Cynthia Andoniadou. At the WIBR Prof. Nicoletta Kessaris and Dr. Lorenza Magno. Thanks also to Dr Caroline Griffiths, Dr. Anthony Wallersteiner, Dr. Elizabeth Chare, and John Ing for their support.

Finally, I would like to thank my family for their support both before and during this work. In particular my Father, my brother Max and his wife Alice, and Emma Broom were always there for me. Thank you to Anna Wulf who was constantly supporting me for the past three years. And to my Mother, who passed away during the PhD, thank you, I will always be grateful for the time we had.

“I have been given much and I have given something in return; I have read and travelled and thought and written. Above all, I have been a sentient being, a thinking animal, on this beautiful planet, and that in itself has been an enormous privilege and adventure.”

Oliver Wolf Sacks

1933-2015

Contents

Abstract

The Class II Phosphoinositide 3-kinases (PI3Ks) are a family of structurally similar enzymes that phosphorylate the 3-position of the inositol ring of phosphoinositides (PIPs), lipids that control membrane identity and cell signalling. Two of the members are ubiquitously expressed, including in the central nervous system (CNS): PI3KC2α and PI3KC2β. Studies from immortalised cells have demonstrated that these two enzymes have important roles in vesicle cycling and nutrient signalling, respectively. PI3KC2α generated phosphatidylinositol-3,4-bisphosphate [$PI(3,4)P_2$] recruits and activates Sorting Nexin 9 to late stage Clathrin-coated pits at the cell surface, which provides the constriction necessary for Dynamin-mediated scission from the plasma membrane. PI3KC2β meanwhile plays important roles during low nutrient signalling, inhibiting cellular growth and promoting autophagy by generating $PI(3,4)P_2$ at the lysosome leading to 14-3-3 protein mediated inhibition of mammalian target of rapamycin complex 1 (mTORC1), a key member of the PI3K-AKT signalling pathway. Here we wanted to investigate how these two proteins contribute to normal brain function.

By generating a brain specific knockout of PI3KC2α in mice, we were able to show that these mice were viable and had normal development and behaviour. Synaptic cycling was found to be mostly unaffected as was synaptic transmission. However, we found accumulation of Synaptotagmin 1 in neurons lacking PI3KC2α, suggesting an underlying defect in maintaining homeostatic protein levels. Together these data suggest PI3KC2α may be largely dispensable in postmitotic neurons in the CNS.

We then assessed the role of PI3KC2β in the CNS, using PI3KC2β null mice as a model, demonstrating that loss of the enzyme in mice resulted in elevated mTORC1 signalling within the hippocampus and cortex. Stereological analysis demonstrated no change in the density of excitatory and inhibitory neurons within the CA1 region of the hippocampus, and glial coverage was also unaffected. However, we found electrophysiological defects in acute CA1 hippocampal recordings, with network hyperexcitability reminiscent of epilepsy. This was confirmed by collaborators via identification of patient mutations in PI3KC2β

associated with focal epilepsies and drug specific epileptogenesis in mice. The mTORC1 activation was shown to be reversable with acute rapamycin treatment, and our collaborators demonstrated epileptogenesis was acutely reversible in the mouse model. This data opens the possibility of a future pathway for treatment of human PI3KC2β type epilepsies.

These data unveil distinct and important roles of the Class II PI3Ks in the CNS that have implications in human health and disease.

Zusammenfassung

PI3KC2α und PI3KC2β besitzen eine ähnliche Struktur und gehören zur Klasse 2 der PI3-Kinasen. Diese Enzyme phosphorylieren die dritte Hydroxylgruppe des Inositolrings von Phosphoinositiden (PIPs). PIPs sind Lipide, die nicht nur die Signaltransduktion der Zelle kontrollieren können, sondern auch die Identität von zellulären Membranen bestimmen. PI3KC2α und PI3KC2β werden im gesamten Körper exprimiert, einschließlich des zentralen Nervensystems. Ergebnisse von immortalisierten Zelllinien zeigen eine wichtige Rolle dieser Enzyme im Vesikelrecycling und der Nährstoff-kontrollierten Signaltransduktion.

PI3KC2α produziert PI(3,4)P_2 an „clathrin coated pits“ (Clathrin-bemantelten Grübchen), wodurch SNX9 zur Plasmamembran rekrutiert und dort aktiviert wird. Das ermöglicht die Abschnürung der Vesikel durch Dynamin von der Membran.

PI3KC2β kann das Zellwachstum inhibieren und Autophagie einleiten, weswegen es wichtig bei geringer Nährstoffzufuhr ist. Die Produktion von PI(3,4)P_2 durch PI3KC2β an der Lysosomenmembran führt zur Inhibierung von mTORC1, einem wichtigen Bestandteil des PI3K-AKT Signalweges. Wir wollten untersuchen, welche Rolle PI3KC2α und PI3KC2β für die Gehirnfunktion spielen.

Trotz der spezifischen Ausschaltung von PI3KC2α im Gehirn von Mäusen, waren diese lebensfähig und wiesen eine normale Entwicklung und normales Verhalten auf. Der synaptische Zyklus, wie auch die synaptische Transmission wurden nicht beeinflusst. Jedoch zeigten wir, dass der Verlust von PI3KC2α zu einer Akkumulation von Synaptotagmin 1 in Neuronen führt, die auf einen Defekt im Aufrechterhalten des homöostatischen Proteinlevels hinweisen könnten. Diese Ergebnisse deuten darauf hin, dass PI3KC2α größtenteils entbehrlich in postmitoschen Neuronen des zentralen Nervensystems ist.

Anschließend untersuchten wir die Rolle von PI3KC2β im zentralen Nervensystem. Wir konnten eine erhöhte Signaltransduktion von mTORC1 im Hippocampus und Cortex in Folge des Verlusts von PI3KC2β feststellen.

Stereologische Analysen zeigten keine Veränderung der Dichte von exzitatorischen und hemmenden Neuronen in der CA1 Region des Hippocampus. Auch war die Verteilung von Gliazellen unverändert. Jedoch konnten wir einen elektrophysiologischen Defekt in akuten CA1 hippocampalen Aufzeichnung feststellen, die an die Übererregbarkeit von Netzwerken in Epilepsie erinnern. Unterstützen zu diesen Ergebnissen identifizierten Kollaboratoren Patienten mit Mutationen in PI3KC2β, die mit fokaler Epilepsie und Medikament-spezifischen Epileptogenese in Mäusen assoziierten wird. mTOR Aktivierung konnte durch akute Behandlung mit Rapamycin rückgängig gemacht werden. Zusätzlich stellten unsere Kollaboratoren fest, dass auch die Epileptogenese in Mausmodellen zurück ging. Dieses Ergebnis eröffnet eine neue Möglichkeit Epilepsie mit PI3KC2β Mutationen in Menschen zu behandeln.

Durch diese Arbeit konnten wichtige und krankheitsrelevante Rollen von Klasse 2 PI3Ks im zentralen Nervensystem nachgewiesen werden.

1 Introduction

1.1 Neuronal Signalling and the Chemical Synapse

The human brain contains nearly 90 billion neurons, highly polarised cells that have a unique architecture. These cells are arranged in complex interlinked networks which generate signalling patterns that govern both conscious behaviour and unconscious control of bodily function. To form these patterns, neurons transmit a signal first along their cell body via electrical conduction, known as an action potential (AP). At rest, a neuron maintains a negative intracellular voltage, typically -70mV (Hodgkin & Huxley, 1952), maintained by active transport of Na^+ ions out of the cell via Na^+/K^+ pumps (Thomas, 1972). However, upon innervation, the membrane potential becomes more positive until -55mV is reached, upon which voltage gated Na^+ channels open, initiating an AP. An AP is caused by the influx of Na^+ down its electrical and chemical gradient which further raises the membrane potential in the local area, leading to a cascade of voltage gating across the length of the neuron. However, for an AP's signal to be transmitted to the next neuron/neurons in a circuit, it must be transmitted across the space between two cells, at special junctions known as chemical synapses.

The chemical synapse comprises three main components: the presynapse, synaptic cleft, and postsynapse (Figure 1). To transmit a signal the sending neuron must convert the electrical AP into a chemical signal, this occurs at the axon terminal in the presynapse, also known as the presynaptic bouton. The chemical signals, known as neurotransmitters, are secreted into the synaptic cleft, the extracellular space between neurons. The size of the cleft is maintained at 20 nm to allow for fast and efficient signal transfer (Clements et al., 1992; Savtchenko & Rusakov, 2007). Neurotransmitter diffuses across the cleft to reach the receiving neuron at its postsynaptic density (PSD) and this in turn, depending on the type of neurotransmitter secreted, can lead to excitation or inhibition of the receiving neuron.

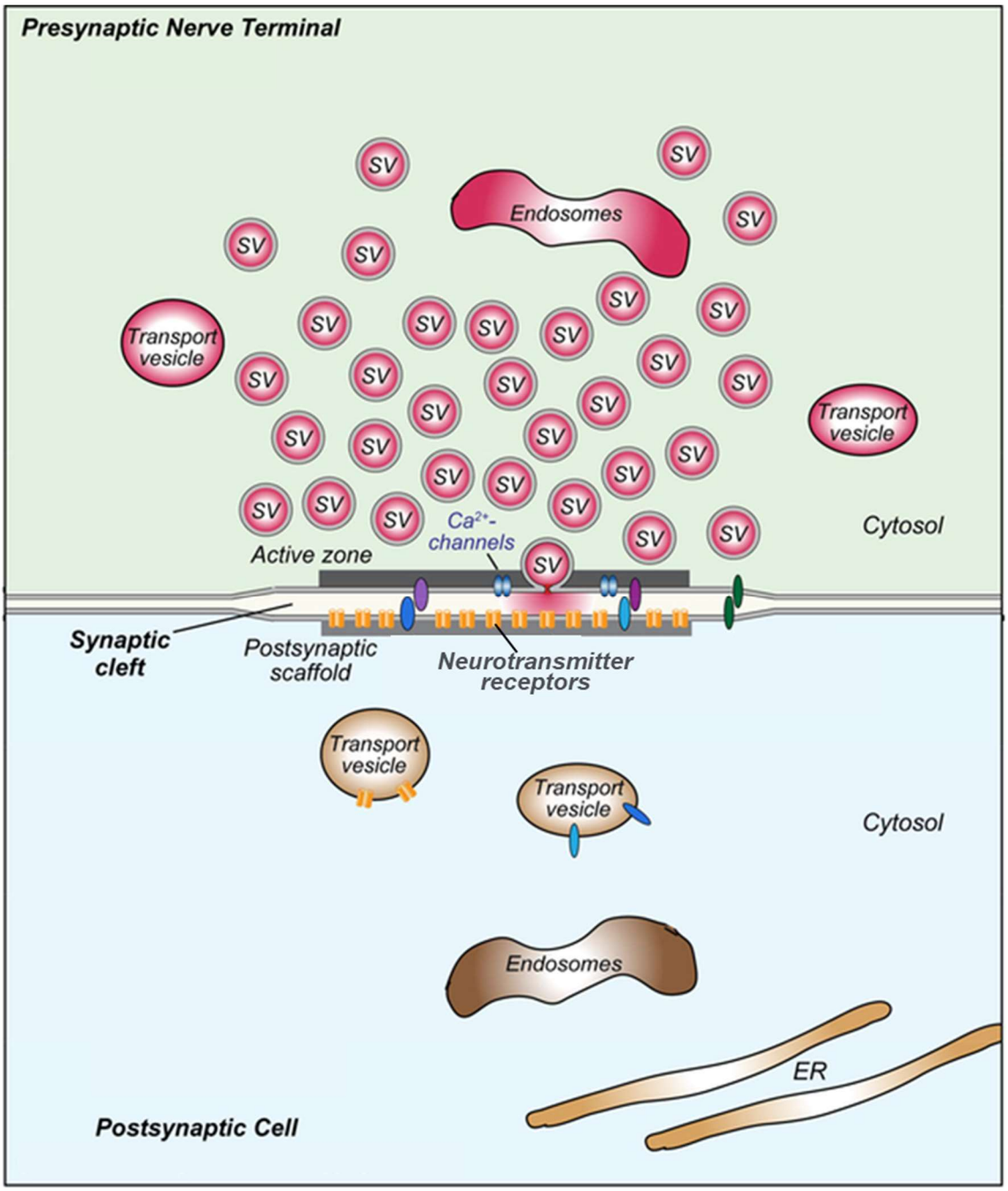

Figure 1: The chemical synapse. A simplified view of the membrane compartments of the synaptic unit, formed of a presynapse, synaptic cleft and postsynapse. The upper presynapse contains primarily secretory compartments known as synaptic vesicles as well as some transport vesicles and recycling compartments known as endosomes. Upon Ca^{2+} influx caused by APs gating of Ca^{2+} channels, vesicles fuse with the presynaptic membrane depositing neurotransmitter into the synaptic cleft, which diffuses across the cleft and binds to postsynaptic neurotransmitter receptors, which leads to ion influx and AP generation. The postsynapse consists primarily of sorting compartments that insert or remove receptors from the PSD, and ER for Ca^{2+} buffering. Adapted from (Südhof, 2018).

Given that most neurons have multiple synaptic inputs, and each of these inputs may have varied strength, time of release and inhibitory or excitatory effect on the postsynaptic neuron, the integration of signals from even a small network generates an exponentially higher computational power than the same number of neurons operating in isolation (Diering & Huganir, 2018; Liaw & Berger, 1996; Tremblay et al., 2016). Understanding how these mechanisms are controlled and modulated has been of key interest to the research community.

1.1.1 The presynapse and synaptic vesicles

Both the presynapse and postsynapse are highly adapted structures for their functions of sending and receiving synaptic signals. The presynapse is an oval shaped structure with a diameter of between 300 – 500 nm (Chéreau et al., 2017). The compartment contains mitochondria and some endoplasmic reticulum (ER), but most notably contains roughly 200 spherical membrane compartments of ~40 nm diameter, known as synaptic vesicles (Schikorski & Stevens, 1997; Takamori et al., 2006). These vesicles are filled with neurotransmitters such as glutamate, GABA, or acetylcholine, and can secrete these into the synaptic cleft by fusing with the protein dense membrane known as the active zone.

Vesicles are conventionally thought to reside in three “pools” which serve linked but separate functions (Denker & Rizzoli, 2010). The readily releasable pool (RRP) is formed of vesicles ready to fuse with the active zone upon AP arrival to the axon terminal, they are either directly docked to the active zone or clustered within the periactive zone ready to replace docked vesicles upon fusion. The number of docked vesicles is tightly regulated (Schikorski & Stevens, 1997; Siksou et al., 2007) and changes in this number have been associated with neurological diseases (Buckmaster et al., 2016). This pool is rapidly depleted upon moderate frequency stimulation and requires replenishment from the recycling pool.

The recycling pool accounts for roughly 10 - 20% of synaptic vesicles, and scales linearly with the total vesicle number (Marra et al., 2012). These highly mobile vesicles can replenish the RRP under moderate stimulation and are thought

to be sufficient for most physiological stimuli (Denker et al., 2011; Richards et al., 2003).

The final pool is the reserve pool, which contains the majority of vesicles (up to 80%, Südhof, 2004). This pool is characterised by immobile vesicles clustered to the cytoskeleton by the phosphoproteins known as Synapsins (Vasileva et al., 2012). Upon intense stimulation Synapsins undergo phosphorylation by CaM kinase which leads to a dissociation of Synapsins from the vesicles resulting in an increase of free moving vesicles which could replenish the recycling pool (Jovanovic et al., 2001; Vasileva et al., 2012).

Other proposed models exist, suggesting a spatial mixing of the reserve and recycling pool (Rizzoli & Betz, 2005), a shared pool of vesicles across multiple synapses (Darcy et al., 2006), and the possibility of a pool of vesicles that have previously fused with the active zone and await further fusion events before retrieval, the "readily retrievable pool" (Fernández-Alfonso et al., 2006; Rizzoli & Jahn, 2007), however these still require further investigation and the traditional model remains mostly intact (Denker & Rizzoli, 2010).

1.1.2 Synaptic vesicle loading, docking and release

As previously stated, synaptic vesicles are loaded with a high concentration of one of several neurotransmitters. This is done by creating a high electrochemical gradient via active transport of protons into the vesicle lumen by a V-ATPase (Farsi et al., 2017), then loading of neurotransmitters through their specific vesicular transporters (Gasnier, 2000). The H^+ gradient is universally required for neurotransmitter loading, with monoamines and acetylcholine loading driven by the chemical gradient, glutamate by the membrane potential and GABA equally driven by both elements (Edwards, 2007). The copy number of these proteins per vesicle appears to be tightly regulated (only 1 - 2 V-ATPase per vesicle, (Mutch et al., 2011; Takamori et al., 2006)), and changes in transporter copy number lead to altered neurotransmitter loading resulting in perturbed synaptic signalling (Takamori, 2016; Wilson et al., 2005; X. S. Wu et al., 2007).

Within the RRP a proportion of vesicles are docked to the plasma membrane which are then primed for an AP to trigger neurotransmitter release. The process of docking and priming revolves around the assembly of complexes of conserved transmembrane proteins known as SNAREs (soluble N-ethylmaleimide-sensitive fusion protein attachment protein receptors), which are located on both the vesicles and the presynaptic membrane (Kaeser & Regehr, 2017). The vesicle interacting vesicle-SNARE (v-SNARE) Synaptobrevin-2 interact with the target membrane target-SNAREs (t-SNARE) Syntaxin and SNAP-25 to form a trans-SNARE complex via their α-helix SNARE domains (Ramakrishnan et al., 2012). The initial docking is thought to be stabilised by the vesicle bound small GTPase Rab3 interacting with active zone cytomatrix linking protein RIM (Mittelstaedt et al., 2010; Y. Wang et al., 1997), which also acts as a link to voltage gated calcium channels required for vesicle fusion (R. He et al., 2018; Kaeser et al., 2011), Subsequent SNARE complex formation is orchestrated by Munc18 and Munc13 (Dulubova et al., 1999; Zilly et al., 2006). Munc18 is bound to closed Syntaxin 1, however upon Munc13 mediated opening of Syntaxin 1, Munc18 is displaced which binds and stabilizes the SNARE complex at the active zone. The final priming step involves formation of a complex of the vesicle bound calcium sensor synaptogamin 1, the SNARE complex, and the fusion clamp Complexin (Zhou et al., 2017).

Upon AP arrival at the bouton, the change in membrane potential leads to opening of the voltage gated calcium channels which leads to an influx of Ca^{2+} ions down their electrochemical gradient. This influx leads to Ca^{2+} binding to the C2A and C2B domains of Synaptotagmin-1 which leads to an increased affinity for phospholipids (Shin et al., 2009), leading to structural changes in the SNARE complex (X. Han & Jackson, 2006), which in turn displaces complexin leading to further SNARE conformational changes (Junjie Xu et al., 2013). The membranes of the vesicle and active zone are forced together by the SNARE complex trans to cis transition, causing the membranes to fuse and an opening (known as the fusion pore) to form which leads to the vesicle lumen to be exposed to the synaptic cleft (Lai et al., 2013). It is thought that this culminates in a full collapse of the vesicle into the active zone (Figure 2) leading to vesicle bound proteins to require retrieval

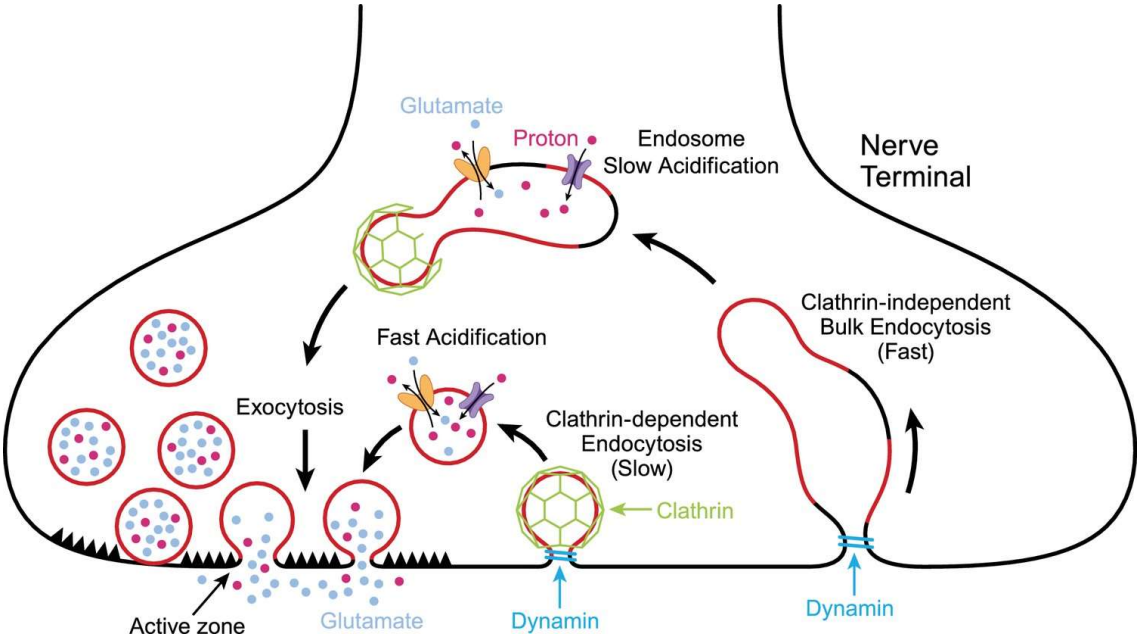

Figure 2: The synaptic vesicle cycle. Primed vesicles at central synapses are thought to fully collapse into the active zone and therefore require retrieval via endocytosis. Upon endocytosis the compartment is acidified to allow for neurotransmitter loading down an electrochemical gradient. After endocytosis occurs, there may be further sorting required via endosomes, however this remains unclear. Adapted from. (Gross & von Gersdorff, 2016).

(Heuser & Reese, 1981). It has been suggested that full collapse may not always occur, instead resulting in a brief pore opening known as kiss and run, however whether this occurs at central synapses remains controversial (L.-G. Wu et al., 2014).

It is clear that vesicle bound proteins such as Rab3, Synaptotagmin-1 and Synaptobrevin-2 have integral roles in vesicle docking and fusion and copy number per vesicle seems to have little deviation (Takamori et al., 2006). This suggests effective sorting of these membrane bound proteins is required to maintain reliable synaptic signalling from the presynapse. In turn, effective sorting of these proteins requires that membrane compartments are clearly defined, so that proteins pass through clear checkpoints to be placed correctly back into synaptic vesicles. Key players in these checkpoints are the lipids of the membranes themselves (to be discussed later).

1.1.3 The postsynapse

Traversing the synaptic cleft, the opposite function of converting a chemical signal back into initiating or inhibiting electrical APs must be achieved. Postsynapses of the central nervous system (CNS) can be located either at the cell soma or at specialised sites along the neuronal dendrite known as dendritic spines, and occasionally onto the axon, though these are primarily GABAergic synapses at the axon initial segment (Nathanson et al., 2019). Though these synapses have diverse location and function, the key feature of all is the clustering of neurotransmitter receptors within a 300 – 500 nm diameter membrane area (E Kim & Sheng, 2009) known as the postsynaptic density (PSD). This highly protein rich area of membrane appears extremely dense under electron microscopy (EM), is roughly 30 – 60 nm thick at excitatory synapses (Carlin et al., 1980), but less defined at inhibitory synapses (Gray, 1959).

The localisation of receptors to the PSD is stabilised by scaffold proteins that link the membrane proteins to the cell's cytoskeleton. At excitatory synapses receptors interact with the membrane-associated guanylate kinases, the best studied of which is PSD-95 (Hunt et al., 1996; Eunjoon Kim & Sheng, 2004). PSD-95 links these channels to a polymeric structure of the proteins Shank and Homer (M. K. Hayashi et al., 2009), which is then in turn bound to filamentous actin via small linker proteins (Naisbitt et al., 1999; Qualmann et al., 2004).

At inhibitory synapses the major scaffolding protein is gephyrin (Giesemann et al., 2003), which may directly link receptors to microtubules (Prior et al., 1992). However gephyrin is only partially required for GABA receptor clustering (Gamlin et al., 2018; Legendre, 2001; Lévi et al., 2004).

Besides the classical excitatory and inhibitory receptors, many modulatory receptors reside at most synapses, though also are located outside the PSD. The mechanisms of how these receptors are localised to specific synapses or the other areas they reside on the cell surface is still poorly understood.

Due to their localisation in the plasma membrane all neurotransmitter receptors are implanted into membrane at the rough ER before passing through

the Golgi apparatus and the Trans Golgi Network (TGN) for proper protein folding (Kennedy & Ehlers, 2006; Shao & Hegde, 2011). These receptors must then be trafficked to the synapse and inserted in the membrane via exocytosis, with the number of each receptor at the PSD determining synaptic strength (Kennedy & Ehlers, 2006), thus control of membrane dynamics needs tight regulation to maintain effective receptor levels.

As mentioned previously, there may be multiple presynaptic inputs to one postsynapse, and depending on how many of these inputs are active and how closely timed the inputs are can lead to a summation of neurotransmitter signals more likely to elicit a postsynaptic response. This is known as spatiotemporal summation.

1.1.4 Direct synaptic transmission

The immediate effects of excitatory or inhibitory signalling are mediated via ionotropic neurotransmitter receptors. Upon neurotransmitter binding, these ion selective channels open allowing for ion flux across the postsynaptic membrane.

In the case of typical central excitatory synapses, glutamate binding to the ionotropic glutamate receptors of the AMPA, NMDA and Kainate receptor families leads to the inrush of cations down their electrochemical gradient (Nicholls, et al. 2012). Upon glutamate binding, AMPA receptors show fast gating (i.e. fast channel opening), leading to a selective influx of Na^+ and, depending on channel subunits, Ca^{2+} ions leading to fast depolarisation (Edmonds et al., 1995). The less common kainate receptors have comparable ion conductance to AMPA receptors, but have slower gating properties, the ratio of these receptors at a synapse may aid the timing of AP generation due to slower depolarisation (Huettner, 2003). The final contributor to excitatory direct transmission is the NMDA receptors. These have much slower gating due to the voltage dependant blockage of the channel by extracellular Mg^{2+} ions which only dissociate from the channel upon a positive membrane potential caused by an AP (Mayer et al., 1984; Nowak et al., 1984). This results in an inrush of Ca^{2+} ions that can lead to secondary APs being generated.

However, these channels are better known for their indirect effects in synaptic transmission whereby Ca^{2+} acts as a second messenger.

Direct inhibitory transmission relies on the transit of the anion Cl^- entering through GABA or glycine receptors. Upon GABA or glycine binding to their respective receptors (Coombs et al., 1955), Cl^- ions enter the postsynapse down their chemical gradient, and subsequently the membrane potential shifts, becoming more negative thus inhibiting AP propagation.

Some ionotropic receptors such as kainate and GABAa receptors are also located at the presynapse. These can lead to changes in the probability of secondary depolarisations leading to changes in further release. Neurotransmission to these receptors can occur either from axoaxonic synapses or via the synapse itself, so called autoreception (MacDermott et al., 1999).

1.1.5 Indirect transmission

Synaptic transmission in the CNS does not only lead to immediate gating of ion channels, but instead leads to second messenger mediated effects that can cause long lasting changes in synaptic excitability and function.

As described previously, Ca^{2+} ions have a key role in indirect transmission. Cytoplasmic calcium is kept at very low concentrations, around a 10,000 fold difference to the synaptic cleft, leading to a high chemical gradient between the intra- and extra-synaptic space (Fierro & Llano, 1996; E. Neher & Augustine, 1992). This difference means that if Ca^{2+} conducting channels such as the NMDA receptors are activated/open, a large influx can occur even against the cation's electrical gradient. Furthermore, small changes in Ca^{2+} concentration within the postsynapse can evoke large changes, due to the high availability of Ca^{2+} dependent effector proteins, such as calmodulin and calpains. Due to the fast binding of these proteins to Ca^{2+} ions that enter through NMDA receptors, Ca^{2+} tends to have rather local changes in concentration near the receptor, known as calcium microdomains (Berridge, 2006). These microdomains containing Ca^{2+} dependent effector proteins can recruit and activate other proteins such as the calmodulin-dependent

protein kinase-II (CaMKII), which requires calmodulin binding and calpain-mediated cleavage to become active (Baudry et al., 2013). CaMKII in turn is recruited to the NMDA receptors of calcium microdomains whereby it phosphorylates neighbour AMPA and NMDA receptor subunits, changing the receptor gating and conductance properties which can enhance or reduce synaptic signal propagation (Coultrap et al., 2014; Hell, 2014). This is an example of how a synapse can modulate the response to the chemical signals of the presynapse, this is known as synaptic plasticity.

Furthermore, Ca^{2+} ion influx is thought to mediate AMPA receptor insertion into the PSD. This occurs due to Synaptotagmin-1 and Synaptotagmin-7 mediated exocytosis of AMPA receptor containing vesicles (M. Park, 2018), leading to fast increase in postsynaptic strength and is a key component of early plasticity.

Ca^{2+} ions may also play a role in detecting aberrant synaptic signalling such as in the case of epilepsy. Ca^{2+} microdomains can lead to activation of lipases such as diacylglycerol lipase which produces endocannabinoids. These lipid neurotransmitters are secreted into the cleft, binding to endocannabinoid receptors in the presynapse which via second messengers inhibit further synaptic vesicle release (Ohno-Shosaku et al., 2005). If the postsynapse receives even higher excitatory signalling, the subsequent large influx of Ca^{2+} ions leads to activation of Calpain. This could lead to Calpain-mediated cleavage of the cytoskeleton which could lead to pruning of the synapse (Schuldiner & Yaron, 2015; Vosler et al., 2008), or even lead to Calpain-mediated caspase cleavage, resulting in apoptosis of the neuron to prevent further damage via excitotoxicity (Cheng et al., 2018; Lam & González, 2019).

The other main route of indirect signalling is via receptors that do not conduct ions, instead activating second messenger pathways within the postsynapse, known as metabotropic receptors. The majority of these transmembrane proteins belong to the super family of G Protein-Coupled Receptors (GPCRs). These GPCRs bind to guanine nucleotide-binding proteins (G Proteins) which at rest are bound to a guanosine diphosphate (GDP). G proteins consist of three subunits (α, β, and γ) with the mixture of these subunits defining

which receptor they bind to and what downstream targets will be. Upon GPCR activation by a stimulus (neurotransmitters, small peptides or even light), GDP is exchanged for guanosine triphosphate (GTP), and the G Protein dissociates from the GPCR, and the α subunit splits from the βγ-subunits to form two second messengers. The targets of these subunits are varied, including protein and lipid kinases, internal calcium reservoirs and ionotropic receptors, and can have effects on both short-term ion influx and endocannabinoid release and longer-term protein turnover and synaptic architecture, modifying synaptic plasticity.

One key group of GPCRs in the CNS are the muscarinic receptors. Comprised of five subtypes, M1 – M5 (Caulfield & Birdsall, 1998; Hulme et al., 1990), they all share an affinity for acetylcholine, but differ in their precise G protein coupling meaning that depending on the M-type present at a synapse, different downstream effects occur upon acetylcholine signalling. The M2 and M4 receptors have been shown to lead to postsynaptic inhibition by activation of K^+ channel opening, which leads to K^+ ion efflux down its chemical gradient, which in turn hyperpolarizes the postsynapse, preventing AP generation (Horn & Dodd, 1983; Wickman & Clapham, 1995). These two channels are also at the presynapse of most acetylcholine secreting boutons, and act as autoinhibitors for cholinergic signalling by inhibiting Ca_v channels (Allen & Brown, 1993).

The M1, M3, and M5 receptors are thought to have primarily excitatory roles on the postsynapse (Brown, 2010). These receptors primarily act on various K^+ channels in the postsynapse, inhibiting hyperpolarization, though may have effects on other cation channels (B. Lu et al., 2009), and are thought to have long term neuromodulatory affects (Dennis et al., 2016; Ohno-Shosaku et al., 2003).

While the M2 and M4 receptors act on their targets directly by G protein subunits binding to the cation channels (Fernández-Fernández et al., 2001; Wickman & Clapham, 1995), the M1, M3, and M5 receptors instead have effects via tertiary messengers, in particular through the metabolism of a phospholipid known as PIP_2 (Brown et al., 2007), a member of the phosphoinositide family of lipids that have far reaching roles in signalling and membrane control.

1.2 Phosphoinositides in Membrane Dynamics

Phosphoinositides (PIPs) are phosphorylated varieties of phosphatidylinositols (PI), glycerophospholipids with an inositol ring headgroup (Figure 3). PI can undergo phosphorylation at positions 3, 4 and 5 of the inositol ring (phosphorylations of positions 2 and 6 have not been found in nature, (Balla, 2013)) and the combinations of these give rise to seven unique PI species (Figure 4). The glycerophospholipid family of phospholipids represents the majority of the phospholipids within the cell membrane, however PIs are only a small contributor, roughly 15% of all phospholipids in the cell, with about 10% being PI and 5% all PIPs combined (Matteis & Godi, 2004). Though PI is present on the membrane of mycobacteria, PIPs' emergence on cytoplasmic membrane leaflets correlates evolutionarily with the appearance of internal membrane structures of more complex organisms (Balla, 2013).

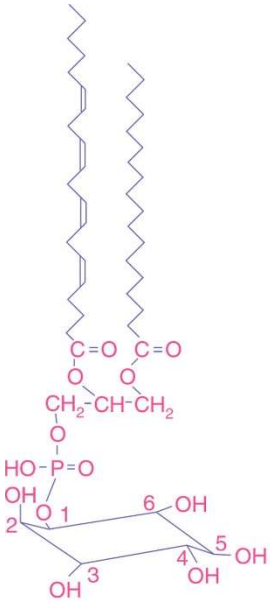

Figure 3: Phosphatidylinositol. PI is an uncommon lipid within membranes, and its derivatives are known as key molecules regulating cell signalling and membrane identity. In nature, the inositol ring can be phosphorylated at the 3, 4, and 5 position in any combination with many proteins having affinity for a specific PIP species (R. Irvine, 2000).

As previously stated, membrane compartments such as synaptic vesicles, ER, and TGN are not static structures, but have high throughput of membrane compartments both fusing and budding from them. This can lead to the exchange of transmembrane proteins that should be placed on specific organelles to allow that compartment to function. Furthermore these organelles may have to be trafficked large distances to reach their precise site of action in the cell (Vukoja et al., 2018). As such, it is conceivable that these membranes must have a mechanism to define the identity of each compartment to allow the correct proteins to interact

with each organelle. Early experiments showed that upon cholinergic drug stimulation of amylase secretion from secretory vesicles of the pancreas, a corresponding increase in phospholipid phosphorylation was observed (Hokin, R.; Hokin, 1953). This was the first hint that the lipids of the membranes themselves may have a role in membrane dynamics.

The distinct stereochemistry of the hydroxyl groups on the inositol ring of PIs (described as a chair layout, or more imaginatively, as the limbs of a turtle, (Agranoff, 2009; R. F. Irvine, 2005), means that each of the PIP species are distinct from each other, making them good candidates as membrane based identifiers for protein interactions. Furthermore, multiple lipid kinases and phosphatases have been identified, allowing for PIP species interconversions which reflect changes in membrane identity or state. These enzymes all convert only one position of the inositol ring, and generally have a preferred species as a substrate (for example the Class-4 inositol polyphosphate-5-phosphatase can dephosphorylate the phosphate on the 5 position of any PI5P species, but has a tenfold higher affinity for $PI(3,4,5)P_3$ (Kong et al., 2000).

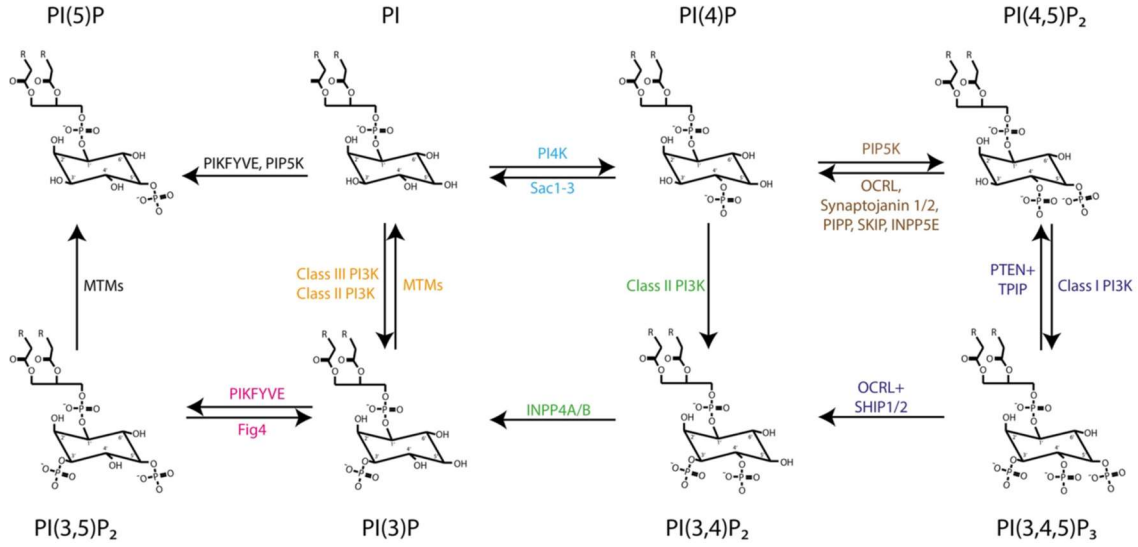

Figure 4: Phosphoinositide metabolism. PIPs can be inter converted between species by PI-kinases and PI-phosphatases. These enzymes can be recruited in a spatial-temporal manner to denote compartmental state (Wallroth & Haucke, 2018).

1.2.1 Phosphoinositides in exocytosis and Clathrin mediated endocytosis

As discussed earlier in the context of synaptic vesicles, docking, and fusing of vesicles is both spatially regulated with predefined release sites and temporally regulated through step by step assembly of protein release machinery. But the membranes themselves also have a role to play in this regulation in both the release of vesicles and the subsequent retrieval in the exo-endocytic cycle.

$PI(4,5)P_2$ is predominantly found at the plasma membrane and is produced by PIP5Ks α – γ from PI4P (Yang et al., 2018, 2019). It has been suggested that several exocytic proteins can interact with $PI(4,5)P_2$, in particular Syntaxins may cluster $PI(4,5)P_2$ into concentrated microdomains which in turn interact with synaptotagmin in the final docking steps of vesicles (Aoyagi et al., 2005; Honigmann et al., 2013). Acute depletion of $PI(4,5)P_2$ was recently shown to result in vesicles becoming undocked from the membrane of insulin secreting cells and a reduction of subsequent membrane fusion events (Ji et al., 2017).

Upon this vesicle release, it is necessary to retrieve the release machinery from the surface and efficiently sort it into new vesicles for further release. This is especially true at the synapse due to the long trafficking distance from the soma to replenish these transmembrane proteins. The limited number of release sites at the synapse is thought to be blocked by used release machinery and requires clearance before further release can occur (Jäpel et al., 2020; Neher, 2010). Furthermore, vesicle fusion adds extra membrane to the release site, both reducing surface tension, required for fusion, and also potentially increasing the distance between Ca^{2+} channels and release sites, lowering release probability (Heuser & Reese, 1981; Lou, 2018). Finally, at a wider context all cells need to maintain the protein landscape of the plasma membrane, from regulation of channels and surface receptors for extracellular signalling, to the uptake of large molecules which cannot pass though the membrane or channels. All these processes are conducted via membrane intake, known as endocytosis.

There are thought to be several mechanisms of endocytosis, but the most common and well understood mechanism across cell types is the highly structured mechanism known as clathrin mediated endocytosis (CME). CME is a highly conserved mechanism present in all eukaryotes to regulate the plasma membrane landscape and to internalise external substances. It has been shown to have key roles in cell signalling, cell motility, and metabolism (Haucke & Kozlov, 2018; R. Lu et al., 2016). It is defined by the assembly of a lattice structure formed from a triskelion shaped molecule known as Clathrin (Kanaseki & Kadota, 1969). Until recently CME was proposed to be the predominant form of synaptic endocytosis, though several other forms of endocytosis have been described, newer studies suggest that though CME is present, it is not dominant at the synapse (Milosevic, 2018; Saheki & De Camilli, 2012; Soykan et al., 2017). However, it is still believed that CME is a contributor in synaptic vesicle recycling, being possibly important for synaptic vesicle reformation from endosomal structures (Kononenko et al., 2014; Milosevic, 2018). It is particularly useful due to its highly structured steps, which lead to fully formed synaptic vesicles which can directly re-enter the RRP and recycling pool without the need for further sorting (Milosevic, 2018).

This structured process can be divided into four steps: Initiation, Maturation, Scission, and Uncoating. Each of these steps involves an evolving interplay of proteins that carefully segregate target proteins and progressively bend the membrane until a point where it can be separated from the plasma membrane and the endocytic machinery removed, all under the control of PIP checkpoints ensuring proper progression of the steps.

Initiation pertains to the targeting of membrane interacting adaptor proteins to selected cargo which begins the assembly of the Clathrin lattice. The heterotetramer AP-2 is known to associate to the plasma membrane via its α and β2 subunits interacting with $PI(4,5)P_2$ (Kelly et al., 2014; Shih et al., 1995; Traub et al., 1999). These interactions cause a conformational change in the complex, which allows for cargo interaction with the μ2 subunit (Jackson et al., 2010),which in turn is thought to open two $PI(4,5)P_2$ binding sites on the μ2 subunit (Höning et al., 2005; Rohde et al., 2002), which stabilises AP-2 at the membrane. AP-2 can then

recruit PI4P 5-kinases via the μ2 subunit generating a concentrated pool of $PI(4,5)P_2$ which leads to further AP-2 complex recruitment (Krauss et al., 2006). The increase of $PI(4,5)P_2$ concentration thus plays a key role as a checkpoint to ensure cargo selection has occurred before the progression of the clathrin coated pit (CCP), and acute reduction of $PI(4,5)P_2$ has been shown to lead to a loss of CCP number and delayed progression of the pits (Zoncu et al., 2007). Several known synaptic proteins that have been shown to be endocytic cargos are Synaptotagmin-1 which is recruited to AP-2 via its cargo adaptors SV2, Stonin 2, and recently SGIP1α (Diril et al., 2006; Kaempf et al., 2015; Lee et al., 2019), and Synaptobrevin-2 via AP180 and CALM (Koo et al., 2011, 2015). Once at the membrane, AP-2 begins to recruit Clathrin molecules via interaction of mobile appendages of AP-2's α and β2 subunits to beta propeller on the terminal domain of the Clathrin heavy chain (Praefcke et al., 2004; Shih et al., 1995; ter Haar et al., 1998). As each Clathrin molecule is a triskelion composed of three light and heavy chains, multiple AP-2 complexes can bind to one Clathrin, as well as other adaptor proteins such as Amphiphysin 2, Arrestin 3, and AP180 (Smith et al., 2017). The Clathrin lattice assembly is thought to displace the PI4P 5-kinases, resulting in the end of $PI(4,5)P_2$ production denoting the end of the initiation phase (Borner et al., 2006; Wallroth & Haucke, 2018).

Maturation is the increase in curvature of the pit until it resembles a U shape whereby constriction and scission occur. This stage is characterised by the remodelling of the membrane by proteins, and the exchange of PIPs to promote progression. Until recently it was thought that Clathrin itself generated the initial curvature of the membrane as the curvature of a CCP matched that of Clathrin molecules (Cocucci et al., 2012; Kirchhausen, 2009), however it was recently shown that Clathrin first forms in a flat lattice before curvature, without an increase in the quantity of Clathrin molecules during bending (Avinoam et al., 2015; Haucke & Kozlov, 2018). Instead bending is caused by both large insertions into the membrane that disrupt the uniform lipid plain, and curved scaffold proteins, particularly Bin-Amphiphysin-rvs (BAR) domain containing proteins, that when recruited to the CCP provide external curvature to the pit (Campelo et

al., 2008; Haucke & Kozlov, 2018). At a yet undefined timepoint during Initiation/Maturation, PI5-phosphatases such as Synaptojanin, SHIP2, and OCRL are recruited to the CCP and convert PI(4,5)P_2 to PI4P (Erdmann et al., 2007; Nakatsu et al., 2010; Perera et al., 2006). This reduction in PI(4,5)P_2 towards the end of maturation intersects with an increase of PI(3,4)P_2, attributed to the Class-II PI3-kinase Alpha (PI3KC2α), which leads to the end of Maturation of the pit and induces Scission.

1.2.2 PI3KC2α and late stage Clathrin-mediated endocytosis

The PI 3-Kinases are a family of enzymes that all phosphorylate the 3 position on the inositol ring of PIPs. This family is split into three classes which are defined by their structural similarity and substrate preference. The best described enzymes are the Class I PI3Ks, which use PI(4,5)P_2 to generate PI(3,4,5)P_3, they are involved in cell signalling, in particular receptor mediated signalling such as Receptor Tyrosine Kinases (RTKs) and GPCRs (Leevers et al., 1999; Vanhaesebroeck et al., 2010). The Class I PI3Ks have been the subject of extensive study due to their role in multiple cancers, but also play a role in the brain, as second messengers for LTP formation (De Santis et al., 2019; Man et al., 2003). VPS34 is the sole member of Class III PI3Ks, it uses PI as its substrate to produce PI3P, which is involved in the control of endosomal sorting after endocytosis and also in controlling autophagy (Jaber & Zong, 2013; Vanhaesebroeck et al., 2010).

The Class II PI3Ks however had until recently remained enigmatic. Comprised of three members, the proteins are classified by having an unstructured N-terminal, a Ras-binding domain, a PI3K core followed by a phosphoinositide

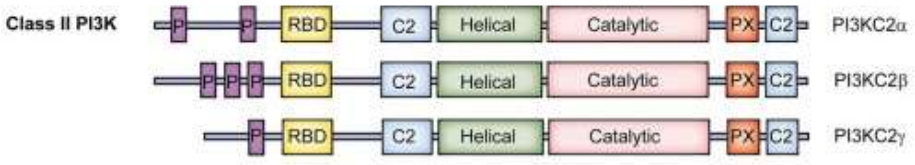

Figure 5: The Class II PI3Ks. The PI3K family is divided into three classes, defined by structural similarities. The Class II PI3Ks have an unstructured N-Terminus, Ras binding domain, two C2 domains, a PX domain and a PI3K core (Durrant & Hers, 2020).

binding Phox homology (PX) domain and a membrane interacting C2 domain (Figure 5). The first two members of the family, PI3KC2α and PI3KC2β are ubiquitously expressed, while PI3KC2γ was thought to be expressed primarily in the liver and pancreas, however recent data suggests expression in other tissues (Juyoung Kim et al., 2020; Kok et al., 2009; Muller et al., 2006). Class II PI3Ks primarily use PI4P as a substrate to produce PI(3,4)P_2 (Marat et al., 2017; Posor et al., 2013; Wallroth & Haucke, 2018), though there is some data that suggests PI as a substrate also (K. He et al., 2017), however this remains controversial.

PI3KC2α was shown to play a role in late stage CME, and its deletion results in delayed endocytosis and an increased number of stranded U shaped CCPs on the cell surface (Posor et al., 2013). This study also demonstrated that acute PI(3,4)P_2 depletion via the inducible recruitment of the PI4-Phosphatase INPP4B to the plasma membrane results in stranded CCPs, and expression of a PI3P-only producing PI3KC2α in knockdown cells does not rescue the phenotypes observed, suggesting PI3KC2α produced PI(3,4)P_2 is vital in the late CME stage of Scission. It is thought that PI3KC2α is recruited to the neck of the pit, interacting with Clathrin via a Clathrin binding domain (CBD) in its unstructured N-terminal region (Gaidarov et al., 2001; Schöneberg et al., 2017). Scission during CME involves the constriction of the vesicle neck until the CCP is Omega shaped (Ω), and eventual fission of the vesicle away from the plasma membrane. The best known proteins involved in this step are Dynamins, which is a key family of GTPases that conduct the final fission of the membrane (Praefcke & McMahon, 2004). However, it has been shown that Dynamin associates with highly constricted membranes with a diameter of 20 nm (Y. J. Chen et al., 2004). To achieve this high curvature, the maturing CCPs must be constricted from the U shape previously described to the Ω shape (Figure 6).

One protein shown be involved in constriction is a member of the sorting nexin family, SNX9. There are three members of the subgroup, SNX9, SNX18 and SNX33, all have the same organisation of domains: An N-Terminal SRC Homology 3 (SH3) Domain, a PX domain then a C-terminal BAR domain (Lundmark & Carlsson, 2009). Potentially having overlapping roles (J. Park et al., 2010), it has

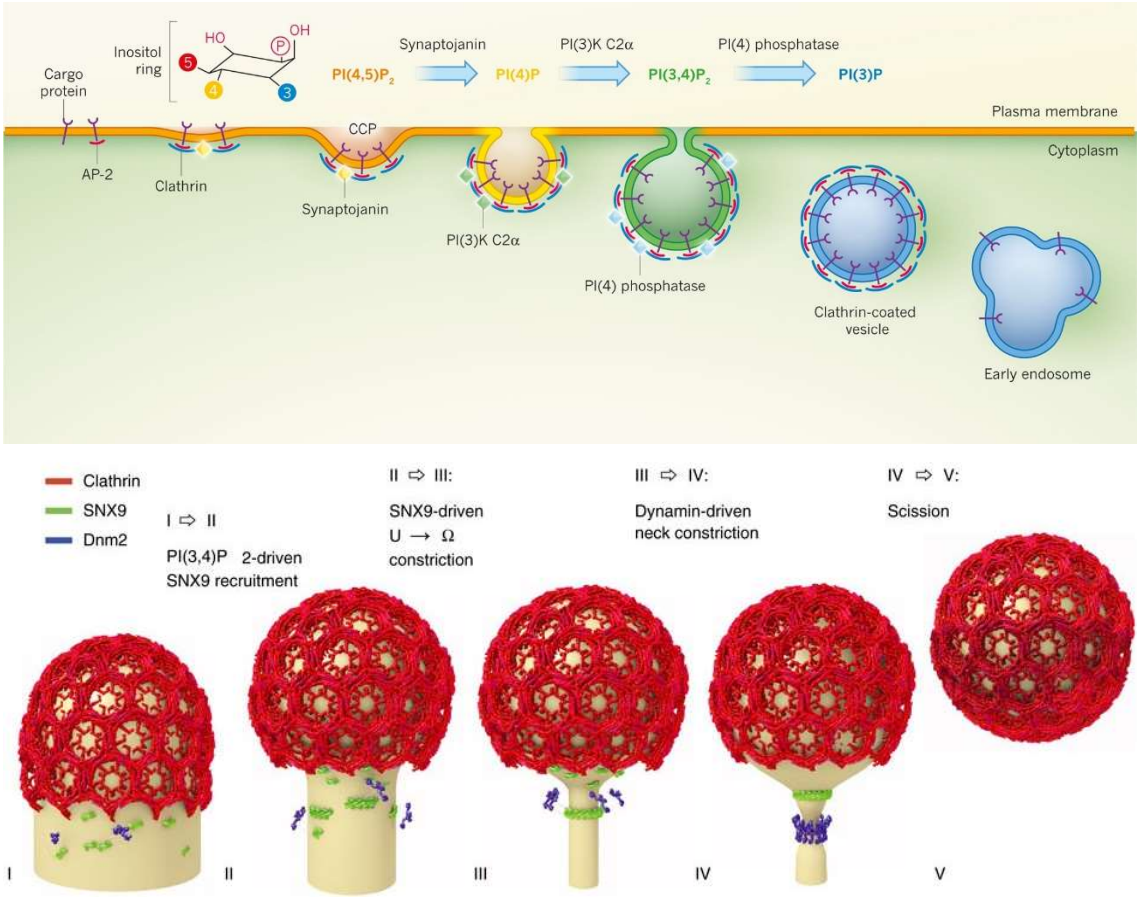

Figure 6: PI(3,4)P_2 mediated neck constriction. PI3KC2α was shown to be recruited to late stage CCPs, converting PI4P to PI(3,4)P_2. This results in the recruitment and activation of SNX9, leading to self-assembly of a ring that constricts the neck to within a diameter of 20 nm, whereby highly curved dynamin can be recruited which further constricts the neck, resulting in eventual fission. Adapted from (Schmid & Mettlen, 2013 and Schöneberg et al., 2017).

been shown that SNX9 and SNX18 are important for the U to Ω transition, with co-knockdown of them resulting in increased number of U CCPs and a tendency for prolonged endocytosis (Schöneberg et al., 2017).

The PX-BAR domain of SNX9 interacts with a stretch within the linker region between its SH3 and PX-BAR domain resulting in autoinhibition (Lo et al., 2017). However, upon interaction at the CCP with the AP-2 alpha ear, the ear binds to this linker region, displacing the PX-BAR domain. SNX9 is now free to interact with PI(3,4)P_2 via its PX domain, which allows SNX9 activation, leading to SNX9 ring self-assembly and membrane remodelling (Schöneberg et al., 2017). PI3KC2α produced PI(3,4)P_2 is thus essential for efficient SNX9 assembly and constriction

of the neck, with acute depletion of $PI(3,4)P_2$ or loss of PI3KC2α resulting in an a loss of SNX9 at the CCP (Posor et al., 2013). The constriction of the neck allows for Dynamin attachment and ring assembly, which then via GTP mediated constriction separates the vesicle neck resulting in completed fission.

Finally, the vesicle undergoes the mechanism of Uncoating, removing the endocytic machinery and the start of the sorting process of its cargo. Auxilin is recruited to the centre of the Clathrin triskelia followed by three copies of HSC70 which disassemble the coat via an ATP dependent mechanism (Greene & Eisenberg, 1990; Rothnie et al., 2011). At the same time, it is believed the PI4-Phosphatases INPP4A/B are recruited to the vesicle, converting $PI(3,4)P_2$ to PI3P, giving the vesicle a more endosomal identity.

Overall, it is clear PIPs are vital for maintaining CME checkpoints, and of interest to this study PI3KC2α produced $PI(3,4)P_2$ appears vital to late stage progression of CME.

1.3 Phosphoinositides in mTOR Signalling

Phosphoinositides are not purely limited to the control of membrane identity and trafficking but play important roles in cellular signalling and cell fate decisions. One such example of this is the conversion of external nutrient signals in the control of autophagy. Autophagy is the process of "eating of self", which involves the regulated breakdown of proteins, membranes, and even entire organelles. This is conducted for several reasons: to clear damaged organelles or misfolded proteins, destroy pathogens, and as a source of energy and nutrients in times of insufficiency. The activation or inhibition of autophagy thus has downstream effects on cell survival, growth, and signalling. Due to autophagy both suppressing growth yet promoting cellular survival, it has become a pathway of key interest in Cancer Biology, with Janus-faced tumour suppressor and promotor effects (Yun & Lee, 2018).

However autophagy is also thought to have key roles in synaptic transmission, neuronal homeostasis, and has impacts on animal behaviour

(Lieberman & Sulzer, 2020). Modulation of autophagy has been shown to have acute effects on synaptic vesicle numbers and release in striatal dopaminergic neurons and it also has a role in removal of defective release machinery (Hernandez et al., 2012; Hoffmann et al., 2019). It is also seen to be a key regulator of LTP and LTD induction, and perturbation of the normal control effects spatial memory (Glatigny et al., 2019; Nikoletopoulou et al., 2017; Shehata et al., 2012). Autophagy is also of key importance within the Hypothalamus, detecting nutrient levels and controlling feeding behaviour (Cota et al., 2006). One emerging field of study is how disfunction of autophagy may play a role in epileptogenesis (Giorgi et al., 2015; McMahon et al., 2012). However, this is a developing field which requires further investigation.

Autophagy involves the process of forming a large membrane compartment to degrade target cargo. During formation, the developing membrane sheet (known as a phagophore) extends and can encircle large structures such as mitochondria or large protein aggregates. Once fully formed into an enclosed compartment, the autophagosome as it is now known can fuse with multivesicular bodies, a type of late endosome which contains vesicles that have inwardly budded that have proteins marked for recycling on their surfaces. Finally, the mature autophagosome fuses with lysosomes containing digestive enzymes, allowing for cargo degradation, and recycling. This ensures effective recycling of cytosolic components.

1.3.1 mTOR control of autophagy and growth signalling

One key question concerning autophagy is how cells incorporate environmental signals in the decision for growth or recycling. One central player in translating these external signals is the protein mammalian target of rapamycin (mTOR). As the name implies, mTOR and its Yeast homolog TOR were discovered to be the target of the inhibitor rapamycin via the prolyl isomerase FKBP12 (Cafferkey et al., 1993; Kunz et al., 1993; Sabers et al., 1995).

mTOR is known to associate in two complexes, mTORC1 and mTORC2 which are both components of the PI3K-AKT pathway, with mTORC1 being a central regulator of the process, however mTORC2 is less well described. The two complexes are comprised of different subunits and have different localisation, mTORC1 being primarily located on the lysosome while mTORC2 is located on ER or at the plasma membrane (Betz & Hall, 2013).

The PI3K-AKT pathway is thought to incorporate multiple extra- and intracellular signals such as glucose levels, amino acid availability, and signals from certain GPCRs (Hemmings & Restuccia, 2015; New & Wong, 2007). The best described stimuli for the PI3K-AKT pathway though are growth factor signals such as Insulin, IGF, or EGF, which bind to their respective RTKs leading to dimerization and autophosphorylation of Tyrosine residues (Lemmon & Schlessinger, 2010; Wee & Wang, 2017). Ligand binding to RTKs leads to activation of Class I PI3Ks at the plasma membrane, either via direct interaction via the phosphorylated tyrosine residues on the activated receptor with the Src Homology 2 domain (SH2) domain of the p85 regulatory subunit of the PI3K or via adaptor proteins such as Gab1 (Mattoon et al., 2004; Wee & Wang, 2017). The interactions of Class I PI3Ks with GPCRs is less well characterised, though direct interactions do exist between certain GPCRs and a subset of Class I PI3Ks (New et al., 2007), and may both be excitatory or inhibitory to the pathway (Jewell et al., 2019; Martelli et al., 2010). Once active, the Class I PI3Ks convert $PI(4,5)P_2$ to $PI(3,4,5)P_3$ on the plasma membrane, which in turn recruits and activates Akt via its Pleckstrin homology (PH) domain (Franke, 2008; Hemmings & Restuccia, 2015). The level of $PI(3,4,5)P_3$ is tightly regulated by the PI3-Phosphatase PTEN, with mutations in the phosphatase being highly associated with tumorigenesis (C. Y. Chen et al., 2018; Stambolic et al., 1998). Akt activation also requires interactions with mTORC2 and PDK1 which may be a coincidence detection mechanism for $PI(3,4,5)P_3$ (Dibble & Cantley, 2015).

Once active, Akt phosphorylates and inactivates Tuberous sclerosis complex (TSC), a complex formed by the two proteins TSC1 and TSC2 (Gao, 2001; J. Huang & Manning, 2009). TSC is a negative regulator of downstream signalling

in the PI3K-AKT-mTOR pathway, and is thought to suppress signalling by sequestering the small GTPase Rheb in a GDP bound state (Garami et al., 2003; Menon et al., 2014), thus inactivation of TSC results in Rheb GTPase activity, which directly acts on mTORC1 either in the mTOR kinase domain or via mTORC1 subunit Raptor (Sancak et al., 2007; Sato et al., 2009). It is then possible for mTORC1 to remove the inhibitory protein PRAS40 from the complex via phosphorylation by Akt and mTORC1 itself, resulting in mTORC1 becoming fully active (Dibble & Cantley, 2015; L. Wang et al., 2008). The steps of how mTORC1 is regulated are still incompletely understood, with likely coincidence detection from indirect PI3K-AKT signalling playing a role (Acosta-Jaquez et al., 2009; Dan et al., 2014), as well as other signalling pathways playing a role, thus further investigation is required.

Once mTORC1 is active, it binds and phosphorylates several targets which effect cell growth, autophagy, and fate decisions. The best-known targets of mTORC1 are Unc-51 like autophagy activating kinase 1 (ULK1) the eukaryotic initiation factor binding proteins (4E-BPs) and Ribosomal protein S6 kinase beta-1 (S6K).

ULK1 resides in a complex of the same name which regulates a secondary Class III PI3K complex VPS34, a key player in initiation of autophagosome formation initiation and therefore also autophagy (Zachari & Ganley, 2017). ULK1 phosphorylates the Beclin-1 subunit of the VPS34 complex leading to increased activity (Russell et al., 2013). Upon the phosphorylation of Ser 757 of ULK1 by mTORC1, the complex is rendered inactive in turn leading to a decline in autophagy (Joungmok Kim et al., 2011).

4E-BPs strongly interact and inhibit Eukaryotic translation initiation factor 4E (eIF4E), a protein that both guides mRNA to ribosomes and initiates translation (Sonenberg & Hinnebusch, 2009). Upon mTORC1 phosphorylation of 4E-BP this interaction is weakened, thus promoting protein translation.

The mTORC1 target S6K and its downstream target S6 ribosomal protein are also important for protein translation. When mTORC1 phosphorylates S6K and

it in turn phosphorylates S6, S6 interacts with the 40S subunit of ribosomes allowing for protein translation (Dufner & Thomas, 1999; Ferrari et al., 1991).

Other targets are also described, including roles in mitochondrial synthesis, lipid metabolism, nucleotide synthesis, and control of transcription, and it is likely many more pathways will be discovered (Ben-Sahra et al., 2013; Cunningham et al., 2007; Napolitano et al., 2018; Porstmann et al., 2008). Furthermore, though the PI3K-Akt pathway is the best described pathway to mTORC1 activation it is by no means the only upstream regulation, with inputs from mitochondria via AMPK being described, and the inputs of mTORC2 and the physiological (I.e. non-rapamycin) regulation of FKBPs are still under investigation (Hausch et al., 2013; Jia Xu et al., 2012). One such pathway that was recently discovered was a novel signalling arch involving mTORC2 and a Class II PI3K known as PI3KC2β.

1.3.2 mTORC1 controls neuronal fate and memory formation

mTORC1 activity has been shown to be a key regulator in LTP formation and maintenance (Hoeffer & Klann, 2010; Stoica et al., 2011), by facilitating protein translation within the postsynapse (Cammalleri et al., 2003; Tsokas et al., 2005). mTORC1 is also thought to play a critical role in cellular fate decisions during neurogenesis, particularly for cortical and hippocampal development. As previously described, the regulation of mTORC1 has direct input into cell division, and increased activation has been associated with macrocephaly (Takei & Nawa, 2014), while conversely inhibition of the pathway leads to inhibited brain growth, and was recently shown to be the cause of microcephaly in Zika virus patients (Cloëtta et al., 2013; Liang et al., 2016). Finally mTORC1 signalling has been demonstrated to play important roles in neuronal migration, with misregulation resulting in poor interneuron migration and linked to autism (LiCausi & Hartman, 2018).

1.3.3 mTORC1 dysfunction in human epilepsies

The implication of the PI3K-AKT-mTOR pathway in epilepsy has been well described (Onda et al., 2002), and has been of particular clinical interest (Galanopoulou et al., 2012; Ostendorf & Wong, 2015). All known epilepsy inducing mutations within the pathway lead to an activation of mTORC1 signalling (J. K. Kim & Lee, 2019). The best described of these syndromes is Tuberous Sclerosis, a congenital disorder arising from mutation of the mTOR negative regulators *TSC1*/*TSC2* which result in multiple symptoms but notably have high occurrence of brain malformations, so called cortical tubers, and epilepsy (Kwiatkowski & Manning, 2005; Ridler et al., 2004). Early embryonic deletion of *Tsc1* or *Tsc2* via neuron specific Cre recombinase results in structural abnormalities, seizures and early death (Meikle et al., 2007; Zeng et al., 2011). However, it is unclear if the seizures are due to developmental abnormality or if there is a change of Excitatory/Inhibitory (E/I) balance within otherwise normal neuronal circuits. Virus mediated Cre recombination of *Tsc1* in adult mice led to *in vitro* neuronal excitability and a difference in susceptibility of seizure inducing kainic acid (Bateup et al., 2013). This adds weight to the argument that mTOR related epilepsies may be acutely treatable. It is key therefore to understand whether novel pathways have an input into mTORC1 signalling, and if dysfunction also leads to epileptogenesis. One such pathway that was recently discovered was a novel signalling arch involving mTORC2 and a Class II PI3K known as PI3KC2β.

1.3.4 PI3KC2β inhibits mTORC1 activity under low growth factor signalling

A recent knockdown study of PI3KC2β showed that upon loss of the PI3K, there is an increase in the phosphorylation of S6K at the Thr389 residue, a common target of active mTORC1 (Holz & Blenis, 2005; Marat et al., 2017; Rosner et al., 2012). Furthermore, loss of PI3KC2β led to an increase in cell size and lysosomal movement from a central to a peripheral location in the cell which indicates a decrease in autophagy and an increase in mTORC1 activity. Pulldown assays of the

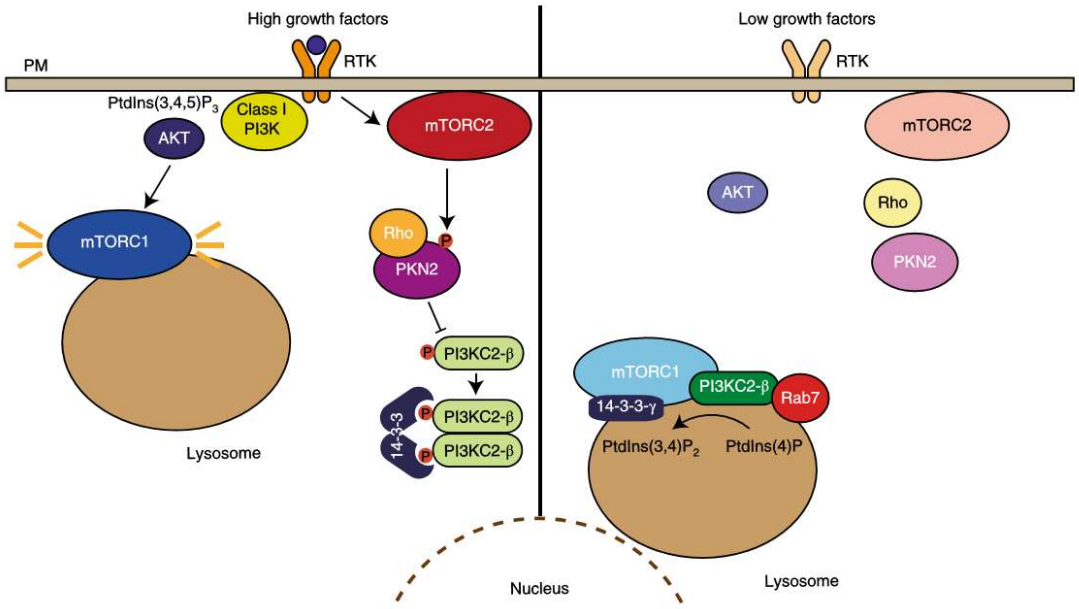

Figure 7: PI(3,4)P_2 mTORC1 inhibition by PI3KC2β. Under high growth factor signalling mTORC2 activates PKN2 which then phosphorylates PI3KC2β leading to 14-3-3 protein mediated dimerization, and sequestration in the cytosol. In the absence of growth factors, PI3KC2β is recruited to the lysosome by RAB7, leading to PI(3,4)P_2 production which recruits 14-3-3γ to the lysosome, inhibiting mTORC1 (Wallroth et al., 2019).

N-terminal region of PI3KC2β followed by mass spectrometry revealed a direct interaction with the Raptor subunit of mTORC1, as well as mTOR itself, and live cell imaging of fluorescently tagged PI3KC2β demonstrated that it associates with lysosomal compartments upon nutrient starvation. These data suggest that PI3KC2β acts as a repressor of mTORC1 in a low nutrient/growth factor environment. Interestingly, Akt signalling was unaffected by PI3KC2β loss and inhibition of AMPK did not affect PI3KC2β interactions with mTORC1, ruling out involvement of the two best known pathways of mTORC1 activation/inhibition, suggesting PI3KC2β inhibition of mTORC1 is activated by an undescribed pathway.

Consistent with the other Class II PI3Ks, it was demonstrated that the preferred substrate for PI3KC2β is PI4P, generating PI(3,4)P_2, and that PI3KC2β produces it during cell starvation. Loss of PI3KC2β resulted in a subsequent loss in 14-3-3 proteins at the lysosome and a decrease in 14-3-3γ interaction to Raptor, a known inhibitor of mTORC1 function (Gwinn et al., 2008), and these deficits were rescued upon exogenous PI(3,4)P_2 administration (Marat et al., 2017).

In a second study, a SILAC-based mass-spectrometry screen for interaction partners of PI3KC2β was performed under growth factor abundant and starved conditions. (Wallroth et al., 2019). Under growth factor abundance, PI3KC2β was shown to interact with 14-3-3 proteins, and pull downs of 14-3-3β against fragments of PI3KC2β suggested interactions in the same region where PI3KC2β binds to Raptor, in particular phosphorylated Thr279, thus blocking this action in fed conditions. A further screening found that this residue is phosphorylated by the two PKC-related serine/threonine-protein kinases N 1/2 (PKN 1/2), and loss of PKN1/2 led to increased PI3KC2β-Raptor interaction. It was then shown that loss of PKN2, but not PKN1 resulted in PI3KC2β association with the lysosome and increased $PI(3,4)P_2$, but interestingly could be rescued by loss of late endosome/lysosome bound small GTPase Rab7. An interaction between PI3KC2β and Rab7 was found and it was suggested this is required for PI3KC2β recruitment to the lysosome. Finally, the study demonstrated that mTORC2 phosphorylates PKN2, and inhibition of mTORC2 results in a loss of PKN2 interaction to PI3KC2β thus linking upstream growth factor stimulation to PI3KC2β inhibition (Wallroth et al., 2019). These studies identified a new pathway for mTORC1 inhibition and demonstrated a new role for PI3KC2β (Figure 7).

1.4 Aims of the study

The Class II PI3Ks PI3KC2α and PI3KC2β have been shown to have key roles in endocytosis and control of growth signalling. Both of these processes are vital to maintaining neuronal signalling and brain function.

At the presynapse, endocytosis is critical for the maintenance of synaptic vesicles and the release machinery to ensure reliable neurotransmitter release. At the postsynapse, the same pathways that control growth in immortalised cells are required for synaptic survival/pruning, memory formation, and synaptic maintenance via removal of defective receptors or protein translation.

This study aims to assess how Class II PI3Ks influence synaptic signalling. Furthermore, we aim to elucidate whether dysfunction of these kinases results in neuronal pathology in animal models, focussing on epileptogenesis translatable to human disease.

2 Materials and Methods

2.1 Materials

2.1.1 Chemicals and consumables

Unless otherwise stated, chemicals were obtained from Carl Roth, Life Technologies, Merck, Sigma-Aldrich and Thermo Fisher. Likewise, consumables were purchased from B. Braun, Biozym, GE Healthcare, Greiner, Millipore, Sarstedt and Schott.

2.1.2 Buffers, media, and solutions

All solutions were diluted in Milli-Q ultrapure water and pH adjusted with 1M HCl and NaOH unless otherwise stated. Where required, buffers were sterilized via autoclaving.

Table 1: Solutions for molecular biology experiments

Solution	Composition
Alkaline lysis buffer	25 mM NaOH 0.2 mM EDTA pH 12
Antibiotic stocks	Ampicillin 100 mg/ml Kanamycin 50 mg/ml
LB medium	1 % (w/v) Yeast extract 0.5 % (w/v) NaCl 0.5 % (w/v) Trypton pH 7.4
LB plates	LB medium 15 g/l Agar-agar
Neutralisation buffer	40 mM Tris-HCl pH 5
10x Orange G DNA loading dye	0.2 % (w/v) Orange G 70 % (v/v) Glycerol
50x Tris-Acetate-EDTA buffer (TAE)	200 mM Tris 100 mM Glacial acetic acid 50 mM EDTA pH 8.2 – 8.4
10x Tris-Borate-EDTA buffer (TBE)	20 mM EDTA 890 mM Tris 890 mM Boric acid

Table 2: Media and solutions for neuronal cell preparation and culture

Solution	Composition
Basic medium for neuronal media preparation	1 x MEM 5 g/l Glucose 200 ml/l NaHCO3 100 mg/l Transferrin
Digestion solution	137 mM NaCl 5 mM KCl 7 mM Na2HPO 25 mM Hepes pH 7.4
Dissociation solution	HBSS (minus Ca^{2+} and Mg^{2+}) 50 mg/l NaHCO3 12 mM MgSO4 1 mM Hepes pH 7.4
Growth medium	1 x Basic medium 5 % (v/v) FCS 0.5 mM L-glutamine 2 % (v/v) B27-supplement 50 U/ml Penicillin 50 µg/ml Streptomycin
Plating medium	1 x Basic medium 5 % (v/v) FCS 0.5 mM L-glutamine 2 % (v/v) B27-supplement 50 U/ml Penicillin 50 µg/ml Streptomycin
Serum solution	HBSS (minus Ca^{2+} and Mg^{2+}) 20% (v/v) Foetal calf serum (FCS) 50 U/ml Penicillin 50 µg/ml Streptomycin
Washing solution	HBSS (minus Ca^{2+} and Mg^{2+}) 50 U/ml Penicillin 50 µg/ml Streptomycin

Table 3: Buffers for live neuronal imaging

Solution	Composition
10 x Imaging stock	1.2 M NaCl 35 mM KCl 40 mM KH2PO4 200 mM TES 50 mM NaHCO3 50 mM Glucose 12 mM Na2SO4 pH 7.4
Imaging buffer	1x Imaging stock 50 mM NaCl 1.2 mM MgCl2 1.3 mM CaCl2 50 µM APV 10 µM CNQX
Unquenching buffer	1x Imaging stock 50 mM NH4Cl 1.2 mM MgCl2 1.3 mM CaCl2 50 µM APV 10 µM CNQX

Table 4: Solutions for immunofluorescent microscopy

Solution	Composition
Blocking buffer	1x PBS 10% (v/v) Normal goat serum (NGS) 0.3% (v/v) Triton X-100 (or Tween-20 where specified)
10 x PBS stock	1.37 M NaCl 27 mM KCl 43 mM Na2HPO 4 14 mM NaH2PO4 pH 7.4
PFA fixative	1x PBS 4 % (w/v) paraformaldehyde (PFA) 4 % (w/v) sucrose pH 7.4

Table 5: Solutions and buffers for immunohistochemistry

Solution	Composition
Anaesthetic	1× PBS 1.2 % (v/v) Ketamin 0.16 % (v/v) Rompun
Cryoprotection solution	1x PBS 15% or 30% (w/v) Sucrose
Fixative solution	1x PBS 4 % (w/v) PFA
Gelatine solution	1% Gelatine powder
0.4 M Phosphate buffer (PB)	85% (v/v) 0.4 M Na2HPO4 15% (v/v) 0.4 M NaH2PO4 NaH2PO4 is added until pH is 7.4
PB blocking buffer	0.125 M PB 10% (v/v) NGS 0.3% (v/v) Tween-20
Section storage solution	0.125 M PB 20% (v/v) Glycerol 2% (v/v)DMSO

Table 6: Solutions and buffers for biochemistry

Solution	Composition
Brain homogenisation buffer	50 mM Tris, pH 7.5 150 mM NaCl 1 % (v/v) Triton X-100 10 % (v/v) Glycerol 1 mM PMSF 0.3% (v/v) Protease inhibitor cocktail (PIC) If required 1 % phosphatase inhibitor cocktail 2 1 % phosphatase inhibitor cocktail 3
2 x Bradford reagent	140 g/l Coomassie G250 200 ml 85 % H3PO4 100 ml ethanol
Buffered sucrose solution	4 mM Hepes pH 7.4 320 mM Sucrose 1 mM PMSF 0.3% (v/v) PIC
Cell lysis buffer	20 mM Hepes pH 7.4 100 mM KCl

	2 mM MgCl2 1 % (v/v) Triton X-100 1 mM PMSF 0.3 % (v/v) PIC 1 % phosphatase inhibitor cocktail 2 1 % phosphatase inhibitor cocktail 3
Membrane blocking buffer	100% Licor Odyssey Blocking Buffer (TBS)
Membrane staining buffer	1x TBS 50% (v/v) Licor Odyssey Blocking Buffer (TBS)
Ponceau solution	0.4 % (w/v) Ponceau-S 1 % (v/v) Acetic acid
Ponceau destaining solution	1 % (v/v) Acetic acid
6x SDS sample buffer	60 % (v/v) Glycerol 18 % (w/v) SDS 30 % (v/v) β-Mercaptoethanol 0.325 M Tris pH 6.8 0.25 % (w/v) Bromophenol blue
4x SDS separating gel buffer	0.4 % (w/v) SDS 1.5 M Tris pH 8.8
4x SDS stacking gel buffer	0.4 % (w/v) SDS 0.5 M Tris pH 6.8
10x TBS	0.2 M Tris pH 7.6 1.4 M NaCl
Wet transfer buffer	25 mM Tris 192 mM Glycine 10 % (v/v) MeOH for low kDA proteins 20 % (v/v) MeOH for high kDA proteins

Table 7: Buffers for electrophysiology and slice incubation experiments

Solution	Composition
Artificial cerebrospinal fluid (ACSF)	120 mM NaCl 2.5 mM KCl 1.25 mM NaH2PO4 24 mM NaHCO3 1.5 mM MgSO4 2 mM CaCl2 25 mM Glucose pH 7.35 - 7.4 Osmolarity 320 For slice incubation with inhibitors DMSO final concentration should be less than 0.01% (v/v)
Dissection ACSF	2.5 mM KCl 1.25 mM NaH2PO4 24 mM NaHCO3 1.5 mM MgSO4 2 mM CaCl2 25 mM Glucose 250 mM sucrose pH 7.35 - 7.4 Osmolarity 320

Table 8: Solutions for seizure experiments

Solution	Composition
Kainic acid solution	0.9% (w/v) NaCl 23.5 mM Kainic acid
Pentylenetetrazol (PTZ) solution	0.9% (w/v) NaCl 72.4 mM PTZ

2.1.3 Enzymes and kits

For tail and ear biopsy genotyping was conducted with Taq DNA polymerase purchased from Bio&SELL.

For small scale preparation of plasmid DNA from *Escherichia coli (E. coli)* grown overnight, NucleoSpin Plasmid Kit from Macherey-Nagel was used for purification. For large scale preparation of plasmid DNA for Neuronal transfection, NucleoBond Xtra Midi Endotoxin Free kit from Macherey-Nagel was used.

For transfection of primary hippocampal cultures with plasmid DNA via calcium phosphate transfection, the ProFection Mammalian Transfection kit was purchased from Promega and used as per the instructions within the kit.

2.1.4 Molecular weight standard markers

For identification of polymerase chain reaction (PCR) fragments for mouse genotyping, FastLoad 100 bp DNA Ladder was purchased from SERVA Electrophoresis GmbH.

For identification of protein weight during protein electrophoresis and immunoblotting, PageRuler Prestained Protein Ladder (10-180 kDa) was used from Thermo Scientific.

2.1.5 Synthetic DNA oligonucleotides

DNA oligonucleotides used as primers in genotyping PCR were obtained from BioTeZ Berlin-Buch GmbH and dissolved to a 100 µM stock concentration in nuclease-free, autoclaved water from Roth. This is diluted again to 10 µM for use in genotyping PCR.

Table 9: Primer sequences for genotyping mouse biopsies

Genotype	Primer	Sequence- 5' to 3'	Size of product
Cre recombinase	TM 63	CCGGGCTGCCACGACCAA	400bp
	TM 64	GGCGCGGCAACACCATTTTT	
PI3K-C2α	Pi3kc2a FW1	AGTCCCAAATGAGCTTGCTCTCTTC	wt: 490bp lox: 700bp
	Pi3kc2a Rev2	ACGTAGTAGCACCCCACAAGC	
PI3K-C2ß Wild Type	c2ßlox3	TGTTAGAACCTGCCGCCTTTAC	251bp
	c2ßlox4	CCGAATCAGCCTCATTTCCTCTC	
PI3K-C2ß Null	c2ß null-1	GGCACACACTAACCACAGCACC	404bp
	c2ß null-2	TCGATGCACGTCTCTCCGC	

2.1.6 Plasmid Vectors

All plasmid DNA was prepared using kits previously described. All were diluted to 1 µg/µl and stored at -20°C.

Table 10: Plasmid DNA constructs for recombinant protein expression

Construct	Backbone	Promoter	Tag	Antibiotic	Source
Syp-pHluorin	pcDNA3.1	Synapsin-1	pHluorin	Ampicillin	L. Lagnado
Syt1-mCherry	pmCherry-C	CMV	mCherry	Kanamycin	N Kaempf
Syt1-pHluorin	pcDNA3.1	Synapsin-1	pHluorin	Ampicillin	M. Wienisch (Wienisch and Klingauf, 2006)

2.1.7 Antibodies

All primary and secondary antibodies in this study were stored at either -20°C or 4°C as specified by the manufacturer for long term storage. Unless specified antibodies were diluted with 50 % (v/v) glycerol to prevent freeze thaw damage, otherwise were aliquoted into single use volumes. As such all dilutions are specific to the diluted glycerol stock or single use aliquot.

Table 11: List of primary antibodies

* Indicates undiluted single use aliquot, + indicates Tween-20 permeabilization

Antigen	Host species	Dilution WB	Dilution ICC	Dilution IHC	Source	Catalogue number
Actin	Mouse	1:10000	-	-	Sigma-Aldrich	A5441
GAPDH	Mouse	1:5000	-	-	Sigma-Aldrich	G8795
Gephyrin	Guinea Pig	-	1:200*	1:200*	Synaptic Systems	147 318
GluR1	Mouse	1:1000	-	-	Millipore	MAB2263
Homer1	Rabbit	1:1000	-	-	Synaptic Systems	160003
Kv1.1	Mouse	1:500	-	-	Antibodies Incorporated	75-007
Kv1.2	Mouse	1:500	-	-	Antibodies Incorporated	75-008-020
MAP2	Mouse	-	1:1000	1:1000	Sigma-Aldrich	M9942
mTOR	Rabbit	1:1000			Cell Signaling	7C10
Parvalbumin	Mouse	-	1:500	1:500	SWANT (acris)	235
P70 S6 Kinase	Rabbit	1:1000	-	-	Cell Signaling	2983
Phospho-mTOR Ser2448	Rabbit	1:1000	-	-	Cell Signaling	5536
Phospho-P70 S6 Kinase T389	Rabbit	1:500	-	-	Cell Signaling	9234
Phospho-S6 Ribosomal Protein (Ser235/236)	Rabbit	1:400*	1:200*+	1:200*+	Cell Signaling	2211
PI3KC2α	Mouse	1:400	-	-	BD transduction	611046

PI3KC2β	Mouse	1:500	-	-	BD transduction	611342
PSD95	Mouse	1:1000	1:400	1:400+	Synaptic Systems	124 011
Rab7	Rabbit	1:1000	-	-	Cell Signaling	9367
S6 Ribosomal Protein	Mouse	1:500*	-	-	Cell Signaling	2317
Somatostatin-28	Guinea Pig	-	1:500*	1:500*	Synaptic Systems	366 004
Synaptophysin	Rabbit	-	1:100	-	Synaptic Systems	101002
Synaptotagmin 1	Mouse	1:5000	1:5000	-	Synaptic Systems	105 011
vGAT-488	Mouse	-	-	1:400	Synaptic Systems	131 011C2
vGLUT	Rabbit	1:1000	-	1:400+	Synaptic Systems	135 302

Table 12: List of secondary antibodies

* Indicates undiluted single use aliquot

Antigen	Host species	Fluorophore	Dilution WB	Dilution ICC/IHC	Source	Catalogue number
Guinea Pig IgG	Goat	AlexaFluor568	-	1:200	Life technologies	A11075
Mouse IgG	Goat	AlexaFluor488	-	1:200	Life technologies	A-11001
Mouse IgG	Goat	AlexaFluor568	-	1:200	Life technologies	A-11031
Mouse IgG	Goat	AlexaFluor647	-	1:200	Life technologies	A-21235
Mouse IgM	Goat	AlexaFluor568	-	1:200	Life technologies	A-21043
Rabbit IgG	Goat	AlexaFluor488	-	1:200	Life technologies	A-11034
Rabbit IgG	Goat	AlexaFluor568	-	1:200	Life technologies	A-11011
Rabbit IgG	Goat	AlexaFluor647	-	1:200	Life technologies	A21244
Guinea Pig IgG	Donkey	IRDye 800CW	1:5000	-	LI-COR	926-32411
Mouse IgG	Goat	IRDye 800CW	1:10000	-	LI-COR	926-32210
Mouse IgG	Goat	IRDye 680RD	1:10000	-	LI-COR	926-68070
Rabbit IgG	Goat	IRDye 800CW	1:5000	-	LI-COR	926-32211
Rabbit IgG	Goat	IRDye 680RD	1:5000	-	LI-COR	926-68071

2.1.8 Bacterial strains

Chemically competent *Escherichia coli* (*E. coli*) from the strain TOP10 (Invitrogen) were used for the storage and amplification of plasmid DNA. For long term storage of plasmid DNA libraries, the TOP10 bacteria were suspended in a 50% (v/v) glycerol solution and stored at -80°C.

2.1.9 Mouse strains

The *Pi3KC2α*$^{Fl/Fl}$ mice come from a C57BL/6J background and had loxP sites inserted to flank exon 2 for Cre-mediated recombination. These mice were originally generated by EUCOMM (European Conditional Mouse Mutagenesis Project). Cre recombination interferes with transcription leading to a loss of the protein. These mice were kindly given to us by Prof. Dr. Emilio Hirsch (MBC Turin).

For inducible knockout in primary hippocampal cultures *Pi3KC2α*$^{Fl/Fl}$ mice were crossed with *Cre-ER*^{TM} from a C57BL/6J background (from now on called *Pi3KC2α-CAG)*. This mouse line ubiquitously expresses a fusion protein consisting of Cre recombinase and a modified ligand-binding domain of estrogen receptor, which has high specificity to tamoxifen (S. Hayashi & McMahon, 2002; Metzger & Chambon, 2001). In absence of tamoxifen Cre-ER is confined to the cytosol, however upon tamoxifen binding it is shuttled into the nucleus where recombination can occur.

For a forebrain specific knockout *Pi3KC2α*$^{Fl/Fl}$ mice were crossed with an EMX-Cre line from a C57BL/6 background, which expresses Cre recombinase from the EMX1 locus (Iwasato et al., 2000). This line has been shown to have Cre recombinase expression in a high percentage of neurons of the cortex and hippocampus.

The *Pi3KC2β*$^{(-/-)}$ line were originally generated by insertion of loxP sites flanking exons 3-5 (Harada et al., 2005). This line was crossed with a line with ubiquitously expressed Cre recombinase, which resulted in germline deletion. These mice were purchased from Charles River Italy and crossed with C57BL/6J mice to generate heterozygotes for breeding purposes.

All mice were cohoused in individually ventilated cages with water and food supplied ad libitum. Cage enrichment was provided, and lighting was controlled on a twelve-hour night day cycle. All experiments and breeding schemes were approved by the ethics committee from the Landesamt für Gesundheit und Soziales (LAGeSo) Berlin. The severity of experiments and mouse lines was monitored throughout the project.

2.1.10 Software

Table 13: List of software

Software name	Source	Application
Adobe Photoshop CS6	Adobe	Preparation of figures
ApE	Jorgensen laboratory, University of Utah	Primer design, DNA Plasmid mapping
Fiji	Online open source (https://fiji.sc/)	Image analysis, figure preparation and macro writing
GeneSys	Syngene	DNA electrophoresis gel imaging
Graphpad Prism 5	Graphpad	Statistical analysis and graph preparation
Image Studio Lite	Licor	Western Blot imaging and analysis
InstarVision	Instar	IP camera control for animal monitoring
Micromanager (µManager)	Online open source (https://micro-manager.org/)	Control of epifluorescence microscope
Office 365	Microsoft	Statistical analysis, graph preparation, text generation and presentations
Patchmaster	HEKA Electronics	Electrophysiological recordings and stimulation management
PDFescape Desktop	PDFescape	PDF file editing
PyRAT Animal Facility Software	Scionics Computer Innovation	Animal management
SigmaPlot 13	Systat Software	Data analysis and graph preparation
Volocity v6.2.1	Perkin Elmer	Control of spinning disk confocal microscope
ZEISS Zen	ZEISS Group	Control of laser scanning microscope

2.2 Molecular Biology Methods

2.2.1 Genotyping of transgenic mice

To determine whether the desired alleles were present in mice, genomic DNA was acquired from either tail or phalanx biopsies in the case of neonates, or from ear biopsies from adult mice. Biopsies were incubated at 95°C in Alkaline lysis buffer (25 µl for tail and phalanx, 50 µl for ear) for 1 hour before inactivation with equal volume of Neutralisation buffer. To amplify the quantity of DNA, PCR was conducted immediately after inactivation of lysis to prevent DNA degradation. Positive controls in the form of wild type and mutant alleles were included to demonstrate the PCR worked as expected, and water as a negative control to demonstrate the PCR mix was free of contamination.

Table 14: Reaction mix for genotyping PCRs

Component	Composition
10x Taq Buffer	1x
$MgCl_2$	2 mM
dNTPs	150 µM each
Primers	375 nM each
10x Orange G DNA loading dye	1x
Template DNA	1 – 2 µl
Taq Polymerase	2 units
Nuclease free water	Up to 20 µl

Table 15: PCR programs for genotyping transgenic mice

Step	Cre	Pi3KC2α	Pi3KC2β WT	Pi3KC2β Null
1. Start	94°C 3 min	94°C 3 min	94°C 5 min	94°C 5 min
2. Denaturation	94°C 30s	94°C 30s	94°C 30s	94°C 30s
3. Annealing	55°C 30s	52°C 30s	60°C 30s	65°C 30s
4. Elongation	72°C 30s	72°C 45s	72°C 1 min	72°C 1 min
5. End	72°C 5 min	72°C 5 min	72°C 5 min	72°C 5 min
6. Store	4°C	4°C	4°C	4°C

Steps 2 – 4 were repeated for 35 cycle

2.2.2 Agarose gel electrophoresis

For DNA fragment identification during mouse genotyping, agarose gel electrophoresis was used. Agarose powder was dissolved 2% (w/v) in 1x TAE buffer, heated in a microwave, while gently agitating every 30 seconds - 1 minute to prevent superheating. Ethidium bromide was then added to a concentration of 100ng/ml, loading combs added and allowed to cool in a fume hood. The gel was then placed into an electrophoresis chamber, covered with 1x TAE buffer and combs removed. FastLoad 100 bp DNA Ladder was added in the first well of each row as a reference, then all reaction mix from each genotyping PCR. The electrophoresis was then performed by applying 10V/cm electrode distance for 30 minutes. The gel was then imaged under UV in a Syngene G Box to detect ethidium bromide intercalated DNA. Detected bands were checked against the reference ladder to see if desired fragment sizes were detected (see Table 9).

2.2.3 Amplification of plasmid DNA using *E. coli*

To amplify plasmid DNA, 5 – 10 µl of bacterial glycerol stock was added to a midi culture of 100 - 250 ml of LB media with the appropriate selection antibiotic using bench aseptic technique. These cultures were incubated in a bacterial shaker overnight at 37°C at 180 rpm in a 500 ml conical flask.

2.2.4 Purification of plasmid DNA from E. coli cultures

After overnight incubation, midi cultures were centrifuged at 4°C, 4000 rcf for 30 minutes. From this step forwards DNA was prepared using the NucleoBond® Xtra endotoxin free (EF) plasmid purification kit (Macherey-Nagel), all incubation time and centrifugation speeds were as recommended by the manufacturer. Cells were lysed in an alkaline SDS buffer followed by centrifugation to remove cell debris while leaving plasmid DNA in the supernatant. DNA is bound to a silica membrane and washed several times to remove remnant proteins and, importantly, endotoxin. Endotoxins are lipopolysaccharides that are plentiful in the outer membrane of Gram-negative bacteria, and have been shown to have effects on *In Vitro* cultures (C. Kim et al., 2016).

Once thoroughly washed, DNA is eluted, then precipitated in isopropanol and ethanol, dried and resuspended in 100- 200 µl ultrapure water. Concentration of DNA, and protein contaminants was then determined with a NanoDrop ND-1000 (Peqlab) according to the Lambert-Beer law (Barker 2005).

2.3 Cell Biology Methods

2.3.1 Preparation of primary hippocampal cultures

Glass coverslips (18 mm for immunofluorescence, 25 mm for live imaging) were acid washed in 1 M HCl for 24 hours in ceramic staining racks, rinsed three times with distilled water and washed in acetone for 24 hours. Finally, the coverslips are washed for 24 hours in 70% (v/v) ethanol, dried and stored in a sterile petri dish for use. On the day of use, the coverslips were coated with 100 – 200 µl (respective of coverslip diameter) 15 µg/ml Poly-L-Lysin (Biochrom). The coating was allowed to incubate at room temperature for 1 – 2 hours, washed three times with water and then allowed to dry for 15 minutes. Coverslips were placed in 12-well and 6-well sterile plates respectively.

After genotyping, 2 - 4 littermates of each desired genotype were selected. The pups were taken at ages p1 – p4 and were sacrificed by decapitation, whole brains removed and placed in ice cold Serum solution. Tail biopsies were taken from each mouse to clarify genotype. Brains were opened down the midline with forceps for easy separation of the hippocampi from their cortical and midbrain connections. Once the hippocampi are separated, any remnant cortical tissue or meningeal projections are removed. Hippocampi are transferred to fresh Serum solution and cut into 4 – 5 equal sized pieces along the coronal axis. The pieces are transferred to a 15 ml falcon, washed twice with serum solution and twice with washing solution.

To digest the tissue, 5 mg/ml Trypsin (Sigma) and 375 U/ml DNase (Sigma) were dissolved in digestion solution and passed through a 0.22 µm syringe filter (Roth), then 2 ml was added to each genotype, which were transferred to 3cm dishes and incubated at 37°C for 15 minutes. Hippocampi were transferred back to

15 ml falcons, washed twice with Serum solution to inactivate trypsin then twice with Washing solution. For dissociation, 375 U/ml DNase was dissolved in Dissociation solution and 2 ml added to each genotype. The hippocampi were then triturated, first with a P1000 micropipette 10 – 15 times, then with a P200 micropipette 20 times. The cells were then centrifuged at 4°C, 400 rcf for 15 minutes. Dissociation solution was aspirated, and the pellet resuspended in 300 – 450 µl of plating media. Cells were counted using a Haemocytometer (Neubauer) and concentration adjusted to 2400 cells/ µl and plated 140,000 cells or 70,000 cells on coverslips respective of coverslip size.

The plates were then incubated in a New Brunswick Galaxy 170 S incubator at 37°C, 5% CO_2 for 1 hour to facilitate cell attachment, then 1 - 2 ml per well (for 12 or 6 well plates respectively) of plating media was then added and the plates were placed back in the incubator. For *Pi3KC2α*$^{Fl/Fl}$ x *Cre-ER*^{TM}, 250 nM Tamoxifen was diluted in the plating media of both Cre positive and negative genotypes.

Feeding occurred on Day In Vitro (DIV) 1 and 2. On DIV1 half the volume of each well was removed and replaced with equal volume Growth medium containing 2 µM β-D-arabinofuranoside (AraC, Sigma) and where applicable 250 nM Tamoxifen. On DIV2, 0.5 - 1 ml was added per well (for 12 or 6 well plates respectively) of growth medium containing 4 µM AraC, and where applicable 250 nM Tamoxifen. AraC is a proliferation inhibitor that was used to prevent overgrowth of astrocytes.

2.3.2 Preparation of primary cortical cultures

Preparation of cortical cultures was required for gathering sufficient material for western blot assays. All steps are the same as primary hippocampal neuron preparation, apart from these subsequent modifications to the protocols.

Instead of coverslips, 3 cm sterile culture dishes were coated with 1 ml 10 µg/ml poly-L-ornithine (Sigma). These were incubated at room temperature for at least 1 - 2 hours, washed three times with water and allowed to dry for 15 minutes. Poly-L-ornithine coating has been shown to promote cortical neuron differentiation and aid culture viability (Ge et al., 2015).

During dissection the cortex was separated down the midline, hippocampi separated to be used in other experiments. Meningeal membranes were removed as well as midbrain, hypothalamus and olfactory bulbs. The cortices were each dissected into 15 – 20 roughly square pieces to aid Trypsin digestion.

Preparation continues unchanged until cell counting, where cells are resuspended in 500 – 1000 µl plating media. A one in ten dilution of the cell suspension was made to aid counting. The dilution was adjusted to 2000 cells/µl and 1.8 million cells were plated per 3 cm dish. Feeding is the same as one well of a 6-well plate of hippocampal neurons.

2.3.3 Calcium phosphate transfection of hippocampal neurons

Primary hippocampal neurons were transfected between DIV6 and DIV9 with endotoxin-free plasmid DNA (see purification of plasmid DNA) using the ProFection Mammalian Transfection System kit (Promega). Aliquots of the culture medium were taken and osmolarity readings taken. The osmolarity of Neurobasal A (NBA, Invitrogen) and HBSS (minus $Ca2^{+}$ and $Mg2^{+}$, Invitrogen) were adjusted by adding D-Mannitol (Sigma) to match the average osmolarity of the culture medium aliquots. The NBA and HBSS were then equilibrated in the incubator for 30 minutes.

The coverslips with primary hippocampal neurons were transferred from culture medium containing plates to plates containing 1 ml of equilibrated NBA. Both plates were placed in the incubator for 25 minutes. This starves the cells which is thought to promote endocytic uptake of DNA-Calcium Phosphate precipitates. During the starvation, the Transfection solution is prepared. Per well, 6 µg of plasmid DNA and 250 mM $CaCl_2$ were dissolved in nuclease free water to a final volume of 100 µl and then mixed 1:1 with 2x Hepes. This is done by adding the DNA solution dropwise to the Hepes while vortexing at low speed. The mix is then incubated in the dark at room temperature for 20 minutes. Afterwards 200 µl was added dropwise to each well of the plate containing neurons, spreading evenly across the well and placed into the incubator for 30-35 minutes. After 30 minutes the cells were checked under a light microscope to see if fine DNA-

Calcium phosphate precipitates had settled on the neurons and then were washed three times with 2 ml of the equilibrated, osmolarity adjusted HBSS before transferring the coverslips back to their original culture medium wells.

2.3.4 Immunocytochemistry

Primary hippocampal neurons were fixed on DIV14 with 4 % (w/v) paraformaldehyde (PFA) and 4 % (w/v) sucrose for 15 min room temperature followed by three quick washes with PBS. The cells were then permeabilised and blocked for 1 hour in Blocking buffer. Primary antibodies were then diluted (see Table 11) in Blocking buffer and applied in 50 – 80 µl drops to parafilm stretched over a culture plate lid. Coverslips with plated neurons were then inverted onto the droplets, the plate lid surrounded with water and a plastic container placed over top to create a humidity chamber and incubated for one hour at room temperature. The coverslips were then washed three times with PBS and then incubated with secondary antibodies (see Table 12) as described above for 30 minutes at room temperature. Coverslips were washed three times and then mounted on microscope slides in Immu-Mount and dried in the dark at room temperature for 1 – 2 hours. Slides were then stored at 4°C.

2.3.5 Electrical stimulation of neuronal cultures for electron microscopy

To detect clathrin intermediates, neurons were stimulated and fixed for transmission electron microscopy. DIV14 primary hippocampal neurons were transferred to an imaging chamber with parallel stimulation electrodes (Warner Instruments) with 37°C osmolarity adjusted Imaging buffer. Postsynaptic receptors were blocked to prevent spontaneous neuronal activity with 50 µM APV (Abcam) and 10 µM CNQX (Sigma). The culture was stimulated by a 40 Hz, 100 mA current for 5 seconds. The cells were then transferred to a 6-well plate containing 4% (v/v) Glutaraldehyde (Sigma) 25 seconds after stimulation. The cells were fixed for 10 minutes at room temperature, then washed three times with PBS before resin embedding and electron microscopy.

2.4 Histology Methods

2.4.1 Transcardial perfusion of mice for brain extraction

To ensure proper fixation of the brains of adult mice, it was necessary to conduct perfusion. Fresh 4% (w/v) PFA in PBS pH 7.4 was prepared on the day and filtered to remove solids. The PFA solution and fresh PBS were both cooled on ice prior to perfusion. Mice were weighed and were given terminal anaesthesia with an intraperitoneal injection of 10 µl/g of 1.2% (v/v) Ketamine (Medistar) and 0.16%(v/v) Xylazine (Medistar) diluted in PBS. Upon loss of pain reflex a small tail biopsy was taken for genotyping and the mouse was transferred to the perfusion chamber consisting of a cork board in a stainless-steel collection tray within a fume hood.

The mouse was affixed to the board, and an incision was made at the base of the abdomen, up both sides of the abdomen, exposing the abdominal cavity and the base of the ribcage. The diaphragm was then opened, and incisions made on both sides of the rib cage. The abdominal wall and frontal ribcage were pinned above the head to expose the heart. A needle connected to a PeriStarPRO pump (WPI) was placed into the left ventricle, PBS perfusion started to maintain pressure and then the right atrium is severed rapidly.

The mouse was then perfused with PBS at a rate of 5 ml/min until the liver is visibly drained of blood, then switched to PFA for 3 minutes. The skull was severed at the neck, opened up the midline to separate the skull plates and the nasal bone severed between the eyes to enable brain removal. The left and right hemispheres were separated and placed in PFA on a roller overnight at 4°C for post fixation.

2.4.2 Cryoprotection of brains

To protect the tissue from ice crystal formation, brains were cryoprotected via sucrose gradient. After post fixation, PFA was exchanged for 15% sucrose (w/v) in PBS and placed back on a roller for 6-12 hours until tissue sinks in the tube. Solution was then exchanged for 30% sucrose (w/v) in PBS and stored at -80°C.

2.4.3 Cryosectioning of brains

One hemisphere was affixed to a Microm HM430 Sliding Microtome (Thermo Scientific) by placing the central face of the hemisphere downwards, olfactory bulb facing the cutting blade, onto 1 – 2 cm^2 of Tissue-Tek O.C.T (Sakura) and frozen to -30°C to obtain sagittal sections. Stereological representative sampling principles were used while acquiring sections and the entire brain was sectioned: 7 series of 40 µm sections were acquired yielding 11-12 hippocampus containing sections per series. Sections were placed in 5 ml Eppendorf tubes, suspended in Section storage solution and stored at -80°C.

2.4.4 Fixation and sectioning of acute hippocampal slices

Acute slices were prepared as described in the Electrophysiology section and incubated either with DMSO or 1 µM Rapamycin in the slice incubation chamber for 2 hours. Slices were then transferred to 4% (w/v) PFA, pH7.4 and stored at 4°C overnight. The comparable hippocampi were isolated away from the slices and then embedded in 4% (w/v) agarose dissolved in PBS. The sections were then resliced using a T1000 S Vibrating blade microtome (Leica) to yield 6 - 8 40 µm sections per slice.

2.4.5 Preparation of gelatinized slides

Microscope slides were gelatinized to aid with section mounting. Two days prior to mounting, Slides were immersed in 60°C Gelatine solution for 30s and then a clip affixed to the label portion of the slide to allow them to stand on their side, allowing excess gelatine drainage. Slides were allowed to dry for two days at room temperature before use.

2.4.6 Immunohistochemistry

All incubation and washing steps were conducted on a Standard Model 1000 shaker (VWR) at 120 rpm.

After thawing, one series of sections were transferred to a 12-well plate (1 well per mouse), washed three times 0.125 M Phosphate buffer (PB) for 10 min each, and then blocked and permeabilised in PB blocking buffer for 2 - 3 hours at

room temperature. Primary antibodies were dissolved in PB blocking buffer (see Table 11), 500 µl added to each well and incubated at 4°C for two days. Sections were washed three times with PB blocking buffer, 30 min each at room temperature. Secondary antibodies were dissolved in PB blocking buffer (see Table 12), 500 µl added to each well and incubated at 4°C overnight. Sections were washed three times with PB blocking buffer, 30 min each at room temperature and then once with 0.125 M PB for 30 min. Sections were then mounted in order in the same orientation on gelatinised slides, excess PB removed, and 20 µl VECTASHIELD Antifade Mounting Medium (Vector laboratories) added to each section. Coverslips were placed on top, sealed with nail varnish, and stored at 4°C.

2.5 Light Microscopy Methods

2.5.1 Principles of fluorescence microscopy and Epifluorescence

Fluorescence microscopy is a powerful technique to visualize cellular compartments, structural changes and molecules via fluorophore tagging. Fluorophores are molecules that have a high absorbance of a particular wavelength, which re-emit light at a longer wavelength. With careful selection of fluorophores with consideration to absorption-emission spectra, multiple fluorophores can be used in one sample to target multiple components.

Generally, a bright light source is passed through an excitation filter to filter the desired wavelength or a single wavelength laser is used (Some other sources may also be used). This light is reflected off a dichroic mirror and through an objective to illuminate the sample. The target fluorophore will absorb light and enter an excited energy state, and slowly returns to it ground state via vibrational energy relaxation. During this relaxation a photon of longer wavelength is emitted, can pass through the dichroic mirror and a secondary emission filter finally encountering a detector whereby it is recorded. This whole sample illumination method is known as Epifluorescence or Widefield microscopy. Due to its brightness and speed this method is used for live cell imaging.

Further adaptations can improve resolution, sample penetrance and remove background at the cost of sample illumination and speed. All microscopes were mounted on air tables to negate external vibrations.

2.5.2 Principles of confocal microscopy

Confocal microscopy achieves a relatively high image resolution by exciting a much smaller portion of the sample and blocking out of focus background light. Excitation light from a laser is passed through a confocal pinhole, focussing light onto the dichroic mirror at a specific angle which when reflected onto the sample, focuses light onto a much narrower area. The re-emitted signal passes through the dichroic mirror, it encounters a secondary confocal pinhole which will focus light from the sample onto the detector while out of focus light is scattered (Jonkman & Brown, 2015). Two methods of confocal microscopy were used in the study: Laser scanning and spinning disk microscopy.

2.5.3 Laser scanning confocal microscopy

A laser scanning microscope (LSM) is a high-resolution confocal microscope that relies on a single scanning beam. This uses the traditional confocal setup described above to have a highly focussed excitation beam illuminating a single point of the sample. This point is moved by movable mirrors known as galvanometers that shift the beam in the x and y plane. Theses mirrors are rotated so the beam can scan the entire sample within the field of view. Meanwhile a variable pinhole can be adjusted to prioritise either z-resolution or sample illumination. This type of microscopy provides high resolution imaging in x, y, and z planes at the expense of speed as accurate scanning is slow. This has in part been mitigated by the innovations of resonant galvanometers which increase scanning speed, and highly sensitive Gallium arsenide phosphide (GaAsP) detectors, which have enabled low photon imaging which allows simultaneous imaging of multiple fluorophores. In this study the LSM was used for imaging of immunohistochemical samples. The LSM used in this study was an LSM780 (Zeiss) fitted with a 34-Channel QUASAR Detection Unit (Zeiss) and a Definite Focus system for z-focus assistance (Zeiss). The controlling software was ZEISS Zen (Zeiss).

2.5.4 Spinning disc confocal microscopy

A spinning disk confocal microscope contains a large array of pinholes on Nipkow disks which can illuminate multiple points of a sample simultaneously. As the disk rotates light passes through different pinholes and is focussed onto other areas of the sample. This gives the spinning disk confocal the advantage of high speed of image acquisition, however the field of view is relatively small and out of focus light from multiple pinholes leads to poor z-resolution. This method of imaging was used for thin samples such as cultured neurons and was primarily used for speed and availability. The spinning disk microscope used in this study was an Axiovert 200 inverted microscope (Zeiss) fitted with an UltraView ERS spinning disk system (Perkin Elmer) and a C9100 EM-CCD camera (Hamamatsu). The software used was Volocity (Perkin Elmer).

2.5.5 Epifluorescent live-cell imaging of pHluorins

During synaptic exo- and endocytosis the internal membrane of synaptic vesicles encounters changing pH depending on the stage of synaptic cycling. Vesicles are acidified by vATPase to create a high proton gradient which drives loading of neurotransmitter anions. This leads readily releasable vesicles to be pH 5.5. Upon fusion with the active zone the vesicle lumen is exposed to the synaptic cleft which under physiological conditions is maintained at around pH 7.3 – 7.4, however small fluctuations occur during synaptic signalling (Chesler, 2003; Krishtal et al., 1987). After endocytosis, the internal endocytic membrane is shielded from the synaptic cleft and undergoes re-acidification to again facilitate neurotransmitter loading. This stage dependent pH change has been exploited via the development of a pH-sensitive GFP known as pHluorin (Miesenböck et al., 1998). GFP fluorescence relies principally on a tripeptide: Ser65, Thr66, and Gly67, known as SYG. In GFP, the backbone of SYG is cyclysed at the Ser65 carbonyl group and the Gly amino group, and oxidation of the C^{α}-C^{β} bond of Tyr66 results in a fluorescent residue of SYG (Heim et al., 1994). This tripeptide is at the centre of a tight beta-barrel which occludes solvents and prevents protonation of Thr66. However, in pHluorin several mutations make this barrel less staple and thus the Thr66 residues susceptible to protonation, leading to fluorophore quenching. It

has been shown that the pK_a of pHluorin is 7.1 and its dynamic range is 5.5 – 9.5 (Sankaranarayanan et al., 2000), making it a good monitor within the range of synaptic pH. Chimera proteins have been made, binding pHluorin to the luminal domains of various synaptic proteins, meaning they should be trafficked through exo-endocytosis.

Hippocampal cultures were transfected with pHluorin constructs as described by Calcium phosphate transfection of hippocampal neurons, and on DIV13 – DIV14 were transferred to an imaging chamber with parallel stimulation electrodes (Warner Instruments) with 37°C osmolarity adjusted Imaging buffer. Postsynaptic receptors were blocked to prevent spontaneous neuronal activity with 50 µM APV (Abcam) and 10 µM CNQX (Sigma). Imaging occurred in a temperature-controlled container affixed to a Nikon Eclipse Ti epifluorescence microscope with an automatic stage controlled by MicroManager ImageJ plugin to control acquisition framerate and exposure time, 200 watt mercury lamp (Prior Scientific) and a mNeo sCMOS camera (Andor). All pHluorin experiments were imaged at a framerate of 0.5 Hz, an exposure of 100 ms and pixel binning of a 2 x 2 frame. Where surface and total pHluorin level acquisition was required, an in-house built perfusion/aspiration system was used for buffer exchange.

2.5.6 Stereological imaging of CA1 region of the hippocampus

Stereology allows for three-dimensional information to be extracted from two dimensional profiles. In stereological imaging, 2D images are taken at known z-intervals, and it requires representative sampling and an element of random sampling to form an unbiased quantitative estimate of the geometry of a structure. To conduct stereological imaging of the CA1, sections were collected and processed as described in the Histology section and were imaged with the LSM780 as it provides accurate xyz resolution and coordinates.

To start, the border of the subiculum and the CA1 of a slice was placed at the border of the frame of the 40x oil objective (1024x1024 pixel image, 354.25x354.25 µm, pinhole set for 1 µm z-acquisition). A dice was rolled, with the result defining the start position of image acquisition (1-2 = 0 µm, 3-4 = 100 µm 5-

6 = 200 µm away from subiculum) introducing random sampling. Two images were acquired with a z-separation of 10 µm, this distance allows the possibility for a nucleus to be observed in both images. The field of view was repositioned 400 µm rostrally and a further z-stack taken. This was repeated until the border of CA1-CA2 was reached whereby no further images were acquired. The process was repeated across all sections to achieve representative sampling of the entire structure.

2.6 Image analysis

All image analysis and regions of interest (ROIs) selection was conducted using Fiji opensource software. All macros were developed in the ImageJ Macro language, full scripts are provided in appendix.

2.6.1 Analysis of pHluorin time-lapse images

Initially pHluorin recordings were passed through a quality control to assess the reliability of the culture. This was done by checking that at least 15 – 20 synaptic boutons responded to the electrical stimuli. As many ROIs as available up to a maximum of 50 were selected from responding boutons. The Fiji plugin Time Series Analyser Version 3 was then run to record raw intensity values, which were saved as csv file for analysis in Microsoft excel.

It is occasionally possible for dead neurons to display synaptic release but they do not conduct endocytosis, these boutons were removed from analysis and a mean fluorescence was calculated from all remaining boutons (F). For analysis of vesicle exocytosis the average fluorescence of the boutons pre-stimulus was taken to obtain F0, and F was then divided by F0 to generate a graph showing fold change from baseline (F/F0), and the peak of the graph was taken to calculate relative exocytosis (Fmax). For comparing endocytic rates F0 was subtracted from F (ΔF). By dividing ΔF by peak fluorescence a normalised graph is generated (ΔF/F) where mean pre-stimulus baseline = 0 and peak fluorescence = 1. The endocytic time constant (τ) was calculated as the value of x where $y = 1/e$ (e= Euler's number).

For experiments demonstrating the differential expression of Synaptotagmin 1 a secondary normalisation was used as the average fluorescence

from an ammonium chloride pulse (FAmmonia) in the calculation of ΔF/F. For these experiments endocytic time constant (τ) was calculated as the value of x where $y=$ (Peak exocytic F)$(1/e)$.

2.6.2 Analysis of stereological images

Images for stereological analysis were acquired as described in the Stereological imaging section. Three 40 μm square ROIs were placed at equal intervals along the structure using the DAPI channel for localisation. The counting of nuclei was conducted across both z-planes, any nuclei present in both images were counted only once, this provides an estimate of overall cell density. Then within the same ROI, the number of cells with the desired marker were also counted. Note that where a staining is diverse (E.g. phosphorylation level of S6), the brightness of the image was adjusted to a level which would only show the top 10% intense pixels in the control group and the settings then applied to all images.

Each count was recorded and a mean was generated from the six counts per image, leading to an estimate of the number of cells within a 40x40x10 μm cube. This could then be converted into cells/mm^3.

2.6.3 Analysis of synapses via electron microscopy

Cells were stimulated and processed as described in the previous section. Embedding and imaging was conducted by Dr. Dmytro Puchkov. Images of both stimulated and non-stimulated synapses were obtained.

In non-stimulated neurons, the number of vesicles directly adjacent to the active zone were counted, and the length of the active zone measured to obtain an estimate of the readily releasable pool (vesicles/nM). For stimulated neurons the number of clathrin intermediates were normalised to the area of the bouton (vesicles/μm^2).

2.7 Biochemical Methods

2.7.1 Preparation of cortical neuron lysates

DIV7 cortical cultures were washed once with PBS and then 140 µl of ice-cold Cell lysis buffer was added to each plate. Cells were removed with a cell scraper and transferred to an 0.5 ml Eppendorf tube. The cells were lysed on ice for 20 min, with brief vortexing every 5 min. The samples were then centrifuged at 17,000 g in a Micro Star 17R Microcentrifuge (VWR) at 4°C for 10 min. The supernatant was transferred to a new Eppendorf, a sample taken for protein quantification, then SDS sample buffer was added and the samples were stored at -20°C.

2.7.2 Preparation of mouse brain lysates

Adult mouse brains were homogenised in 5 ml per gram of brain of Brain homogenisation buffer. The brain and buffer were placed in a tube and homogenised 20 times with a EUROSTAR power basic stirrer (IKA) at 900 rpm. The samples were placed on ice for 10 min and then centrifuged at 17,000 g in a Micro Star 17R Microcentrifuge (VWR) at 4°C for 10 min. The supernatant was transferred to a new Eppendorf and centrifugation repeated to remove any remnant debris. The supernatant was again transferred to a new Eppendorf, a sample taken for protein quantification, then SDS sample buffer was added and the samples were stored at -20°C.

2.7.3 Preparation of crude synaptic vesicles (LP2) from mouse brains

To obtain synaptic vesicles, subcellular fractionation was conducted. At each step, 500 – 1000 µl aliquots were taken from each supernatant and pellet. To start, 10 – 15 mouse brains were placed in 50 ml ice cold Buffered sucrose solution and homogenised with 12 strokes of the EUROSTAR power basic stirrer at 900 rpm (Yielding H). A further 50 ml of buffered sucrose was added, and the mix was centrifuged in a Thermo Scientific Heraeus Megafuge 16R (Thermo Scientific) at 800 g, 4°C for 10 min (Yielding P1 and S1). The supernatant was then recentrifuged in a SS-34 fixed angle rotor (Thermo Scientific) using a Sorvall Evolution RC Superspeed Centrifuge (Thermo Scientific) at 9,200 g, 4°C for 15 min (Yielding P2

and S2). The pellet (P2) is resuspended in 120 ml buffered sucrose solution and centrifuged in the same rotor and superspeed centrifuge at 10,200 g, 4°C for 15 min (Yielding P2' and S2'). P2' is resuspended in 13 ml of Buffered sucrose solution, 117 ml of ice-cold water added and homogenised with the power basic stirrer with five strokes at 2000 rpm (yielding L). The lysate was transferred into a beaker containing 1 ml 1M HEPES pH 7.4, 1 ml PMSF and 300 µl PIC and kept on ice for 30 min. The mix is then centrifuged at 25,000 g, 4°C for 20 min (Yielding LP1 and LS1). Centrifugation of LS1 was repeated to remove any contaminants. LS1 was transferred into Beckman hard plastic tubes, filled to top with buffered sucrose, with care taken to ensure complete rotor balance, and then centrifuged in a Type 45 Ti fixed-angle titanium rotor (Beckman Coulter) with a Optima MAX-XP ultracentrifuge (Beckman Coulter), 165000g, 4°C for 2 hours (Yielding LS2 and LP2). Finally LP2 was resuspended in Brain homogenization buffer, homogenised with 10 strokes of the EUROSTAR power basic stirrer at 1200 rpm, passed through a 27 gauge needle 5x and then stored in SDS sample buffer.

2.7.4 Protein quantification via Bradford assay

By analysing the absorbance shift of Coomassie G-250 (Thermo Fisher) within Bradford's Reagent (Prepared 2x stock by Uwe Fink) in the presence of proteins it is possible to determine the protein concentration. Upon binding to proteins, Coomassie G-250's absorbance changes from 465 to 595 nm. A calibration curve of 595 nm absorbance in presence of various protein concentrations was prepared by Uwe Fink using a BioPhotometer Plus (Eppendorf). Samples from cell lysates were diluted 1:200 – 1:1000 in 1x Bradford's Reagent and brain lysates at 1:1000 – 1:10,000, to a final volume of 1 ml. As a control, 1 µl of either cell lysis buffer or brain homogenisation buffer was added to 1 ml 1x Bradford's Reagent.

2.7.5 SDS polyacrylamide gel electrophoresis (SDS-PAGE)

To separate proteins by molecular weight, sodium dodecyl sulfate–polyacrylamide gel electrophoresis was conducted. SDS is a surfactant with an

overall negative charge, which binds to proteins via hydrophobic interactions, interfering with secondary structure and thus denaturing the protein. This applies a broadly uniform negative charge to a protein regardless of protein length, meaning that the primary factor effecting mobility under electrophoresis is molecular weight of the protein.

Gels were cast and run using the Mini-Protean Tetra Cell System (Bio-Rad), casting a 1 mm thick gel, with a 7 cm separating gel and a 3 cm stacking gel. Separating gels were made with 8 – 14 % ROTIPHORESE Gel 30 (37.5:1) Acrylamide/Methylenebisacrylamide mix (Roth), depending on preference of protein weight seperation. A constant current of 10 - 20 mA was applied per gel.

Table 16: SDS polyacrylamide gel composition

Component	Separation			Stacking
	8%	12%	14%	3%
4x SDS stacking gel buffer				0.625 ml
4x SDS separating gel buffer	1.875 ml	1.875 ml	1.875 ml	
MilliQ Water	3.5 ml	2.5 ml	2 ml	1.625 ml
ROTIPHORESE	2 ml	3 ml	3.5 ml	0.33 ml
10 % (w/v) Ammonium persulfate	75 µl	75 µl	75 µl	37.5 µl
TEMED	7.5 µl	7.5 µl	7.5 µl	3.75 µl

2.7.6 Immunoblotting

To detect proteins, immunoblotting (known also as western blotting) was conducted. Wet transfer was performed in a Mini Trans-Blot tank (Biorad) to migrate proteins from the polyacrylamide gel to onto a nitrocellulose membrane

(GE Healthcare) via electroblotting. The gel and membrane were surrounded by three blotting papers and a sponge on each side. The whole stack was equilibrated in Wet transfer buffer while being assembled, with care taken to remove any bubbles during the process. Transfer was conducted at 110 V, 90 min at 4°C or overnight with 30 V at 4°C.

Afterwards, the membrane was stained with Ponceau solution for 15 min at room temperature, followed by 3x 5 min washes in Ponceau destaining solution to assess the quality of the transfer and to cut the membrane. Ponceau was then completely removed with 3x 10 min washes with TBS followed by a 1 hour incubation with Odyssey Blocking Buffer in TBS (Licor). Primary antibodies were diluted as described in Table 11, diluted in TBS with 50% (v/v) Odyssey Blocking Buffer, and incubated with the membrane overnight at 4°C. The membranes were then washed 3x 10min at room temperature in TBS with 0.05 % (v/v) Tween-20. Secondary antibodies were diluted as described in Table 12, diluted in TBS with 50% (v/v) Odyssey Blocking Buffer and incubated with the membranes for 1 hour at room temperature. The membranes were washed 3x 10 min in TBS with 0.05 % (v/v) Tween-20 and then imaged using an Odyssey Fc Dual-Mode Imaging System (Licor).

2.8 Electrophysiology

2.8.1 Preparation of acute sagittal slices for hippocampal field recordings

Before dissection began 500 ml of Dissection ACSF (dACSF) and 1 l of ACSF were prepared. Half of the dACSF was placed at -80°C, 20 - 30 min prior to dissection to have a slush ice constancy to aid slice survival. A BSC-PC slice incubation chamber (Warner Instruments) was filled with ACSF and constantly bubbled with a fine flow of 95% O_2 and 5% CO_2 gas mix. Liquid dACSF was added to the chamber attached to a VT 1200S vibroslicer (Leica) and cooled down to +4°C using a FL300 freezer (Julabo).

Mice were sacrificed by cervical dislocation followed by decapitation, skin removed from the head and incisions made down each side of the skull and down

the midline, and the nasal bone severed between the eyes. The skull was removed to expose the brain which is carefully removed and submerged fully in dACSF slush ice. From sacrifice to submersion must not take longer than 60 s to aid slice survival.

The hemispheres were separated down the midline and affixed to a cutting disk by placing the central face of the hemisphere downwards on to fast setting glue. This was transferred to the vibroslicer, 350 µm slices acquired and transferred to the slice incubation chamber. Slices were rested for at least 1.5 hours before beginning recordings. In the case of 1 µM Rapamycin treatment, slices were split into two chambers, one with Rapamycin and one with DMSO containing ACSF. Slices were transferred to a RC-27L recording chamber (Warner Instruments) and perfused with a constant flow (3 - 5 ml/min) of oxygenated ACSF. Slices were fixed with the slice anchor for RC-27L chamber in place using a BX61WI upright microscope (Olympus) with care not to apply pressure to the recording area. Glass electrodes were prepared using a P-1000 Micropipette Puller (Sutter Instrument), with resistances of 1 – 1.5 MΩ and 1.5 – 2.5 MΩ for the stimulating and recording electrode respectively and filled with ACSF. Recordings were conducted using an EPC9 amplifier (HEKA Electronics) under current clamp, at a sampling rate of 10 kHz, low pass filtered at 3 kHz using Patchmaster software (HEKA Electronics) for stimulus control and analysis. The stimulating electrode was placed within the CA3 Schaffer collateral axons, and the recording electrode either within the CA1 *Stratum pyramidale* (conducted by Dr. Gaga Kochlamazashvili) or the CA1 *Stratum radiatum*. Then, 50 µA test pulses were used to establish whether optimal electrode positioning had been achieved. Then 10 min recordings were taken with a single 50 µA pulse every 20 s to establish slice stability. All recordings in this study measure local field potentials: Excitatory postsynaptic potentials (fEPSPs) or population spikes (PSs).

2.8.2 Input-output recordings

Once optimal electrode depth is reached and a stable baseline maintained, input-output measurements were recorded. This type of recording looks at the relative response within the recording area to a given intensity of fibre volley (FV)

from the stimulated area. This is done by stimulating the Schaffer collaterals with an increasing current from 0 – 200 μA, increasing in 20 μA increments until maximal response is reached. Each stimulus intensity was repeated 3 times with a 20s interval to create an average sweep. The point at which 33% and 50% of the maximum amplitude of response is achieved is noted for later stimulus paradigms. Curves are then calculated as amplitude fEPSP/amplitude FV.

2.8.3 Paired pulse recordings

By applying 2 pulses in rapid succession and varying the time between pulses, it is possible to elucidate further information of the recording area. All paired pulse recordings were represented as percentage amplitude of the second pulse compared to the first.

In *stratum radiatum* recordings, presynaptic facilitation was examined by varying the interpulse interval between 10 – 500 ms using a stimulus that elicits a response of 33% of the maximum (see above). The principle is that when pulses occur within a certain interval, Ca^{2+} is not fully cleared from the synapse, leading to a higher presynaptic calcium concentration upon the second pulse leading to higher vesicle fusion probability. This leads to increased neurotransmitter release, an increased chance of the postsynaptic action potential threshold being reached leading to a larger field response being observed (Castillo & Katz, 1953; Jianhua Xu et al., 2007). This method can be used as a broad estimate of release probability, as changes in response to the first pulse are detected in the facilitation of the second pulse at a given interval.

During recordings within *stratum pyramidale* stimuli were also given with interpulse intervals of 10 – 500 ms, however in this case to examine the contribution of feedback inhibition a supramaximal stimulus of 200 μA was applied (Koo et al., 2015). During stimulation of Schaffer collaterals, the axons are not only synapsing onto Pyramidal neurons, but also onto interneurons which then form perisomatic synapses onto Pyramidal neurons, this is known as feedforward inhibition. Secondly pyramidal neurons themselves synapse onto inhibitory cells of the *stratum oriens* which synapse back onto the soma and basal dendrites of the

Pyramidal neurons (Maccaferri, 2005), this is known as feedback inhibition. Feedback circuits lead to GABAergic inhibition at the *stratum pyramidale* which reduces the chance of action potential propagation of the second pulse if it occurs too soon after the first (Bartley & Dobrunz, 2015; Freund, 2003). This presents itself as a reduced PS in the second pulse.

2.8.4 Activity-dependent disinhibition

To assess the possibility of epileptiform activity, *stratum pyramidale* recordings were subjected to a 1 Hz stimulus for 60 s (Koo et al., 2015). This results in a short-term hyperexcitability in the CA1, via a temporary increase in glutamatergic signalling (B. Davies et al., 2001) and a complementary decrease in feed forward and feedback inhibition (Thompson & Gahwiler, 1989). Traces are represented as percentage increase of area under the curve of response to stimuli "n" compared to the first stimulus, and the number of slices exhibiting polyspiking activity was also recorded.

2.8.5 Long-term potentiation induction via theta-burst stimulation

Long-term potentiation (LTP) is a prolonged strengthening of synaptic transmission induced by certain stimulus paradigms (Bliss & Gardner-Medwin, 1973; Lømo, 2003). One highly effective stimulus paradigm is so called theta-burst stimulation (TBS), consisting of repetitive high frequency bursts of pulses which resemble physiological LTP inducing signals (Larson et al., 1986); with the optimal stimulus train thought to be 4 pulse 100 Hz bursts repeated at a rate of 5 Hz (Heckly & Dimmick, 1978). TBS induces LTP in a multistep manner, with bursts happening during time points where feedforward inhibition is undergoing recovery (C. H. Davies et al., 1990) and thus exerting maximum excitation on the postsynaptic neuron which is thought to lead to NMDA receptor currents which lead to LTP formation (Larson & Lynch, 1988). In field recordings LTP is seen as an increased amplitude of response to a given stimuli. In this study, in *stratum radiatum* recordings a 50% maximum stimulus was given every 20 s for 10 min as a baseline. Then TBS consisting of 8 bursts of 4 pulses at 100 Hz, repeated at a rate of 5 Hz, was applied 5 times at 20 s intervals. Finally, the same 50% maximum stimulus as before was applied every 20 s for 1 hour to record LTP.

2.9 Behavioural Studies

All mouse studies were conducted in a quiet room with normal room lighting, experiments were performed between 1 - 6 pm with sex matched littermates. The order of mouse genotype recorded was alternated to ensure time of experiment was not a factor. New cages were used, and behaviour equipment cleaned between uses to prevent smell being a factor effecting experiments. An IN-8015 HD infrared camera (Instar) was used to record experiments for later analysis. For seizure induction experiments, a second researcher (Prof. Dr. Tanja Maritzen) was always present to aid with drug administration, help with scoring the phenotypes and to ensure severity limit was not exceeded.

2.9.1 Home cage observation

Initially, all mice were observed for 10 min recordings of their movement in the home cage to detect any aberrant behaviour such as compulsive jumping or seizures. In no genotype was an obvious phenotype observed.

2.9.2 Elevated plus maze

As a measure of anxiety, mice were placed in the elevated plus maze (Ugo Basile). The mice were placed facing the corner of a closed arm and allowed to freely explore for 5 mins of observation. The number of times and overall time exploring the open arms was scored.

2.9.3 Seizure induction and scoring

To test for genotype specific seizure susceptibility, several protocols were used. Experiments involving Kainic acid and Pentylenetetrazol (PTZ) were conducted at the FMP, Berlin and were approved by the Berlin LAGeSo (see mouse strains). Experiments involving Pilocarpine were conducted in collaboration by the group of Prof. Dr. Emilio Hirsch, UNITO, Turin and were approved by the Italian governing body.

Drugs were dissolved in saline solution 1 hour before use as described in Table 8. The dose chosen was designed to elicit seizures in 50% of control animals; 15 mg/kg for Kainic acid (Bateup et al., 2013; Umpierre et al., 2016) and 50 mg/kg

for PTZ (Hentschke et al., 2006), which were injected intraperitoneally. Mice were then rapidly transferred to an empty home cage and behaviour was observed for up to 2 hours or until the first tonic-clonic seizure occurred. Mice were then sacrificed via cervical dislocation and a tail biopsy taken to clarify genotype.

3 Results

Though as previously described PI3KC2α and PI3KC2β have been shown to be present in brain homogenates, the location of the kinases within the neuron is still unknown. Current antibodies do not work in immunocytochemistry, so instead we conducted subcellular fractionation to detect a potential synaptic enrichment of the Class II PI3Ks.

Indeed, we found an enrichment of both PI3KC2α and PI3KC2β within synaptosomes (fraction P2, P2′) and within the crude synaptic vesicle fraction (LP2) (Figure 8), which opens the possibility of a role of these kinases in synaptic maintenance. Knowing their respective roles in CME and mTORC1 signalling, we conducted two projects, the first focussing on PI3KC2α's effect on vesicle cycling, the second on PI3KC2β/mTORC1 synaptic maintenance and neuronal control.

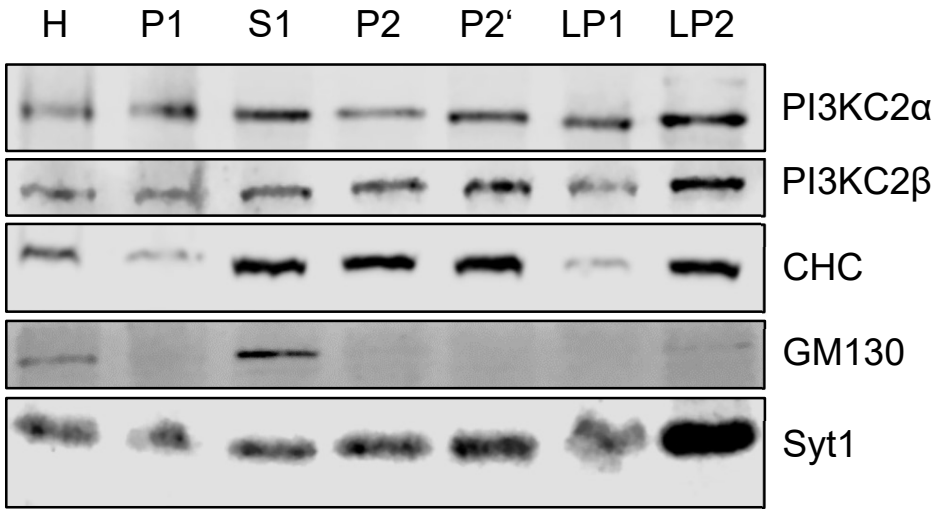

Figure 8: Enrichment of Class II PI3Ks at synaptic membranes. Fractionation from whole wildtype mouse brains (40 µg protein per lane; n=3 independent experiments). Both PI3KC2α and PI3KC2β are enriched within synaptosomes (P2, P2') and furthermore within small synaptic compartments (LP2), compared to homogenate (H) and nuclear membranes (P1). PI3KC2α also appears to have some enrichment within smaller somal membranes (S1) Control for soma compartment (GM130). Positive control for synaptic membranes (Syt1). Positive control for Clathrin coated vesicles (CHC).

3.1 PI3KC2α and Synaptic Endocytosis

3.1.1 Effective deletion of PI3KC2α in primary hippocampal neurons and in mouse forebrain

As constitutive knockout of PI3KC2α is embryonically lethal in mice (Yoshioka et al., 2012), and unpublished work kindly provided by Prof. Dr. Emilio Hirsch (Molecular Biotechnology Centre, Turin, Italy) suggests that deletion in adult mice is also lethal in a manner independent of brain function, it was necessary to create conditional mouse lines to study neuronal roles of PI3KC2α. A previously generated "floxed" PI3KC2α (*Pi3KC2α*$^{Fl/Fl}$, (Franco et al., 2014)) was kindly provided to us by Prof. Dr. Emilio Hirsch. These mice have loxP insertions flanking exon 2 of PI3KC2α. The loxP sites are recognised by Cre-recombinase, which excises exon 2 from the genome resulting in termination of gene transcription. We created two mouse lines to either conditionally knockout PI3KC2α in the forebrain during neuronal differentiation (*Pi3KC2αFl/Fl-EMX)* or globally upon tamoxifen administration (*Pi3KC2αFl/Fl x Cre-ERTM)*.

For tamoxifen inducible Cre recombination, *Pi3KC2α*$^{Fl/Fl}$ were crossed with *Cre-ER*^{TM} and mice from the 1st and 2nd generation were re-crossed until only offspring with homozygous floxed *Pi3KC2α* were present and Cre was only present in one parent (Figure 9A). Offspring with the Cre allele express a chimera protein consisting of Cre recombinase and a modified ligand-binding domain of estrogen receptor with high tamoxifen affinity, which under steady state is sequestered in the cytosol. Only upon binding to the estrogen receptor antagonist tamoxifen, the nuclear location sequence (NLS) is exposed, and trafficking into the nucleus occurs (Figure 9B). This allowed for Cre recombination to be conducted in a time dependent manner within primary hippocampal cultures. Low dose tamoxifen treatment of 0.25 μM was shown to be sufficient for complete loss of PI3KC2α in as little as 5 days (Figure 9C & D, performed by Dr. Natalie Kaempf).

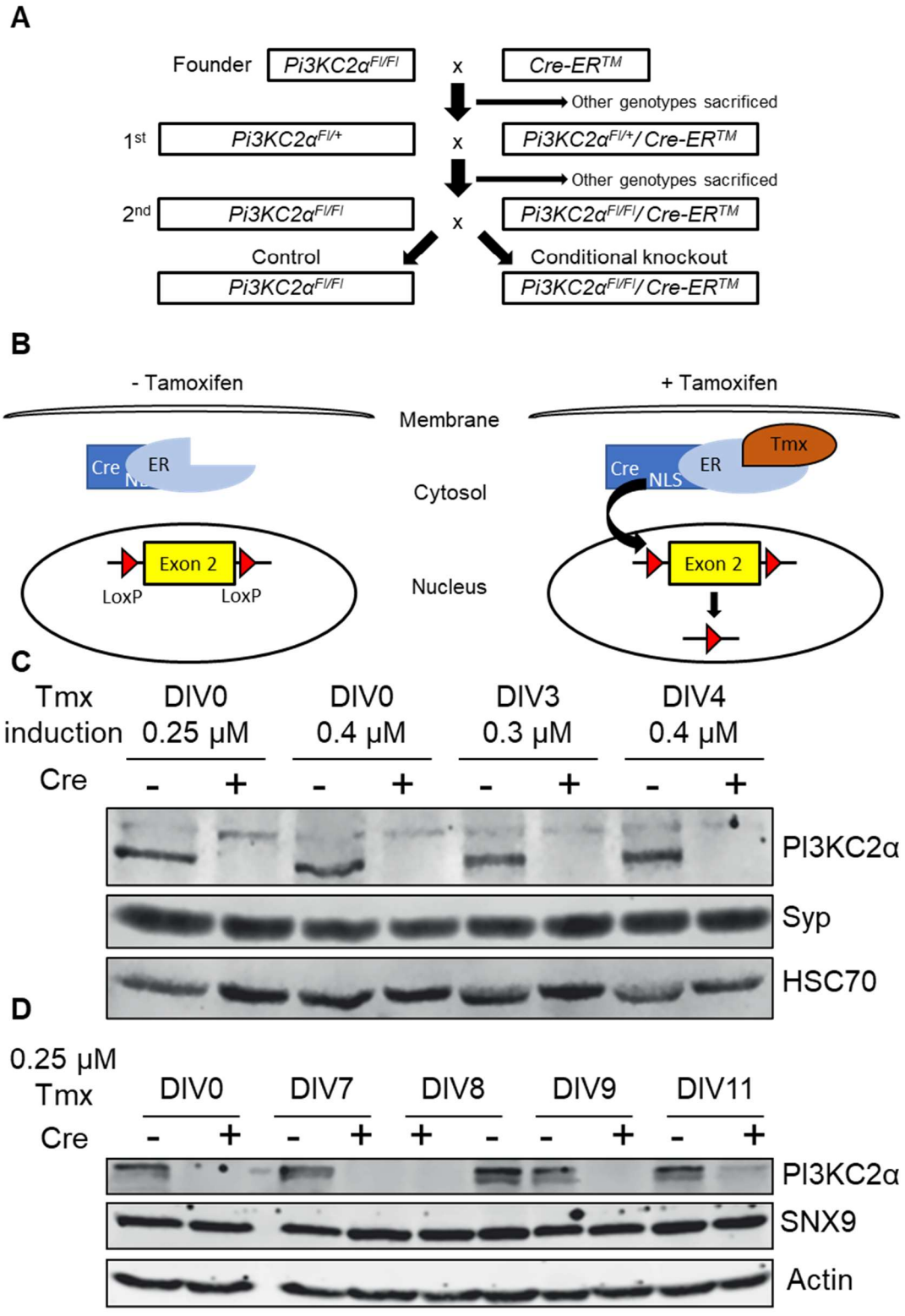

Figure 9: Tamoxifen mediated loss of PI3KC2α. **(A)** Breeding scheme for efficient generation of Cre positive and negative mice in a single breeding. **(B)** Visualisation of Tamoxifen inducible Cre. Tamoxifen binding to Estrogen receptor-Cre results in conformational change in chimera protein, exposing the NLS, leading to nuclear translocation which allows recombination. **(C & D)** Low

concentration Tamoxifen induction is sufficient for complete deletion of PI3KC2α in cultured cortical neurons. 0.25 μM incubation when applied as late as DIV9 leads to efficient knockout of PI3KC2α as detected via western blot in lysates at DIV14 (30 μg protein per lane n=3 independent experiments, conducted by Dr. Natalie Kaempf).

For forebrain specific deletion, *Pi3KC2α*$^{Fl/Fl}$ were crossed with an *Emx1-Cre* line, which expresses Cre recombinase from the Emx1 locus (Iwasato et al., 2000). Emx1 is expressed by neural stem cells of the developing hippocampus and cortex. Mice heterozygous for floxed *Pi3KC2α* were bred together, with one parent heterozygous for *Emx1-Cre* so WT, HET and KO offspring were possible within a single breeding (Figure 10A). Mice were born at mendelian ratios (Figure 10B) and passed a general health screen (Not shown). During postnatal development to adulthood all genotype weights were comparable (Figure 10C). Adult mice were sacrificed and loss of PI3KC2α was confirmed in Hippocampal and Cortical lysates (Figure 10D).

Creation of these two lines allowed for assessment of acute PI3KC2α loss *in vitro* and for prolonged loss *in vivo*.

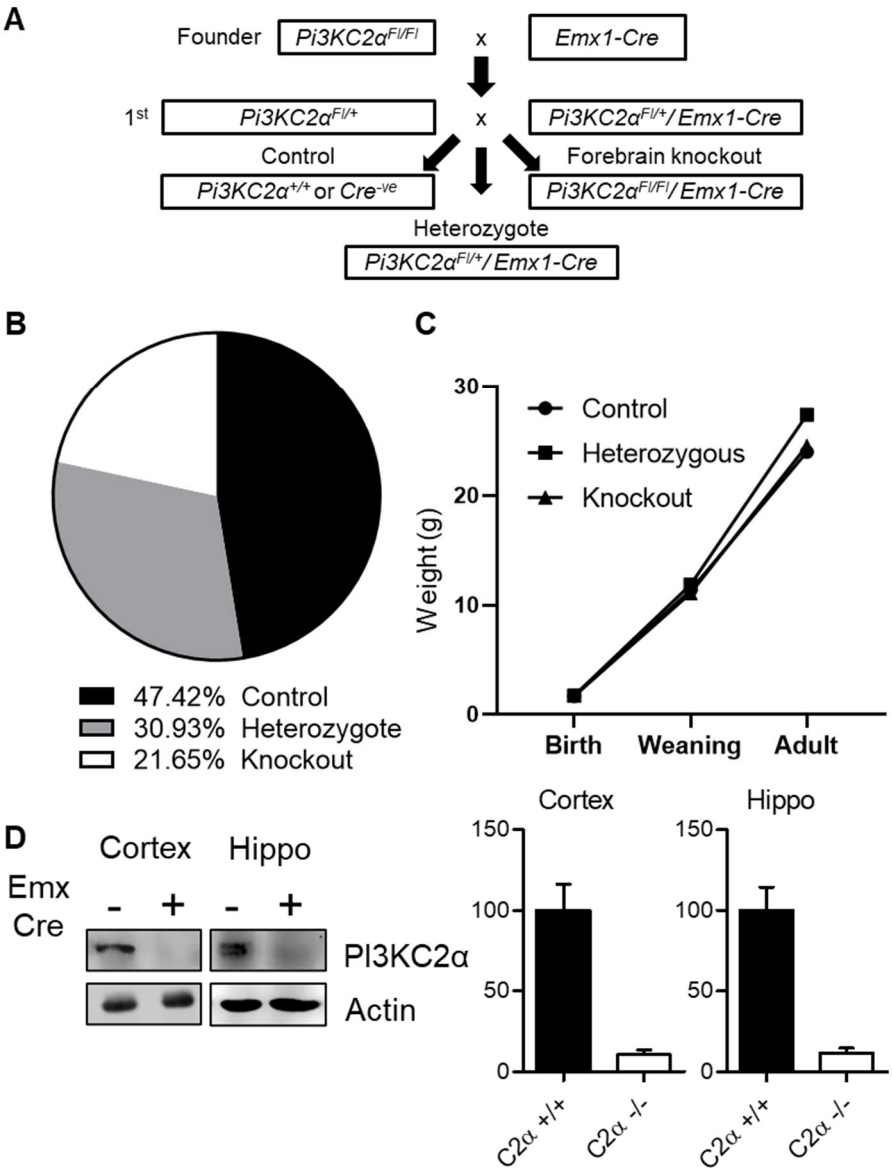

Figure 10: Forebrain loss of PI3KC2α. **(A)** Breeding scheme for efficient generation of Cre positive and negative mice in a single breeding. **(B)** Genotype ratios of mice born are within expected mendelian ratios (N=97 mice) **(C)** Mice of all genotypes show no significant change in weight to adulthood (One-way ANOVA N=25 mice). **(D)** Cortex and hippocampus lysates of 8 week old mice show efficient deletion of PI3KC2α (n=6 mice).

3.1.2 Deletion of PI3KC2α in forebrain does not affect behaviour or synaptic transmission

Impaired endocytosis at the synapse has been implicated in several diseases previously, including epilepsy, Parkinson's disease and neurodegeneration (Dhindsa et al., 2015; Kyung et al., 2018; Medeiros et al., 2018). To assess the

presence of such phenotypes in our *Pi3KC2α*$^{Fl/Fl}$ x Emx*1-Cre* mouse line, we conducted behavioural and electrophysiological assays. During home cage assessments no control or knockout mice showed any signs of epileptogenesis or movement disorders (not shown), nor were seizures evoked by tail suspension (Figure 11A) as seen in previous synaptic endocytosis studies (Koo et al., 2015). Anxiety was tested using the elevated plus maze behavioural test, no difference was detected in the number of entries to the open arms nor the time spent on open arms (Figure 11B). Field electrophysiological recordings in the *stratum radiatum* provided by Dr. Gaga Kochlamazashvili showed no differences in Input-Output measurements, or in paired pulse ratio, suggesting broadly normal synaptic signalling withing the CA3-CA1, and no defects in LTP formation.

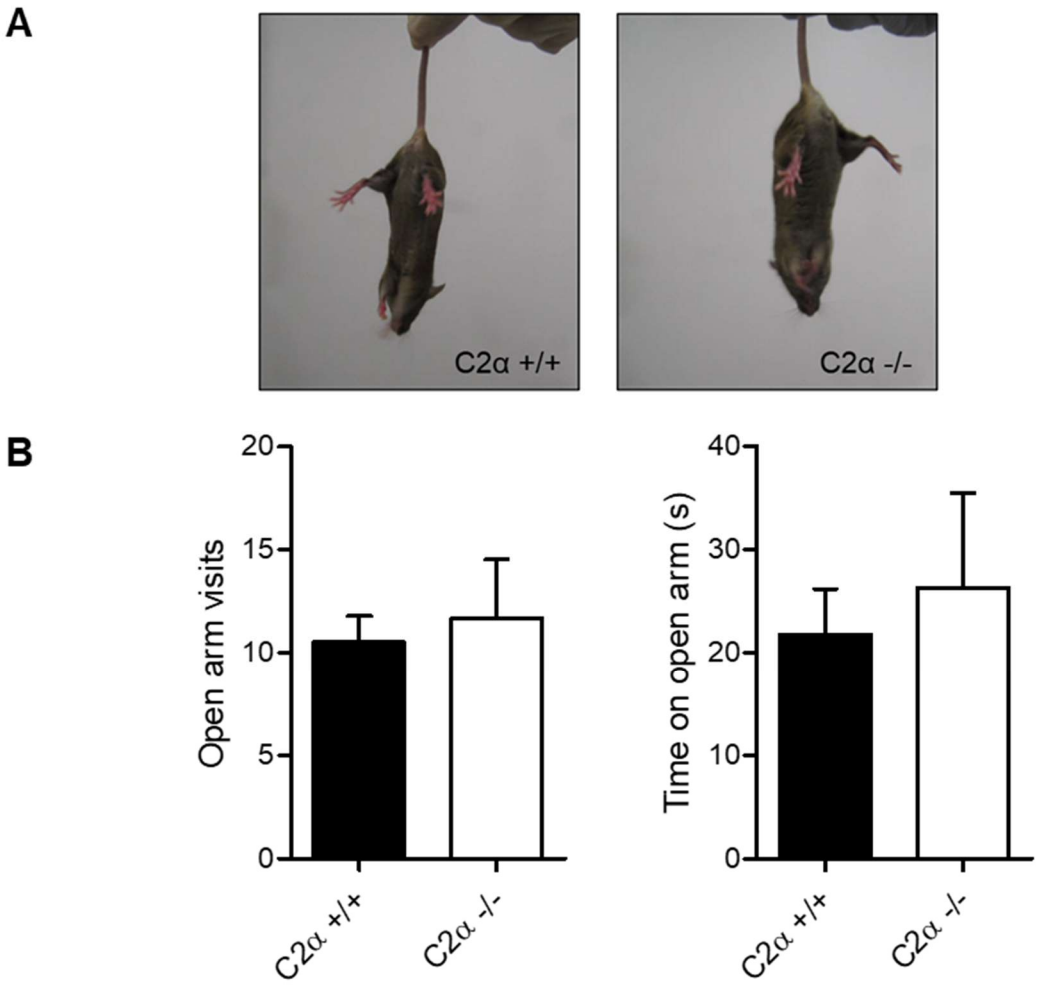

Figure 11: ***Pi3KC2α*** $^{Fl/Fl}$ **x Emx*1*-*Cre* have normal behaviour(A)** PI3KC2α knockout mice show normal response to tail suspension test, with no seizures observed or muscle limpness. **(B)** No change in elevated plus maze open arm entries or dwell time (Two-Tailed student´s t-Test, N=5 Control and 4 Knockout mice).

3.1.3 Increased Synaptotagmin 1 expression after PI3KC2α loss

To examine whether in neurons PI3KC2α played a similar role in endocytosis, as seen in other models (Posor et al., 2013), we overexpressed Syt1-pHluorin in primary hippocampal cultures of *Pi3KC2α*$^{Fl/Fl}$ x *Cre-ER*^{TM} and imaged at DIV14. Syt1 is present on synaptic vesicles and under physiological conditions copy number per synaptic vesicle is tightly regulated (Takamori et al., 2006). Upon electrical stimulation of 40 Hz for 5 s, no apparent change in endocytic speed upon PI3KC2α loss was observed (Figure 12A), but instead a significant increase in apparent exocytosis, due to an increased peak fluorescence post stimulus caused by more exposure of Syt1-pH to the neutral pH of the extracellular imaging buffer (Figure 12B). We then conducted the same paradigm with a different marker, Synaptophysin1-pHluorin (Syp-pH). Synaptophysins are transmembrane proteins with high abundance exclusively at synaptic vesicles (Takamori et al., 2006), and have been proposed to aid endocytic efficiency by clustering other vesicle proteins such as Synaptobrevin (Adams et al., 2015; Kwon & Chapman, 2011). But in the case of Syp-pH, no change in endocytic rate nor in apparent exocytosis were observed (Figure 13A & B).

This divergence of reporters suggested that the apparent increase of exocytosis could be an artifact concerning the overexpression of Syt1-pH. Either the loss of PI3KC2α leads to post-translational modifications leading to changes in vesicle release probability, or alternatively the same effect could be seen by changes in Syt1-pH copy number per vesicle resulting in higher fluorescence per vesicle released. To rule out the first possibility, Syt1-mCherry was co-expressed with Syp-pH and the same paradigm conducted. This did not cause an increase in exocytosis (Figure 13C), suggesting that the apparent exocytosis increase is an artefact specific to Syt1-pH, and Syt1 does not have altered release properties upon PI3KC2α deletion.

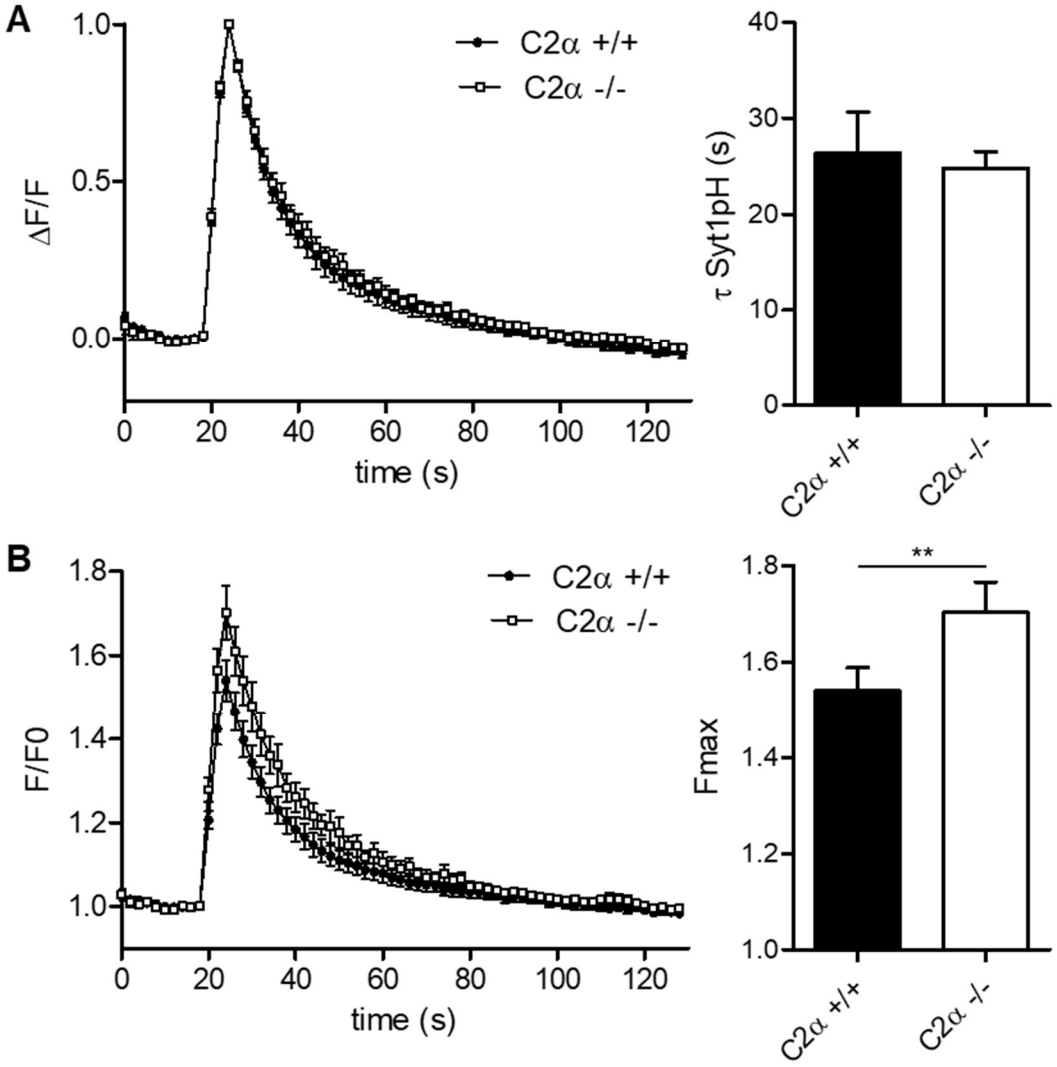

Figure 12: PI3KC2α loss leads to apparent increase in exocytosis of Synaptotagmin 1. (A) ΔF/F normalisation of SytlpH suggests no apparent endocytic defect in PI3KC2α knockout neurons (Paired t test P= 0.7235 n=5 paired experiments). **(B)** Instead, F/F0 normalisation reveals a strong increase in apparent SytlpH exocytosis (Paired t test P= 0.0079 n=5 paired experiments).

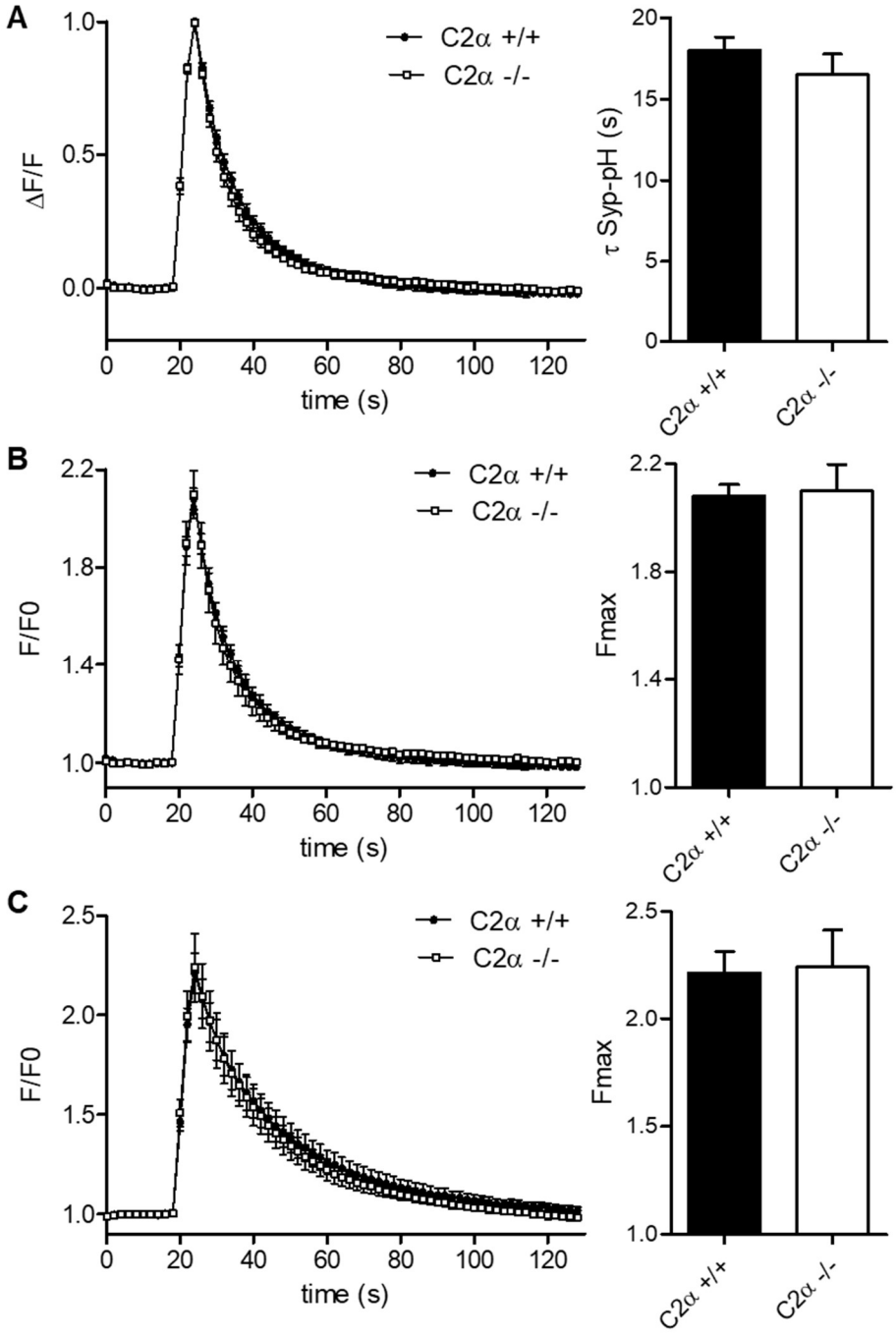

Figure 13: PI3KC2α loss does not affect Synaptophysin 1 exo-endocytosis. **(A)** ΔF/F normalisation of SypIpH suggests no endocytic defect in PI3KC2α knockout neurons (Paired t test P=0.3910 n=4 paired experiments). **(B)** F/F0 normalisation suggests no increase in SypIpH exocytosis (Paired t test P=0.8746 n=4 paired experiments). **(C)** F/F0 normalisation of PI3KC2α knockout neurons overexpressing Syt1-mCherry and SypIpH does not show increased exocytosis (Paired t test P= 0.8611 n=5 paired experiments).

One explanation for this apparent increase of exocytosis would be if changes in the abundance of Syt1 were to occur. Syt1 is trafficked to synaptic vesicles with high specificity (Mutch et al., 2011). In a context of an overabundance of Syt1-pHluorin upon PI3KC2α deletion, this could lead to a higher copy number per vesicle, which upon membrane fusion would lead to an increased fluorescence, thus to an apparent increase in exocytosis. To address this, we conducted an ammonium chloride (NH_4Cl) pulse to alkalize intracellular membrane compartments, thereby revealing the total pHluorin quantity (Roos & Boron, 1981; Sankaranarayanan et al., 2000). This confirmed that the total quantity of Syt1-pHluorin was increased in PI3KC2α knockout neurons (Figure 14).

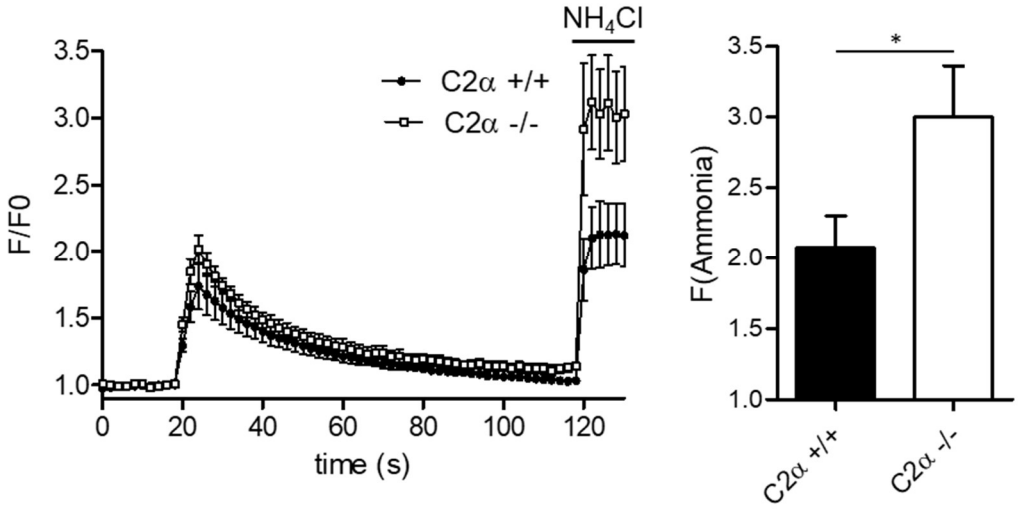

Figure 14: Ammonium chloride unquenching reveals PI3KC2α specific increase in Syt1pH. F/F0 normalisation of hippocampal neurons overexpressing Syt1pH and unquenched with NH_4Cl displays a large increase in total Syt1pH expression (Paired t test P= 0.0387 n=5 paired experiments).

However, the question still remained whether this is an artefact only seen in an overexpression system or if it were to be a physiological effect. When DIV14 hippocampal neurons from *Pi3KC2α*$^{Fl/Fl}$ x *Cre-ER*^{TM} mice were stained for Syt1, a substantial increase in Syt1 fluorescence was seen (Figure 15A & B). Furthermore, an increase in Syt1 levels was detected in *Pi3KC2α*$^{Fl/Fl}$ x Emx*1-Cre* whole brain lysates (Figure 15C & D). Together these data suggest an underlying role for PI3KC2α in controlling Syt1 levels in mouse neurons.

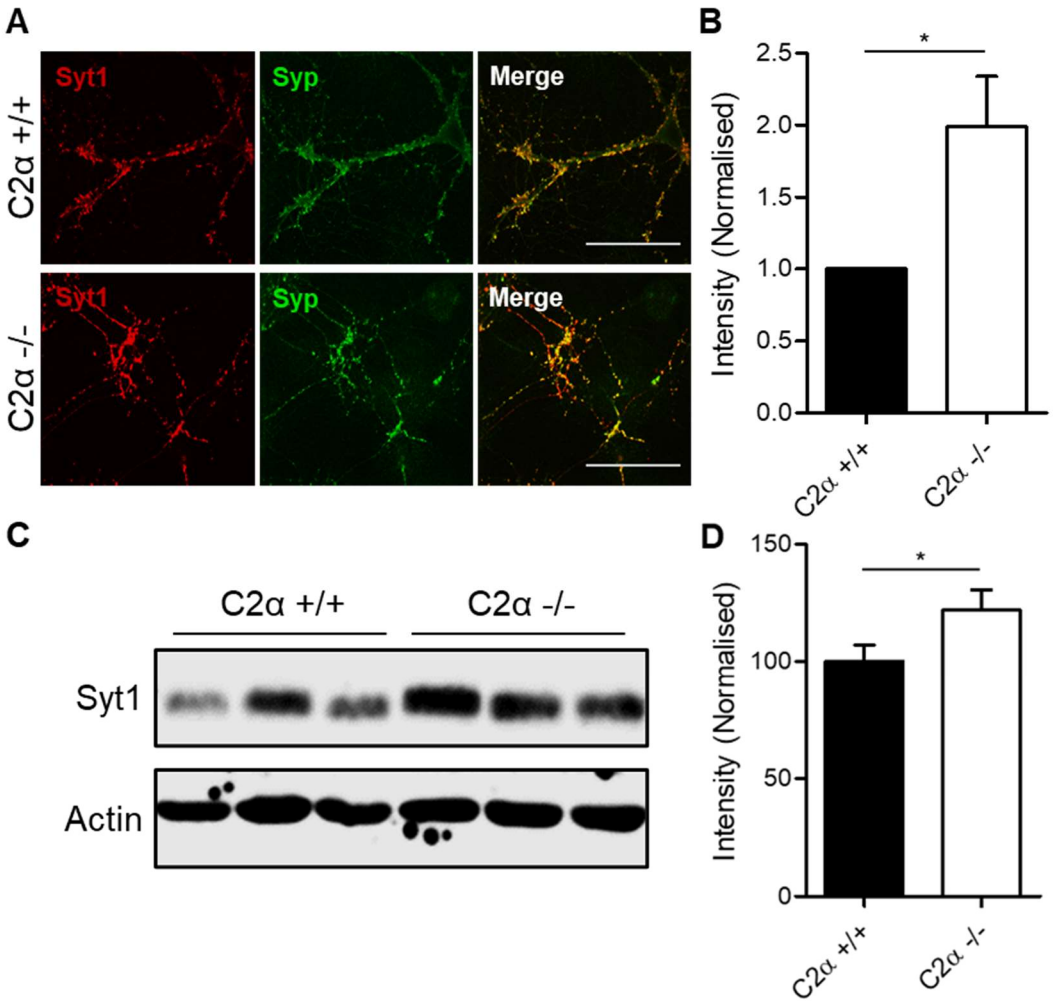

Figure 15: Increased endogenous Synaptotagmin 1 expression in PI3KC2α knockout mice. (A & B) Immunohistochemistry of Syt1 expression using Syp1 as a mask for synapses (scale bar, 50 µm). Levels of Syt1 are increased upon PI3KC2α loss (One sample t test P= 0.0463 n=4 independent experiments) **(C & D)** Cortex lysates from 8 week old mice show increased Syt1 via western blot (Paired t test P= 0.0251 n=6 paired experiments).

3.1.4 Slowed endocytosis in PI3KC2α knockout neurons

As the NH_4Cl pulse revealed an increase in Syt1-pH levels, it became possible to normalise the pHluorin curves to the dequenched expression levels (Figure 16A & B) and analyse the endocytic decay. Though the initial decay rate was relatively similar in both control and knockout neurons, a pool of Syt1-pH still can be seen on the surface of PI3KC2α knockout neurons after 30 s. PI3KC2α was shown in immortalised cells to have a key role in CME progression (Posor et al., 2013), however CME is thought to be mostly dispensable at central synapses (Kononenko et al., 2014; Soykan et al., 2017). This small pool of stranded Syt1-pH appears at the timescale of CME completion, and so may be a pool of stranded CCPs on the surface. To investigate further if there was a delay in CME, electron microscopy of steady state and stimulated neurons was conducted in collaboration with Dr. Dmytro Puchkov. DIV14 hippocampal neurons were either directly fixed or fixed 25 s after stimulation of 40 Hz, 5 s and then subjected to electron microscopy. In unstimulated neurons, no difference was seen in the number of docked vesicles at the active zone (Figure 16C & D). Interestingly in stimulated neurons an increase in the number of Clathrin intermediates was observed in knockout synapses (Figure 16E & F). These data together suggest that PI3KC2α may have a minor role in CME at the synapse together with a potential role in Syt1 maintenance.

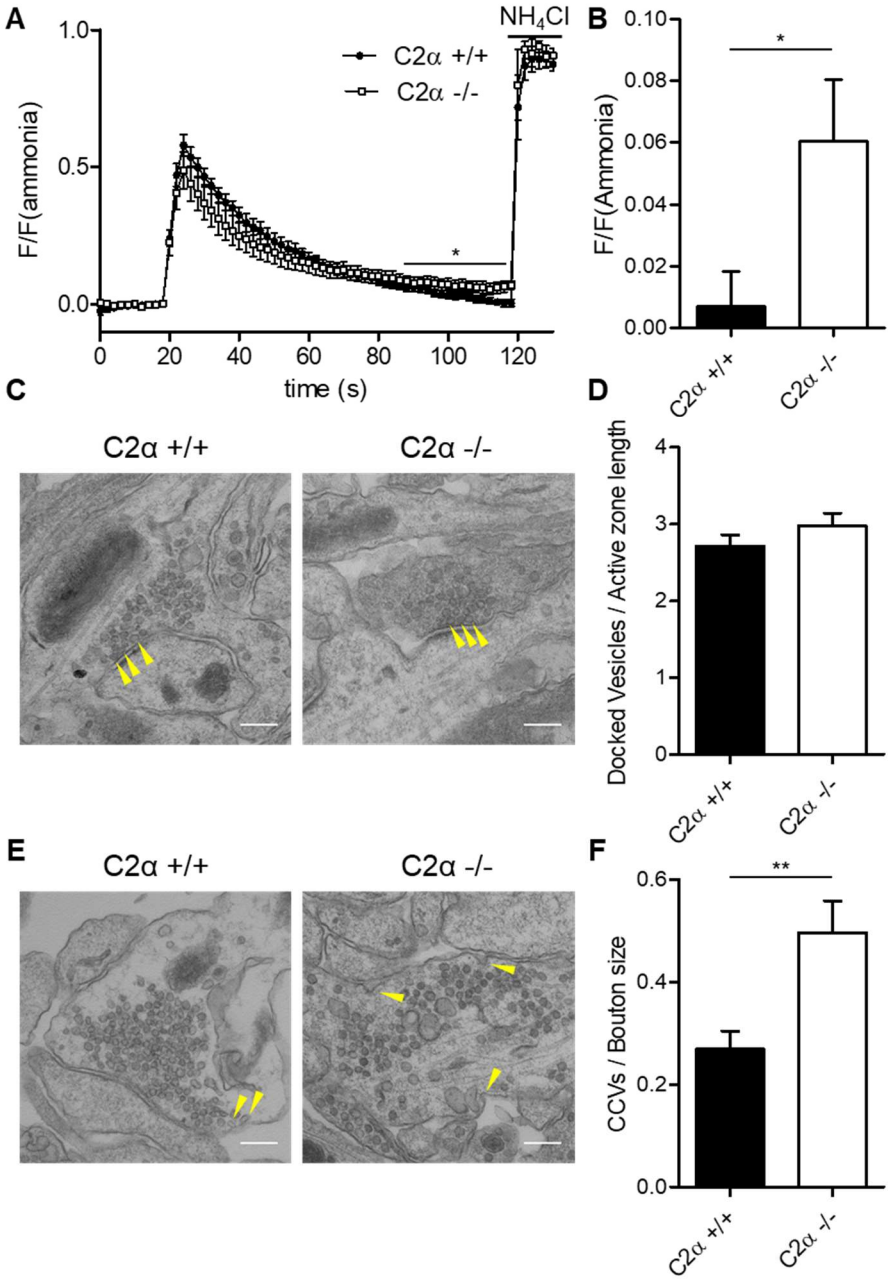

Figure 16: Surface stranding of CCPs in PI3KC2α knockout neurons. (A & B) F/F(Ammonia) normalised neurons show a stranding of surface SytIpH 40s after stimulation (Paired t test P= 0.0470 n=5 paired experiments). **(C & D)** Electron microscopy of unstimulated synapses (scale bar, 200 nm). No change in the number of docked vesicles observed (Unpaired t test P= 0.2595 n=50 synapses control, 32 synapses knockout). **(E & F)** Electron microscopy of stimulated synapses (scale bar, 200 nm). The number of CCPs was increased in synapses lacking PI3KC2α (Unpaired t test P= 0.0016 n=34 synapses control, 31 synapses knockout).

3.2 PI3KC2β Dysfunction Leads to Epileptogenesis

Recent work within our group demonstrated PI3KC2β as a novel mTORC1 repressor via its lipid kinase activity (Marat et al., 2017; Wallroth et al., 2019), which led to the possibility of its involvement in a new type of mTOR related epilepsy. Therefore through a collaboration between the groups of Dr. Tommaso Pippucci (Policlinico S.Orsola-Malpighi Bologna, Italy) and Prof. Dr. Emilio Hirsch (Molecular Biotechnology Centre, Turin, Italy) we decided to conduct an interdisciplinary study into whether PI3KC2β plays a role in epileptogenesis in humans and mice and if such a syndrome could be treated.

To establish whether any epilepsies were associated with PI3KC2β, a technique called collapsing statistical analysis was used to identify rare variants of common diseases (Sun et al., 2011). This collapses all unique small nucleotide polymorphisms (SNPs) within a gene together to identify candidate genes associated with a disease. This analysis was conducted on a patient dataset provided by the S.Orsola-Malpighi University Hospital, Bologna by Dr. Sara Baldassari. The analysis found that PI3KC2β had a significant genetic burden for non-acquired focal epilepsy, which was also confirmed in a separate large whole exome sequencing study, which placed it within the top 200 genes with burden of deleterious ultra-rare genetic variants (Y. C. A. Feng et al., 2019). Of note their analysis found that deleterious SNPs were within the lipid kinase domain and the membrane targeting C-terminal C2 domain, two domains that are thought to be crucial for mTORC1 suppression.

When these mutations were overexpressed in HEK 293T cells, the phosphorylation level of mTORC1's downstream target (Nojima et al., 2003) p70 S6-kinase (S6K) was greatly increased compared to WT PI3KC2β, and an ADP-Glo assay demonstrated that these mutants no longer produce $PI(3,4)P_2$, suggesting a loss of function of the protein.

To assess the neurological consequences of PI3KC2β loss of function, we decided to conduct a functional analysis of PI3KC2β null mice.

3.2.1 Characterisation of PI3KC2β null mouse brains

To further understand how PI3KC2β loss of function contributes to epileptogenesis, PI3KC2β null mice were obtained from Charles River Italy. These mice have a deletion of exons 3 – 5, leading to early termination of gene transcription (Harada et al., 2005). PI3KC2β KO mice are born at Mendelian ratios and have no known health issues (Harada et al., 2005). The mice were crossed with C57Bl/6J mice to generate heterozygotes for a breeding stock to obtain *Pi3kc2β* +/+ and *Pi3kc2β* -/- littermates for comparison.

Whole brain lysates were taken from 8-week old mice to assess whether there was a change in key synaptic proteins or mTORC1 pathway. No changes were observed between genotypes (Figure 17).

We next decided to characterise the Hippocampi of *Pi3kc2β* +/+ and *Pi3kc2β* -/- littermates, as the structure is highly associated with epilepsy in both humans and mice (Chatzikonstantinou, 2014; Riban et al., 2002). As epilepsy is often associated with changes in synapse density (Cossart et al., 2001; Perez, 1996), we first analysed the density of the CA1 excitatory synapses in the *stratum radiatum* and perisomatic inhibitory synapses in the *stratum pyramidale*. No changes were observed (Figure 18A-D). As astrogliosis has been linked to epileptogenesis in TSC models of mTORC1 epilepsies (Wong & Crino, 2012), we also examined glial coverage of the CA1 (Figure 18 E & F). However, again no change was observed in the coverage by GFAP-positive cells.

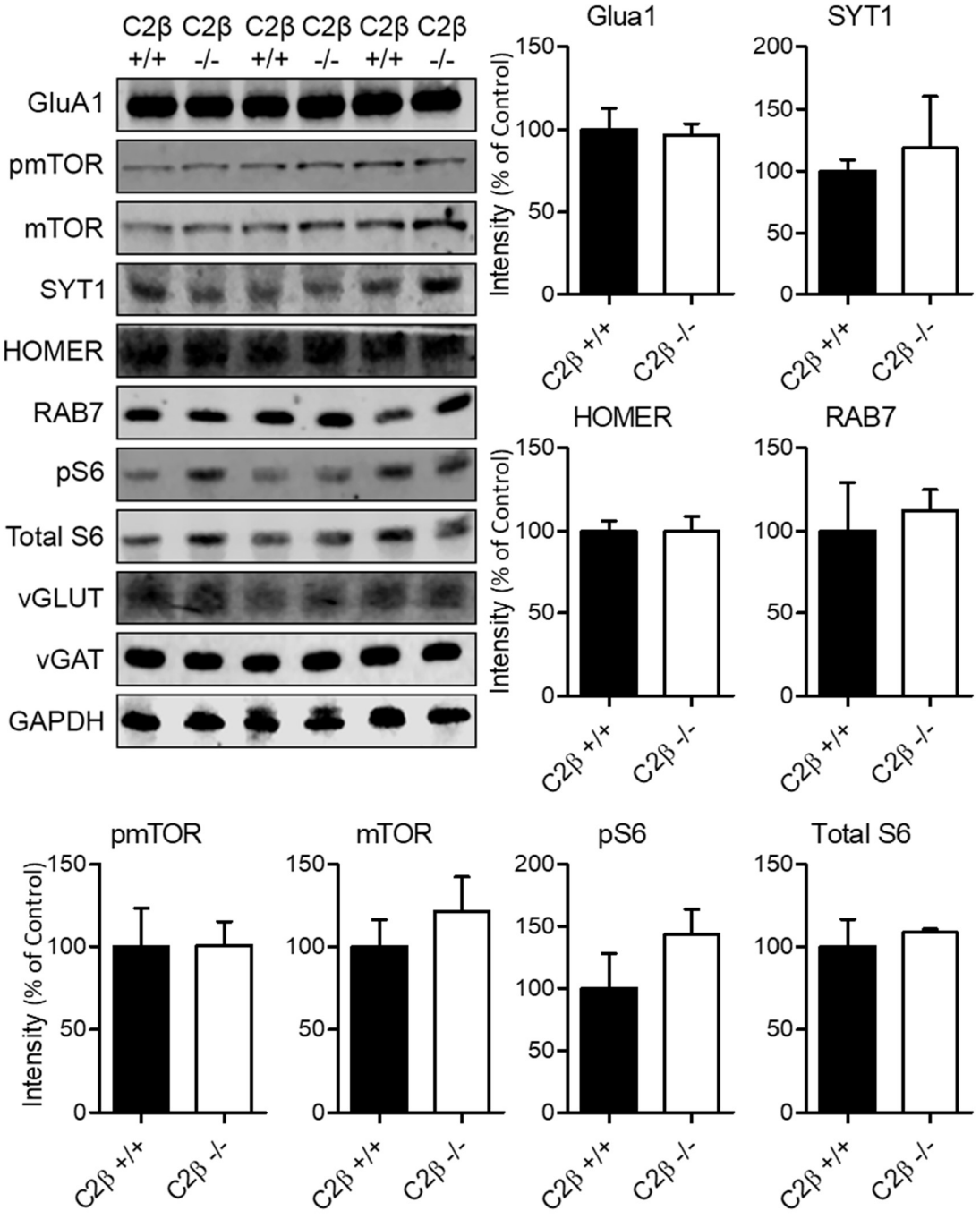

Figure 17: PI3KC2β knockout mice have unchanged levels of key proteins. Western blots of whole brain lysates from 8-week old animals. No significant changes were observed (Paired t test, n=3 paired experiments).

Another proposed mechanism for epileptogenesis is neuronal dysplasia (H. Kim et al., 2013), or changes of neuron number, particularly interneurons (André et al., 2001; Yamawaki et al., 2015). To obtain a detailed characterisation of the cells within each region of the CA1, we used a stereological approach to estimate cell density (Figure 19A & B). Interestingly, though no change in density of cells within the primarily excitatory *stratum pyramidale*, a large increase in density in the *stratum oriens* was observed, and a small but significant increase of cells within the *stratum radiatum*, two relatively low density areas containing mostly inhibitory interneurons. This was accompanied by an increase in Somatostatin-positive interneurons in the *stratum oriens* and a decrease in the *stratum radiatum* (Figure 19C). No change in Parvalbumin-positive interneuron number was observed (Figure 19D). This may indicate a compensatory inhibition to suppress epileptogenesis (Baran et al., 2004).

In summary, no changes were observed in synaptic proteins associated with epilepsy of *Pi3kc2β* -/- mice, no obvious defects were detected within the hippocampus, apart from a small increase in inhibitory interneurons.

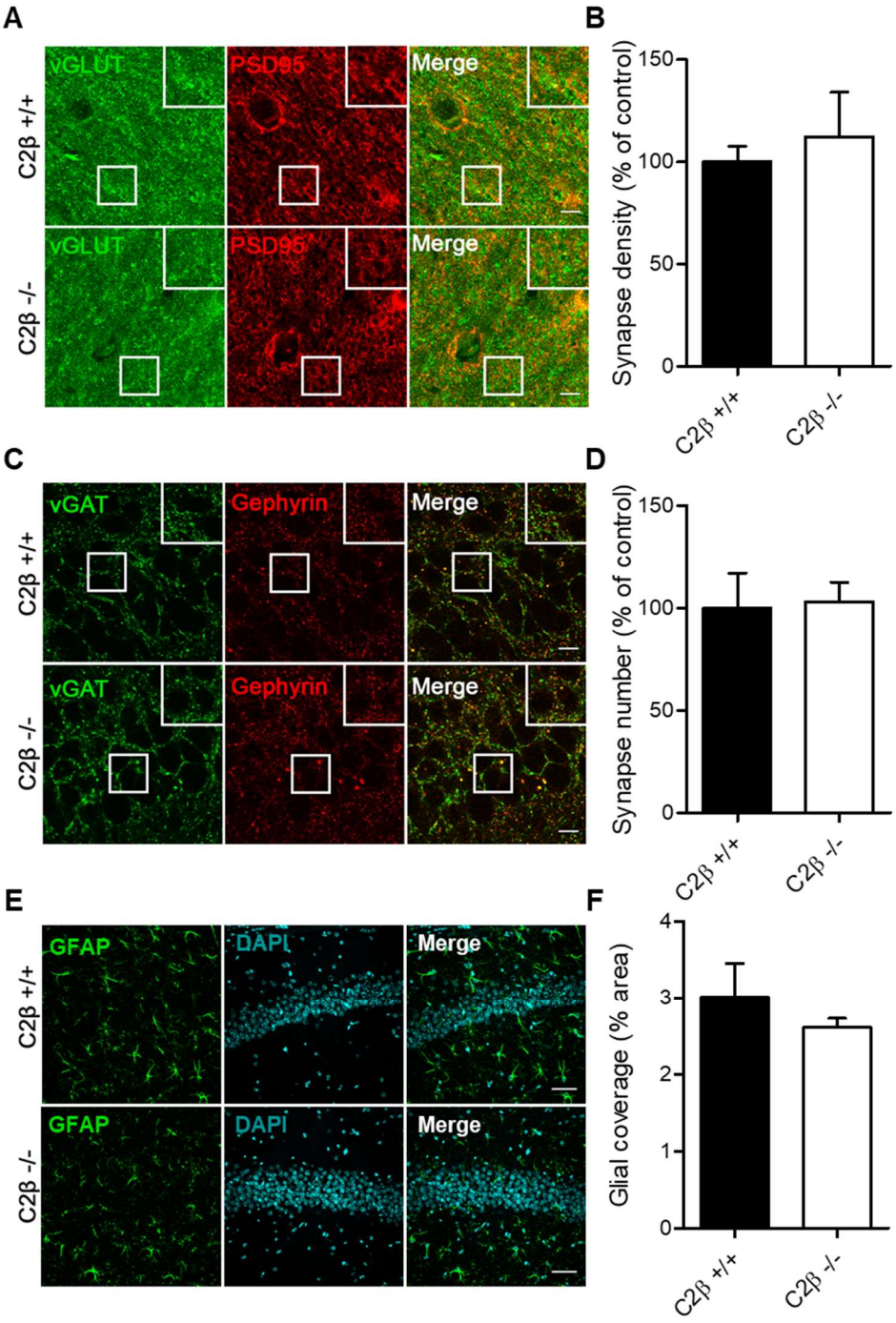

Figure 18: Normal synaptic density and glial coverage in PI3KC2β KO mice. **(A & B)** Immunohistochemistry of excitatory synapses in *Stratum radiatum* (Insert, 20 µm scale bar, 10 µm). Density calculated from colocalising vGLUT and PSD95 (Paired t test, n=4 paired experiments) **(C & D)** Immunohistochemistry of perisomatic inhibitory synapses within the *Stratum pyramidale* (Insert, 20 µm scale bar, 10 µm). Density calculated from colocalising vGAT and Gephyrin (Paired t test, n=4 paired experiments). **(E & F)** Immunohistochemistry of Glial coverage of the CA1 region (scale bar, 50 µm). Coverage calculated by GFAP presence within the total CA1 (Paired t test, n=4 paired experiments).

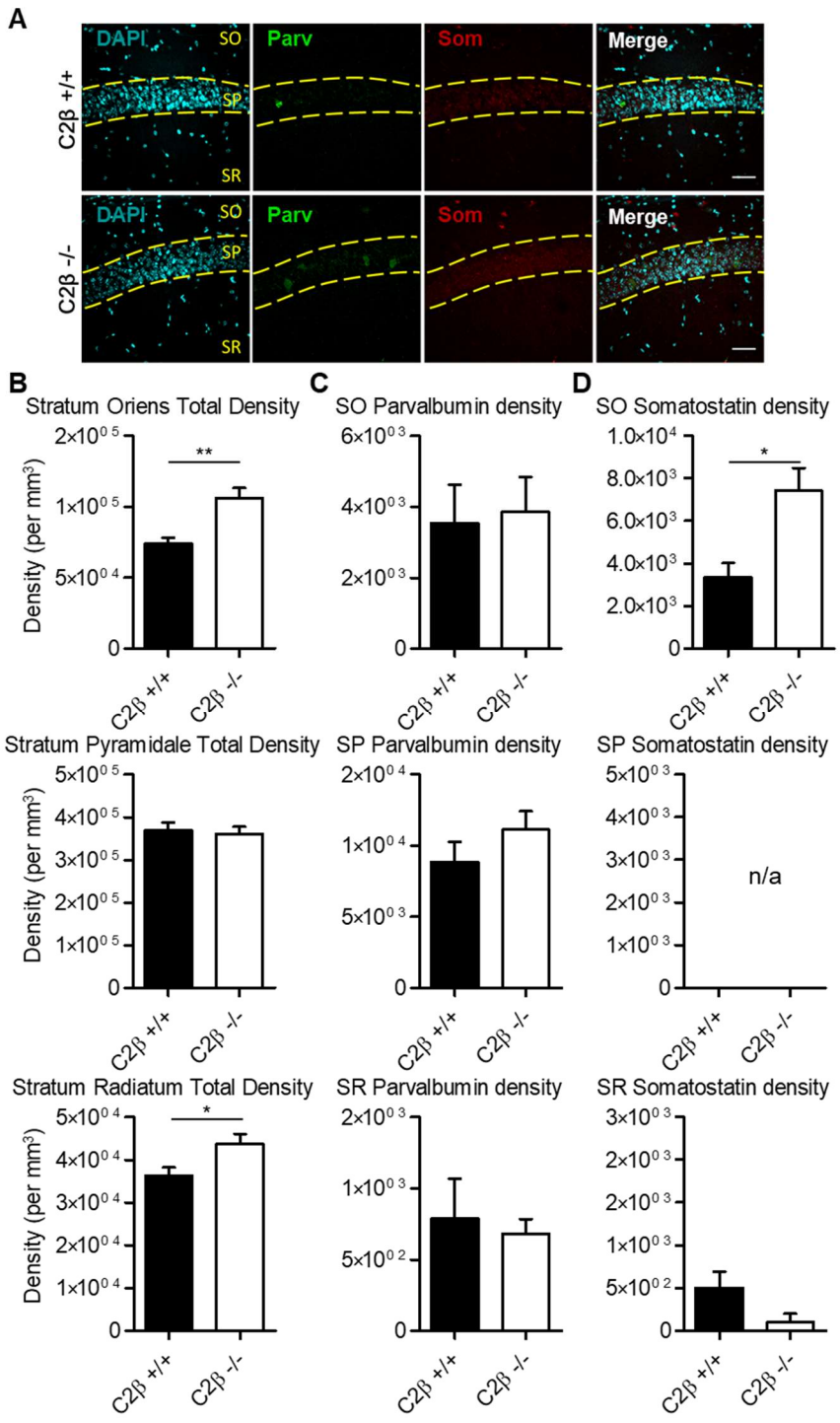

Figure 19: Stereological Analysis of CA1 Total and interneuron density in PI3KC2b KO mice. **(A)** Representative images of Immunohistochemistry of CA1 (SO= *Stratum oriens* SP= *Stratum pyramidale* SR= *Stratum radiatum*, scale bar, 50 µm). **(B – D)** Stereological estimates of cell density per mm³ (Paired t test, *P< 0.05 **P< 0.005 n=4 paired experiments).

3.2.2 PI3KC2β loss leads to hyperactive mTORC1 signalling in neurons

Having seen that loss of function mutations of PI3KC2β led to an increase in mTORC1 activity in immortalized cells, it became our focus to see if a similar elevation could be seen in *Pi3kc2β* -/- neurons. Lysates from DIV7 *Pi3kc2β* +/+ and *Pi3kc2β* -/- cortical neuron cultures were taken, and showed a tendency for increased S6K phosphorylation upon PI3KC2β loss, and a significant increase in the phosphorylation of its downstream target S6 (pS6) was also observed (Figure 20A-C). Furthermore, immunohistochemistry of DIV14 hippocampal confirmed an increase of pS6 intensity (Figure 20D & E).

Attempts to quantify average pS6 levels in vivo within the entire CA1 *stratum pyramidale* by means of immunohistochemistry initially showed no change in mean intensity. Closer investigation indicated that in *Pi3kc2β* -/- hippocampi an increased number of cells had high levels of pS6 compared to neighbouring cells. To assess whether the number of cells with high pS6 levels was increased in *Pi3kc2β* -/- *stratum pyramidale*, we conducted stereological analysis. This demonstrated that as anticipated the number of cells with high pS6 was increased while total cell density within the structure remained unchanged (Figure 21A-C). This demonstrates a physiological increase of mTORC1 signalling in *Pi3kc2β* -/- mice.

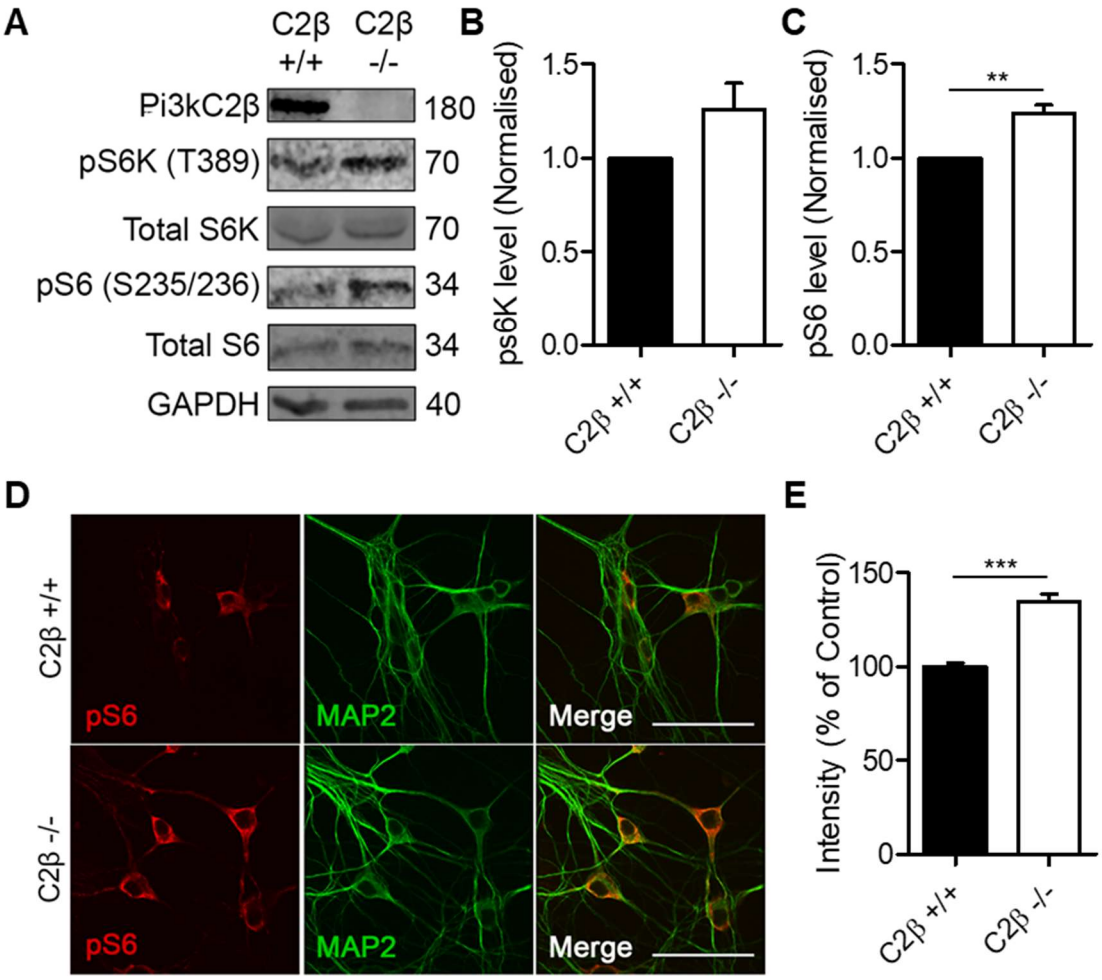

Figure 20: Hyperactive mTORC1 signalling in PI3KC2β null neurons. **(A)** Western blot analysis of DIV7 cortical neuron lysates **(B & C)** Quantification of pS6K and pS6 levels. pS6K shows tendency towards increase in PI3KC2β null neurons (One sample t test P=0.1198 n=6 independent experiments). pS6 levels are significantly increased (One sample t test P=0.0043 n=6 independent experiments). **(D - E)** Immunocytochemistry of DIV14 hippocampal neurons (scale bar, 50 μm). Intensity of pS6 staining is significantly higher in PI3KC2β null neurons (Paired t test, P=0.0006 n=5 paired experiments).

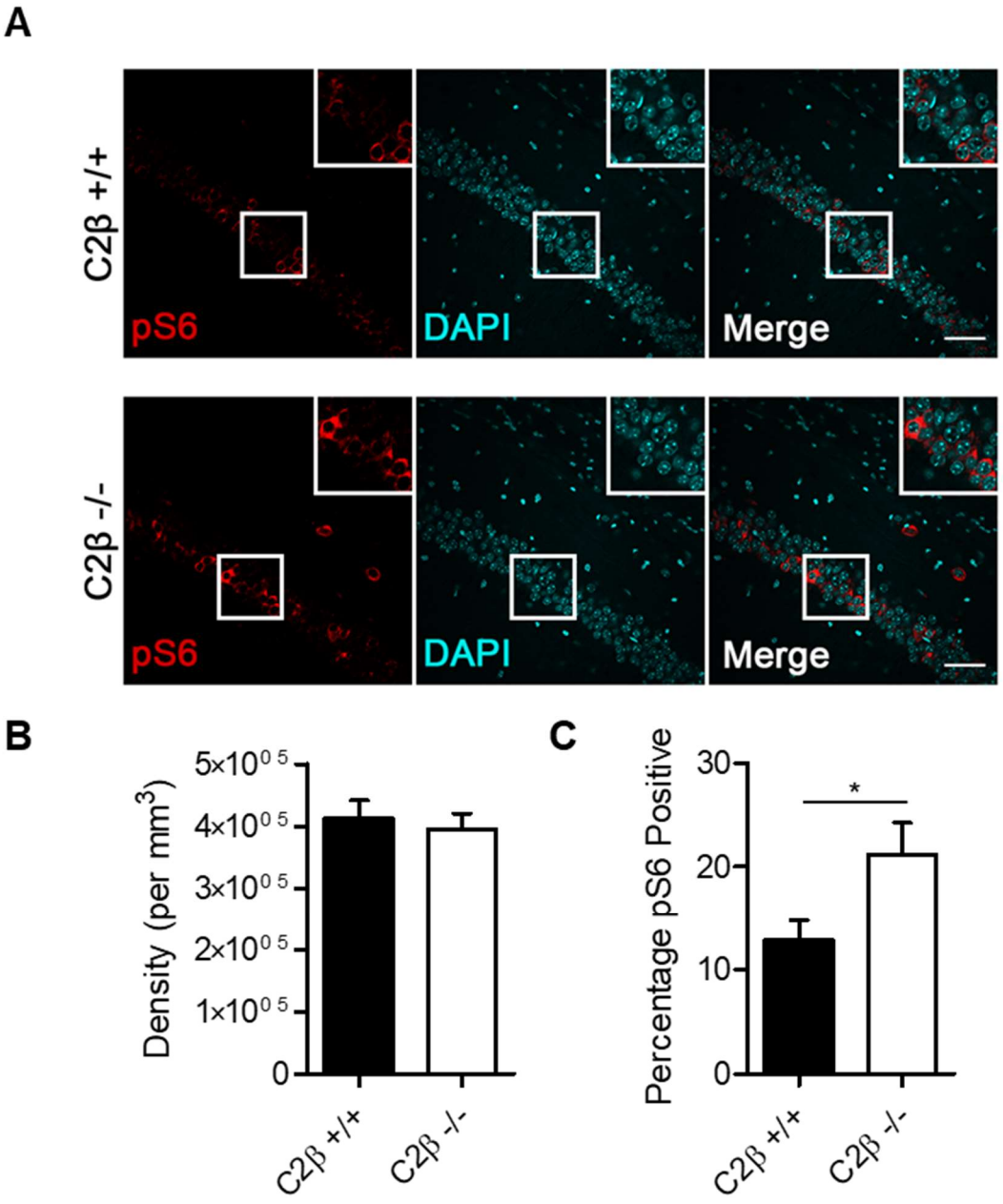

Figure 21: Hyperactive mTORC1 signalling in PI3KC2β null CA1 *stratum pyramidale*. **(A)** Immunohistochemistry of pS6 in the CA1 region of the hippocampus (Insert, 75 µm scale bar, 50 µm). **(B)** Stereological estimate of cell density within the CA1 *stratum pyramidale*, PI3KC2β loss does not affect cell density (Paired t test, P=0.3435 n=6 paired experiments). **(C)** Percentage of cells with high pS6 staining, threshold set at the 10% brightest pixels of control sections. PI3KC2β loss resulted in higher pS6 expression (Paired t test, P=0.0187 n=6 paired experiments).

3.2.3 Altered network activity in PI3KC2β null acute slices

Though no profound histological defects were observed, underlying tendencies for epileptogenesis can be found by examining network properties. We therefore conducted electrophysiological assays within the CA1 to detect for changes in E/I balance, calcium facilitation and synaptic plasticity.

Field recordings were first made in the *stratum radiatum* (Figure 22A), a region containing primarily dendrites of CA1 pyramidal cells with few interneurons, meaning recordings represent near pure responses to glutamatergic signalling of CA3 Schaffer collaterals. Input-Output measurements showed increased responses in *Pi3kc2β* -/- slices (Figure 23B, Data pooled with Dr. Gaga Kochlamazashvili), suggesting an increase in synaptic transmission, but no change in presynaptic calcium facilitation was observed via paired pulse facilitation stimuli (Figure 22C, Data pooled with Dr. Gaga Kochlamazashvili). To examine the effect of PI3KC2β loss on synaptic plasticity, LTP was induced via five theta burst stimuli trains (5x TBS). Surprisingly, facilitation was reduced in *Pi3kc2β* -/- slices (Figure 22D & E, Data pooled with Dr. Gaga Kochlamazashvili). These results suggest a change in excitatory transmission and perturbed LTP in the CA1.

To examine changes in feedforward and feedback inhibition within the CA1, field recordings were taken in the *stratum pyramidale* (Figure 23A). The population spikes in this region represent multiple pyramidal cells firing, and with different stimulus trains can detect inhibition from the few *stratum radiatum* interneurons, as well as the interneurons from the *stratum oriens* and *pyramidale*. Again, Input-Output measurements showed an increased response to stimulus in PI3KC2β null slices (Figure 23B, performed by Dr. Gaga Kochlamazashvili), demonstrating a consistent effect.

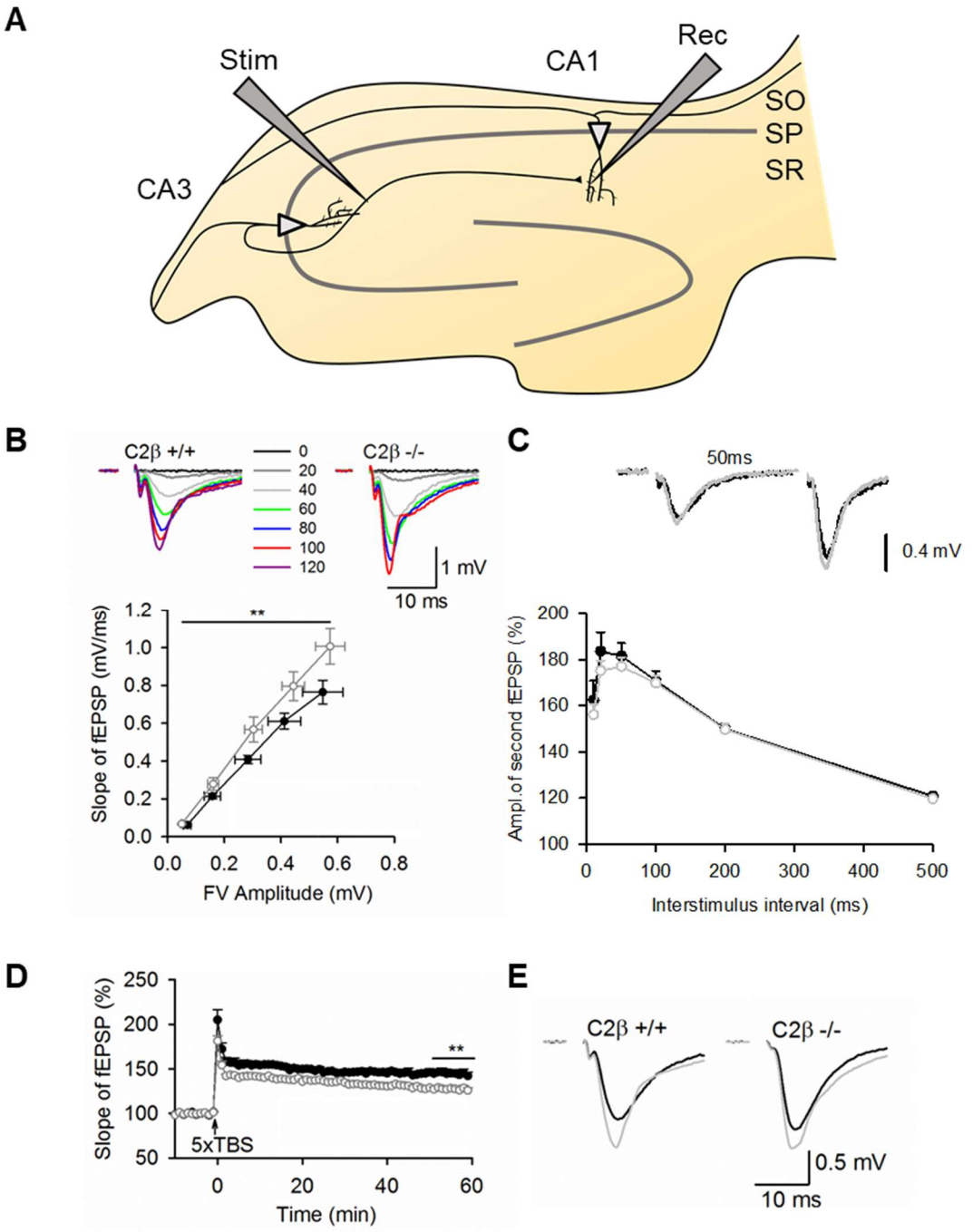

Figure 22: Electrophysiological recordings of *Stratum radiatum* display hyperexcitability and perturbed LTP in PI3KC2b KO mice. (A) Visualisation of electrode placement for *Stratum radiatum* recordings **(B)** Input-Output recordings reveal hyperexcitability in PI3KC2β null recordings relative to the fibre volley input (Two way ANOVA: **P< 0.005 n= 8 slices N= 8 mice per genotype) **(C)** Paired pulse recordings indicate no change in presynaptic calcium facilitation (Two way ANOVA *Pi3kc2β* +/+ n= 17 slices N= 14 mice *Pi3kc2β* -/- n= 15 slices N= 13 mice) **(D & E)** Quantification and example traces of LTP induction. PI3KC2β null slices exhibit less LTP relative to pre-induction baseline (One way ANOVA: **P< 0.005 n= 8 slices N= 8 mice per genotype). Data pooled with Gaga Kochlamazashvili.

Feedback inhibition occurs from the basket cells of the *stratum oriens* which are innervated by pyramidal cells that synapse back onto the latter leading to inhibition which suppresses pyramidal cell firing for a brief period, usually for up to 50 ms (Freund, 2003). To assess the strength of feedback inhibition, paired pulse stimulation was applied. At 10 ms interpulse interval in *Pi3kc2β* +/+ slices, the second stimulation evokes a much smaller response than the first sue to feedback inhibition (Figure 23C, performed by Dr. Gaga Kochlamazashvili), however as can be seen in *Pi3kc2β* -/- slices, the second pulses lead to a response near comparable to the first, and even at longer interstimulus pulses is larger than the control. This suggests a loss of feedback inhibition, a key suppressor of epileptogenesis.

Finally, we wanted to test if an aberrant level of activity dependent inhibition was occurring. Upon regular, moderate to high frequency stimulation, glutamatergic signalling is facilitated (B. Davies et al., 2001) and feedforward/feedback inhibitory signalling is suppressed (Thompson & Gahwiler, 1989). After 30 s of 1 Hz stimuli, *Pi3kc2β* +/+ slices show a 50% increase in PS field potentials measured as area under the curve (Figure 23D & E, performed by Dr. Gaga Kochlamazashvili). However, *Pi3kc2β* -/- slices show an 100% increase in the PS area response, and most interestingly 53% of slices show polyspiking behaviour compared to 12% of *Pi3kc2β* +/+ slices, whereby secondary spontaneous action potentials are generated by the pyramidal cells, which is reminiscent of seizure spiking.

Taken together these electrophysiological experiments demonstrate multiple abnormalities of CA1 network activity, with an E/I imbalance which may indicate an underlying tendency to epileptogenesis.

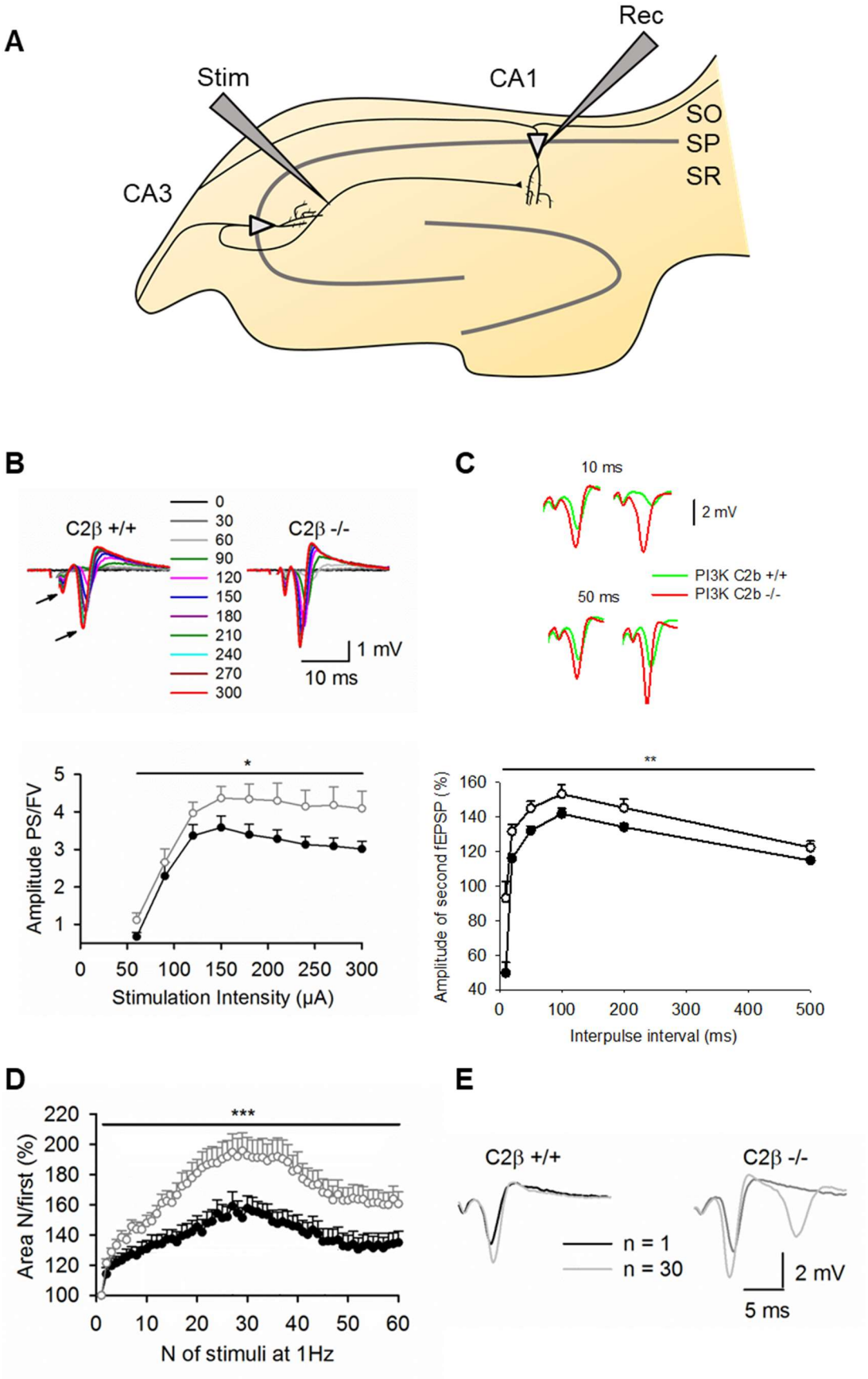
A
Rec
Stim
CA1
SO
SP
SR
CA3
B
C2β +/+
C2β -/-
0
30
60
90
120
150
180
210
240
270
300
1 mV
10 ms
C
10 ms
2 mV
PI3K C2b +/+
PI3K C2b -/-
50 ms
Amplitude PS/FV
Stimulation Intensity (μA)
Amplitude of second fEPSP (%)
Interpulse interval (ms)
D
Area N/first (%)
N of stimuli at 1Hz
E
C2β +/+
C2β -/-
n = 1
n = 30
2 mV
5 ms

Figure 23: Electrophysiological recordings of *Stratum pyramidale* display altered properties of PI3KC2b KO slices. **(A)** Visualisation of electrode placement for *Stratum pyramidale* recordings **(B)** Population spike recordings reveal hyperexcitability in PI3KC2β null recordings relative to the fibre volley input (Two way ANOVA: *P< 0.05 *Pi3kc2β* +/+ n= 17 slices N= 5 mice, *Pi3kc2β* -/- n= 15 slices N= 5 mice) **(C)** Paired pulse recordings reveal potential change in feedback inhibition (Two way ANOVA **P< 0. *Pi3kc2β* +/+ n= 17 slices N= 5 mice, *Pi3kc2β* -/- n= 15 slices N= 5 mice) **(D & E)** Quantification and example traces of repetitive stimulus train. PI3KC2β null slices show increased response to stimuli during the stimulus train (One way ANOVA: ***P< 0.0005 *Pi3kc2β*

3.2.4 PI3KC2β loss results in drug specific epileptogenesis

To first detect for any spontaneous seizure activity, *Pi3kc2β* -/- mice and their littermates were observed for 12 hours in home cages, including day/night light switching, however no spontaneous seizures were observed in either genotype (not shown). However, many mouse models of epilepsy show no spontaneous seizures but instead show increased response to seizure inducing drugs (Bateup et al., 2013; Hentschke et al., 2006). Therefore, we tested several drugs to uncover whether PI3KC2β null mice have a lowered seizure threshold.

A pilot experiment using 15 mg/kg intraperitoneal (IP) injection of the glutamate receptor agonist Kainic Acid saw no obvious tendency for lowered threshold in PI3KC2β null mice (not shown). The GABA receptor antagonist Pentylenetetrazol (PTZ) also showed no change in seizure onset or severity when 50 mg/kg was injected IP (Figure 24).

Interestingly, data by the group of Prof. Dr. Emilio Hirsch demonstrated that cholinergic receptor agonist Pilocarpine elicited potent seizures in PI3KC2β null mice, leading to high rates of mortality. Furthermore, PI3KC2β heterozygotes were also included and showed a susceptibility to Pilocarpine, suggesting a haploinsufficiency effect of PI3KC2β loss. These data suggest a pathway specific route to epileptogenesis in *Pi3kc2β* -/- mice.

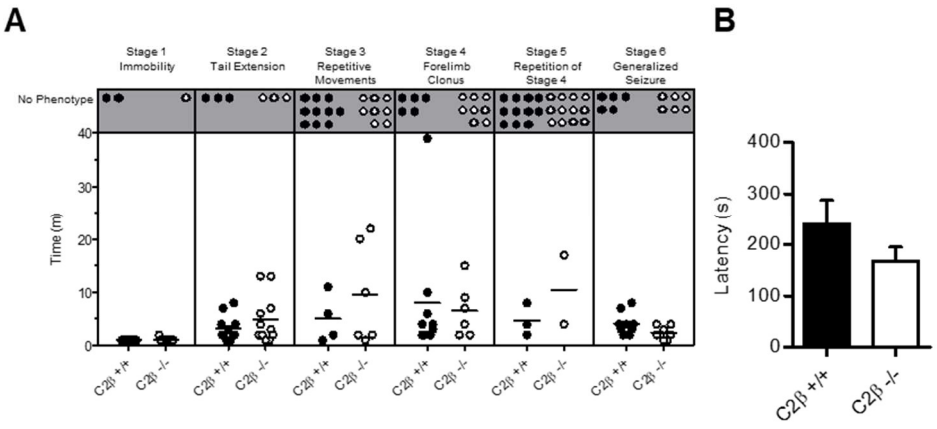

Figure 24: PI3KC2β null mice are not susceptible to PTZ seizure induction. **(A)** Response to Pentylenetetrazol injection. Latency to when phenotype is first observed in each mouse is represented. **(B)** Latency to stage 6 seizure, no significant difference between genotypes is observed (Unpaired t test P= 0.2198 N=9 control and 8 knockout mice).

3.2.5 Rapamycin dissipates PI3KC2β null susceptibility to epilepsy

The macrolide antibiotic Rapamycin has long been known to suppress cellular growth (Houchens et al., 1983), and is regularly used within chemotherapy or as an immunosuppressant after transplant (Calne et al., 1989; Veroux et al., 2013). Rapamycin was found to form a complex with FKBP12 (Bierer et al., 1990), which in turn binds to mTOR via its FRB domain (Banaszynski et al., 2005; Sabatini et al., 1994; Sabers et al., 1995), leading to a strong inhibition of activity (Price et al., 1992). Due to its specific interaction, Rapamycin and its analogues have been proposed as a treatment for patients with tuberous sclerosis (Onda et al., 2002), as well as patients with other mTORC1 related epilepsies (Ghosh Mazumder et al., 2016). Using our PI3KC2β null epilepsy model, we decided to test whether a similar treatment may be applicable to patients suffering from deleterious PI3KC2β mutations.

First, DIV14 *Pi3kc2β* +/+ and *Pi3kc2β* -/- primary hippocampal neuron cultures were incubated with 200 nM Rapamycin or an equal volume of the vehicle DMSO for 1 hour. While DMSO had no effect on the difference in pS6 intensity previously seen, rapamycin incubation reduced pS6 in both genotypes (Figure 25A and B), with levels in *Pi3kc2β* -/- neurons comparable to WT cells. We next aimed to determine if Rapamycin could effectively inhibit mTORC1 and rescue the increase in pS6 seen in *Pi3kc2β* -/- brain slices. Brain slices were incubated in ACSF containing 1 μM rapamycin or an equivalent volume of DMSO for 2 hours and then fixed and re-sectioned. DMSO had no effect on the number of cells within the CA1 *stratum pyramidale* with high pS6 levels, however in both genotypes the number of cells with elevated pS6 levels was dramatically reduced c (Figure 26A & B). Therefore, rapamycin can effectively reduce mTORC1 activity acutely in acute slices.

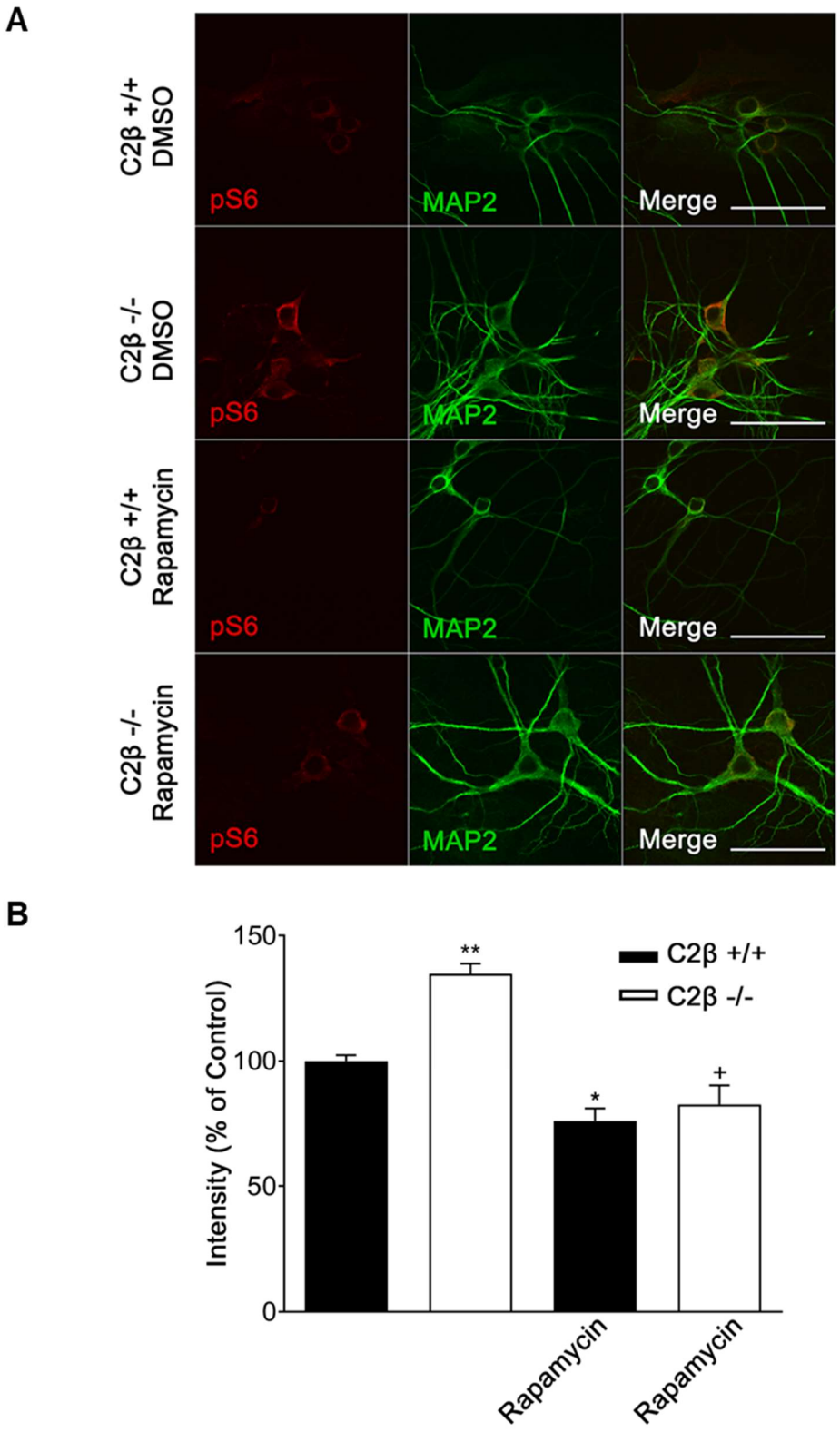

Figure 25: Rapamycin supresses mTORC1 activity in neurons. **(A)** Immunocytochemistry for pS6 of DIV14 hippocampal neurons in the presence of 1 hour DMSO or Rapamycin treatment (scale bar, 50 µm). **(B)** Intensity of pS6 staining is reduced by Rapamycin in both control and PI3KC2β null neurons (One way ANOVA with bonferroni correction: *P< 0,05 **P< 0.005 n=4 independent experiments).

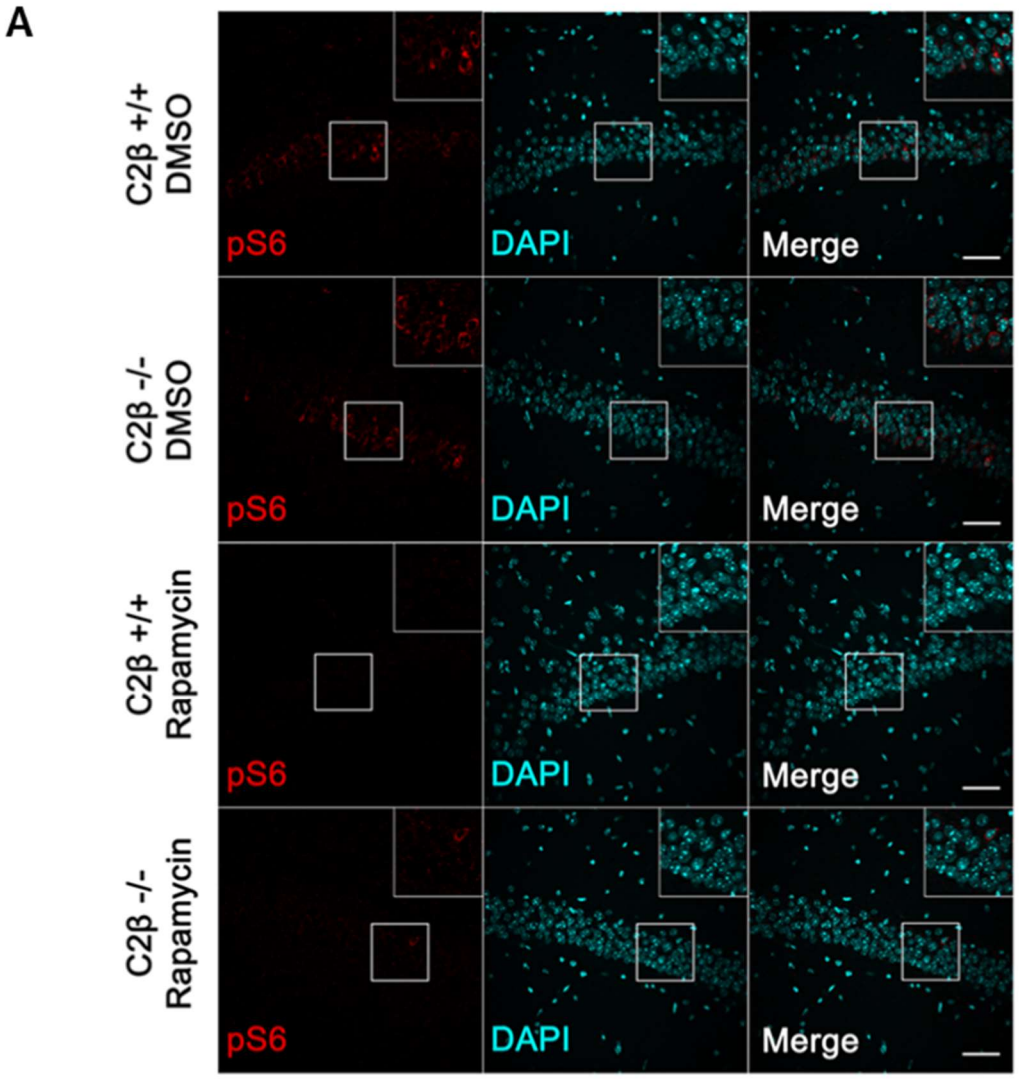
A
C2β +/+ DMSO
C2β -/- DMSO
C2β +/+ Rapamycin
C2β -/- Rapamycin
pS6
DAPI
Merge
B
Procentage pS6 Positive
15
10
5
0
C2β +/+
C2β -/-
**
*
*
Rapamycin
Rapamycin

Figure 26: Rapamycin supresses mTORC1 activity in CA1 hippocampus. **(A)** Immunohistochemistry of pS6 in the CA1 region of the hippocampus (Insert, 75 µm scale bar, 50 µm). **(B)** Percentage of cells with high pS6 staining is reduced after 2 hour incubation with Rapamycin in both control and PI3KC2β null slices (One way ANOVA with bonferroni correction: *P< 0,05 **P< 0.005 n=4 independent experiments).

Finally, to assess if the same effect could be replicated In Vivo, mice were pre-treated with rapamycin before pilocarpine administration, conducted in the group of Prof. Dr. Emilio Hirsch. The number of PI3KC2β null mice exhibiting seizures was reduced after Rapamycin treatment (Figure 27, performed by Luca Gozzelino), and the severity of the seizures decreased. Furthermore, the delay until seizures were first observed was increased to a time comparable with *Pi3kc2β* +/+ mice.

Taken together, these data demonstrate that Rapamycin is an effective treatment to reduce mTORC1 activity and protects against epileptogenesis in our PI3KC2β null mouse model of epilepsy.

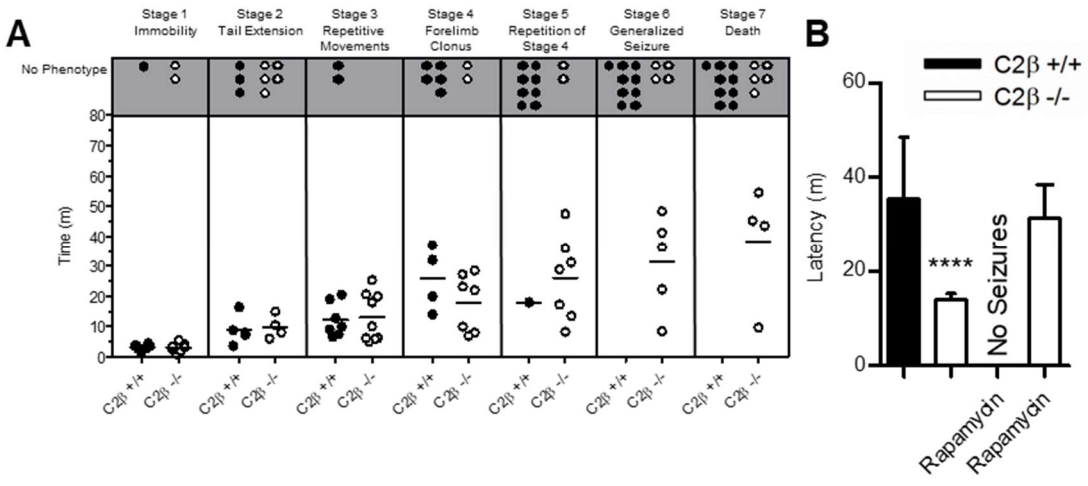

Figure 27: Rapamycin is protective against Pilocarpine induced seizures **(A)** Response to Pilocarpine injection after Rapamycin treatment. Latency to when phenotype is first observed in each mouse is represented. **(B)** Latency to stage 6 seizure, both control and PI3KC2β null mice have reduced susceptibility to Pilocarpine after Rapamycin treatment (One way ANOVA with Bonferroni correction: ****P< 0.00005 N= 9 control and 9 null mice).

4 Discussion

This work investigated the roles of two Class II PI3Ks in neuronal function and disease. In the first half of the study, chronic and acute neuron specific knockouts of PI3KC2α were generated, which revealed that the protein is largely dispensable, but also hinted at an enigmatic role in maintaining appropriate levels of Synaptotagmin1 at the synapse. The second half of the study involved a multi approach assessment of PI3KC2β in neuron homeostasis. It was highlighted that SNPs within the core of PI3KC2β result in loss of function of the protein and in turn activation of mTORC1, which can lead to epileptogenesis in patients. Furthermore, deletion studies in mouse models replicated theses results, demonstrating mTORC1 hyperactivation in neurons of the hippocampus, hyperactivity and LTP defects within local networks, and epileptic susceptibility to certain drugs. Finally, acute treatment with the classical mTORC1 inhibitor rapamycin suppresses the defects found in our mouse model and prevents seizure induction, which hints at a route to treatment for patients suffering from PI3KC2β type focal epilepsy. These data demonstrate that Class II PI3Ks have important functions within neuronal homeostasis.

4.1 The Role PI3KC2α in Synaptic Sorting

Loss of PI3KC2α globally, either constitutively during embryogenesis or acutely in adulthood, leads to lethality in mouse models (Yoshioka et al., 2012), however we found that neuron specific knockout mice are viable and display no obvious abnormalities in behaviour or in network excitability (Figure 10 & 11). It has been proposed that the loss of viability in global PI3KC2α knockout mice is due to loss of genetic stability as it plays a role in mitotic spindle assembly (Gulluni et al., 2017), thus embryogenesis may be disrupted. In the case of global deletion in adult mice via a tamoxifen induction system, data by the group of Prof. Dr. Emilio Hirsch (unpublished) suggests the mortality does not arise from the loss of PI3KC2α in the brain as protein levels from whole brain lysates of deceased mice are comparable to control mice, but loss in other organs is complete (Not shown).

Global deletion of other late stage effector proteins of CME such as Auxilin and Dynamin 1/3 result in at least partially viable mice with few observable defects besides delayed endocytosis (Raimondi et al., 2011; Yim et al., 2010), meaning our brain specific PI3KC2α knockout is in line with these other studies. Interestingly upon Dynamin 1/3 double knockout the frequency of mEPSCs is lower compared to controls suggesting a lower release probability, this is not a parameter we assessed in our electrophysiological recordings and could be further investigated.

4.1.1 PI3KC2α is dispensable at hippocampal synapses

As previously stated, PI3KC2α has been shown to play a key role in CME Maturation/Scission in immortalised cells (Posor et al., 2013; Schöneberg et al., 2017), this study suggest PI3KC2α plays a minor role at the synapse, with no change in endocytic rate. It appears that a small pool of Syt1-pH remains stranded on the surface of synapses of PI3KC2α knockout neurons, and an increase of Clathrin intermediates was observed via EM upon electrical stimulation (Figure 16). The effect of slowed endocytosis is specific to Syt1-pHluorin and not Syp-pHluorin. However, it is clear that the bulk of cargo can be retrieved and the stranding of this small proportion of Syt1 after high intensity stimulus is unlikely to have meaningful repercussions.

This study does not completely rule out a role for PI3KC2α in synaptic cycling, as compensation by the other members of the Class II PI3K family upon loss of PI3KC2α. In particular, we showed that PI3KC2β is also enriched in synaptic fractions (Figure 8). These two members of the family are extremely similar at the kinase core, and indeed within the unstructured N-Terminal region contains a Clathrin binding domain which has been shown to co-immunoprecipitate with Clathrin (Wheeler & Domin, 2006). Furthermore, PI3KC2β has recently been shown to be required for a Clathrin dependant fluid phase form of endocytosis called Clathrin mediated pinocytosis in endothelial cells (Aung et al., 2019), however this group suggest it is required for F-Actin assembly. This places PI3KC2β at the endocytic machinery, yet whether there is redundancy or compensation

between PI3KC2α and PI3KC2β remains as yet uncertain. One surprising study recently found patients from consanguineous parents that completely lack PI3KC2α (Tiosano et al., 2019). Unlike mouse models, the patients have survived adulthood, albeit with a complex syndrome of skeletal, visual, and learning defects. In these patients, high expression of PI3KC2β was observed, which may indicate a partial compensation. Whether this is the case in our model is not clear and requires further investigation

4.1.2 A potential role for PI3KC2α in Synaptotagmin 1 maintenance

One noticeable phenotype observed from both overexpressed Syt1-pHluorin and by examining endogenous expression in cultured neurons and brain lysates was an increase of Syt1 within PI3KC2α knockout neurons (Figures 14 & 15). Though this difference in expression level was only examined for Syt1 due to its use as a tool for monitoring synaptic endocytosis, it is probable other such proteins could also have erroneous expression levels, however this was not investigated in this study.

But how could PI3KC2α be regulating the levels of Syt1? One potential route may be via endosomal sorting at the synapse. As previously described, it was thought that PI3KC2α has a preference for PI4P as a substrate to generate $PI(3,4)P_2$ (Marat et al., 2017; Posor et al., 2013; Wallroth & Haucke, 2018). However other studies have suggested that away from the plasma membrane, PI is used by PI3KC2a to generate PI3P instead (Falasca et al., 2007; Yoshioka et al., 2012), this could occur either due to substrate availability or posttranslational modifications. Importantly, PI3P is a key regulator of endosomal progression, with multiple endosomal proteins such as early endosome fusion molecule EEA1 binding to PI3P via a zinc finger known as a FYVE domain (Burd & Emr, 1998; Stenmark et al., 1996). Some PX domain containing proteins also bind PI3P, including SNXs which conduct constriction on the endosome for budding similar to CME scission (Cullen, 2008; Seet & Hong, 2006). Endosomal sorting aided by PI3P within neurons has been shown to be of importance for regulating protein levels, with disruption of PI3P generation resulting in accumulation of amyloid precursor protein and amyloidogenesis, commonly associated with Alzheimer's disease

(Morel et al., 2013), and interestingly a recent computational study highlighted PI3KC2α as a potential drug target in AD (Z. J. Han et al., 2018). Could loss of PI3KC2α effect endosomal sorting? Indeed a recent study demonstrated that a burst of PI3KC2α generated PI3P was required for Rab11 mediated recycling of cargo from early endosomes (Campa et al., 2018). It is possible that this mechanism is conserved in neurons and without which Syt1 is not effectively sorted to a degrative pathway resulting in accumulation of the protein.

The other mechanism by which PI3KC2α may be controlling Syt1 and other unknown protein levels is via autophagy. PI3KC2α was recently shown to interact with ATG9, a key protein in autophagosome formation (Feng et al., 2016). It was shown that knockdown of PI3KC2α led to less LC3B positive compartments in cell treated with rapamycin, and an accumulation perinuclear endosomes (Merrill et al., 2017). Furthermore, lateral stress applied to epithelial cells was shown to lead to high levels of PI3KC2α at the primary cilium followed by autophagy induction (Boukhalfa et al., 2020). This increase in autophagy as seen by LC3 puncta, could be ablated by knockdown of PI3KC2α. Suggesting a role in the initiation of autophagosome formation. This novel role for PI3KC2α is still not well understood, but merits further study in neurons.

4.2 Identification of a Novel PI3KC2β-mTORC1 Focal Epilepsy

It was previously shown that the Class II PI3KC2β is a novel regulator of nutrient signalling, and an important repressor of mTORC1 activity. In this study through a multifaceted approach we demonstrated that PI3KC2β has important roles in neurons via mTORC1 regulation, with impacts on downstream signalling, network excitability, and pathophysiology. These data appear to be translatable to human focal epilepsy, with patient rare variant SNPs in the protein leading to loss of function and increased mTORC1 activity that is likely a key factor in epileptogenesis. Here we will discuss the meaning of these results and the potential impact of them on the human syndrome.

4.2.1 PI3KC2β mutations are a contributing factor in epileptogenesis

This study was initiated after we were provided data from the group of Dr. Tommaso Pippucci, whereby collapsing statistical analysis highlighted that mutations within PI3KC2β were associated with focal epilepsy within the dataset from the S.Orsola-Malpighi University Hospital. As stated, this analysis appears to be in agreement with another recent study that identified PI3KC2β as one of the top 200 genes of which mutations are associated with burden for non-acquired focal epilepsy (Feng et al., 2019). Interestingly the regulator of PI3KC2β, PKN2 has also been associated with epilepsy (Odgerel et al., 2019), though the mechanism is not known. The SNPs led to a loss of function of PI3KC2β which result in an increased mTORC1 activity**.** Our study agreed with this, showing that deletion of PI3KC2β in mice resulted in a similar increase of mTORC1 activity in both cultured neurons and the mouse hippocampus (Figure 20 & 21). Furthermore, deletion of PI3KC2β in this mouse model led to seizure susceptibility to the drug Pilocarpine (Figure 27, performed by Luca Gozzelino), but notably no spontaneous seizures were observed, either during routine checks and handling or via multiday 12-hour overnight monitoring. It should be stated that this is not proof that seizures do not occur spontaneously in the mouse model, as episodes could be rare or be of low severity, making them difficult to observe. We had considered implanting EEG recording equipment into test mice for continual monitoring but it was decided that this may place excessive burden on the animal with little scientific gain. But it is also true that the origin of seizures in patients is difficult to fully understand. Non-acquired focal epilepsy is defined by seizures originating from one hemisphere, without the presence of lesions, and with at least one familial case of third-degree or less (Perucca, 2018). However, this does not rule out the possibility of factors other than genetic ones on contributing to epileptogenesis.

This study demonstrated a drug specific increased susceptibility to epileptogenesis, with the muscarinic agonist Pilocarpine having profound effects on epileptogenesis, while Kainic Acid and PTZ, drugs effecting excitatory and inhibitory drive respectively, had no effect on acute seizures. How could a model be more susceptible to one drug than others? Muscarinic acetylcholine signalling

is still not well understood, but studies have suggested that agonist binding of muscarinic receptors results in activation of mTORC1 signalling, resulting in high pS6 levels (X. Huang et al., 2010; Slack & Blusztajn, 2008). Furthermore a recent study demonstrated that stimulation of the CNS enriched M1 receptor resulted in phosphorylation of AMPA subunit GluA1 leading to membrane insertion, which could be prevented by administration of an AKT inhibitor, suggesting an involvement of downstream mTORC1 (Zhao et al., 2019). It could be that this direct activation of the mTORC1 signalling is enhanced in the absence of PI3KC2β leading to faster AMPA insertion and thus faster, more severe seizures. Several of these studies used a different cholinomimetic drug called Carbachol, which has similar binding properties to Pilocarpine. It would be interesting in a future study to confirm whether PI3KC2β null mice show a similar susceptibility to Carbachol in epileptogenesis. Furthermore, these two muscarinic agonists are common ingredients in several eye drop solutions, which could also be a contributing factor to epileptogenesis itself, though is unlikely in low doses.

Indeed, the lack of spontaneous seizures and drug specific epileptogenesis in our mouse model could be interpreted as evidence that though PI3KC2β mutations are a risk factor in focal epilepsy, a secondary stimulus may be required to cause an episode. Common risk factors in epilepsy include traumatic brain injury, viral infection, diet, and illicit drug use, the latter two being of particular interest. It is clear that nutrient levels have strong effects on mTORC1 activity as previously described in immortalised cells, and it is conceivable that the effects of such nutrient signalling may affect mTORC1 activity in neurons either directly or via insulin signalling. Investigations into diet restriction on seizure severity are ongoing and have been speculated as a promising treatment for patients with Tuberous Sclerosis to help seizure management (D'Andrea Meira et al., 2019; Stafstrom, 2004). It would be interesting to see if caloric restriction or abundance leads to the occurrence of spontaneous seizures in our PI3KC2β null mouse line. Concerning drug use as a risk factor, studies have shown multiple commonly used drugs can result in increased mTORC1 activity including nicotine, alcohol, and cocaine (Dayas et al., 2012; Knight et al., 2012; Memmott & Dennis, 2010; Neasta

et al., 2010), with excessive use of these drugs being associated with epileptogenesis (Leach et al., 2012). Whether these drugs would lead to epileptogenesis in our model is unclear as they act through non-muscarinic mechanisms. Whether environmental factors play a role in PI3KC2β epileptogenesis is not clear due to the limited patient group size and history collected, and would require a much larger, more detailed investigation to draw any conclusions.

One interesting question that arises from the study is whether PI3KC2β mutations in the patients act in a dominant negative or haploinsufficient manner, with all patients being heterozygous for PI3KC2β mutations. The data from the Hirsch Group's Pilocarpine experiments showed that mice with heterozygous deletion of PI3KC2β are also more susceptible to seizures, suggesting that PI3KC2β copy number is important for effective signalling in neurons. However, the severity of the phenotype is less in heterozygotes than in PI3KC2β mice, and it is possible dysfunctional PI3KC2β may still inhibit the action of its functional counterpart if copy number at the lysosome is tightly regulated. Therefore, a follow up study has been planned to introduce the patient SNPs in mouse PI3KC2β to assess seizure burden, and thus help answer the question of whether there are dominant negative effects in the patients.

4.2.2 Electrophysiological effects of PI3KC2β loss

Acute hippocampal slices of PI3KC2β null mice demonstrated an array of electrophysiological phenotypes associated with epileptogenesis, as well as some alterations that require further investigation. In both *Stratum radiatum* and pyramidale recordings an increased amplitude of response to CA3 Schaffer collaterals was observed (Figures 22 & 23). As these are present in the *Stratum radiatum*, this is an indicator of increased excitatory signalling at the postsynapse, this might be caused via a mechanism of increased surface AMPA receptors arising from increased mTORC1 signalling (Zhao et al., 2019) leading to an increased postsynaptic quantal size to presynaptic signalling. To dissect if this is an increase

of AMPA specific currents one could see if blockage of AMPA specific currents via antagonists such as CNQX could ablate the difference between PI3KC2β null mice and their controls at the *Stratum radiatum*. However, this does not completely rule out a loss of inhibitory drive as a factor further increasing fEPSPs at the *Stratum pyramidale*. The 1 Hz repetitive stimuli led to fast hyperexcitability, which could either indicate perturbed feedforward/feedback inhibitory signalling, even leading to secondary spikes (Figure 23). This result is interesting as it clearly denotes an excitatory/inhibitory imbalance that could underly epileptogenesis, and is similar to a mouse model with spontaneous seizures previously described by our group (Koo et al., 2015).

Perisomatic synapse number appears broadly normal (Figure 18) and the number of interneurons is comparable, except for an increase of somatostatin positive cells in the *Stratum oriens*, which suggests it is unlikely inhibitory drive is affected. It is still possible that these excess interneurons do not integrate correctly into the network leading to weak inhibition, or even synapsing onto each other leading to negative feedback in the inhibitory system. To rule out these possibilities further whole cell patch experiments should be conducted on both the interneurons and pyramidal cells to see if mIPSCs or sIPSCs are reduced in pyramidal cells or increased in somatostatin interneurons. Furthermore, interneurons could be filled with an Alexa Fluo dye to examine if the architecture and projections of the cells has been altered upon PI3KC2β loss. Interestingly, a recent study using heterozygous knockout of Tsc1 in interneurons reported a loss of inhibition in pyramidal cells (Haji et al., 2020), suggesting the phenotype arises from problems with GABA release rather than postsynaptic receptors. Population spikes should be probed in the presence of GABA antagonists such as PTZ or Bicuculline, to see if the change in response size in PI3KC2β null slices is comparable to Controls or if less drug induced hyperexcitability is observed, unveiling whether perturbed GABAergic signalling has occurred. However, it should be stated that increased excitatory drive is the most likely cause of the imbalance.

One final interesting finding from our initial electrophysiological experiments was that LTP formation upon 5xTBS induction is reduced in slices lacking PI3KC2β. This was puzzling as previous data has shown that mTORC1 activity was crucial for effective LTP formation (Hoeffer & Klann, 2010; Stoica et al., 2011), making our data appear on the face as contradictory. This is however not the case, as LTP is measured as a fold change from the basal signalling and thus relies on comparable baselines. We however know from our Input-Output recordings that there is hyperexcitability in response to a given stimulus in the *Stratum radiatum*. It could be that this region in PI3KC2β null slices is near maximal potentiation and it is therefore not possible to increase the excitability upon 5xTBS. This could be explained by previously described studies indicating mTORC1 activities involvement in AMPAR surface levels (Zhao et al., 2019) and may also be involved in NMDA receptor expression (Niere & Raab-Graham, 2017). To examine this possibility one could subject the slices first to a low frequency paradigm (Doyle et al., 1997; O'Dell & Kandel, 1994; Staubli & Lynch, 1990) to see if the baseline shifts, before then inducing LTP. Indeed, we saw hints of such a mechanism when Rapamycin preincubation could rescue this defect in LTP.

4.2.3 Rapamycin acutely supresses epileptogenesis

It is not novel to suggest mTORC1 activity can be rapidly supressed via rapamycin inhibition, and as we have seen in cultured neurons and acute slices (Figures 25 & 26), relatively brief rapamycin treatments result in strong mTORC1 inhibition. In line with this, recent data from Dr. Gaga Kochlamazashvili has demonstrated that the electrophysiological phenotypes seen in the PI3KC2β null mice is acutely rescued by rapamycin pre-treatment, and the greater susceptibility to Pilocarpine induced seizures is also preventable (Figures 27). It is surprising that downstream macro effects of mTORC1 hyperactivity such as adherent protein production and post translational modification, which we believe may cause the seizure reminiscent behaviour, are so rapidly rescued. In the case of the hyperexcitability in the *Stratum radiatum* and LTP deficiency previously described, these phenotypes are abolished upon 2-hour Rapamycin preincubation, similar to

what one might expect from the depotentiation paradigm previously described. This adds weight to the argument that mTORC1 is actually a dynamic member of the potentiation/depotentiation axis, a process associated with neurological disorders such as Schizophrenia (Ryskalin et al., 2018; Sanderson, 2012), indeed PI3KC2β itself was found to be enriched in several screens for rare variants of schizophrenia patients (Fromer et al., 2014; Purcell et al., 2014). This is a line of investigation that would be interesting to explore, to see if PI3KC2β mice have hyperlocomotion in open maze scenarios (Jones et al., 2011), and if so if Rapamycin can again be protective.

The data from Dr. Gaga Kochlamazashvili suggest rapamycin also acutely prevents excessive activity dependent disinhibition within the *Stratum pyramidale*. However, the mechanism of this is not entirely clear as the role of mTORC1 signalling specifically in interneurons is not well understood. Our data agrees with the phenotype of interneuron specific TSC1 knockout mice, in which rapamycin pre-treatment restores inhibitory signalling by an unexplained mechanism (Haji et al., 2020).

The final and most exciting finding is that Rapamycin treatment was found to be protective against Pilocarpine induced seizures (Figure 27), not only delaying seizures in PI3KC2β null mice, but also reducing the seizure severity in control mice. This indicates that Pilocarpine induced muscarinic receptor signalling is occuring in an mTORC1 dependant manner, which is an interesting insight as the Pilocarpine mechanism of action is still poorly understood (Lopes et al., 2013). This also indicates a pathway for future therapeutic approaches for human patients, it would be of high importance to examine whether Rapamycin and other mTORC1 inhibiting drugs may have benefits for sufferers of PI3KC2β related epilepsies. The use of Rapamycin in epilepsy treatment is not a novel idea, with multiple clinical trials reporting at least partial success (Griffith & Wong, 2018). However, a cohort of patients derived only from PI3KC2β type epilepsies may have a better response rate compared to these more generalised studies. This will hopefully lead to improved treatment options for those suffering from PI3KC2β related focal epilepsy.

5 Conclusion

In the past decade, the relatively understudied Class II PI3Ks have come under the spotlight as important regulators of membrane trafficking, genome stability and cell signalling. The findings of this study demonstrate that the importance of this family of proteins extends to maintaining neuronal function in the CNS, and their disruption could result in loss of homeostasis and disease.

In particular, the discovery of a new type of focal epilepsy and the promising results of mTORC1 inhibition may lead to better disease management and future treatments for this subset of patients. Our study focussed primarily on the hippocampus and epileptogenesis, but further investigations could yield new insights into Cortical signalling, Schizophrenia, and other mTORC1 related diseases such as autism. Though the loss of PI3KC2α in the brain resulted in a milder phenotype compared to immortalised cell lines, there are still open questions as to how it is involved in synaptic protein sorting, and whether it plays a role in age related neurodegeneration. There is still much to be explored, as previously stated, investigations are underway as to whether there may be functional redundancy between PI3KC2α/β, which may reveal yet unknown roles for these proteins in cellular function or exacerbate phenotypes of individual loss. Additionally, further studies are planned to ascertain exactly how PI3KC2β is involved in LTP formation, excitatory vs inhibitory signalling and whether it has further implications on animal behaviour.

6 References

Acosta-Jaquez, H. A., Keller, J. A., Foster, K. G., Ekim, B., Soliman, G. A., Feener, E. P., Ballif, B. A., & Fingar, D. C. (2009). Site-Specific mTOR Phosphorylation Promotes mTORC1-Mediated Signaling and Cell Growth. *Molecular and Cellular Biology*, *29*(15), 4308–4324. https://doi.org/10.1128/mcb.01665-08

Adams, D. J., Arthur, C. P., & Stowell, M. H. B. (2015). Architecture of the Synaptophysin/Synaptobrevin Complex: Structural Evidence for an Entropic Clustering Function at the Synapse. *Scientific Reports*, *5*(July), 1–9. https://doi.org/10.1038/srep13659

Agranoff, B. W. (2009). Turtles all the way: Reflections on myo-inositol. *Journal of Biological Chemistry*, *284*(32), 21121–21126. https://doi.org/10.1074/jbc.X109.004747

Allen, T. G., & Brown, D. A. (1993). M2 muscarinic receptor-mediated inhibition of the Ca2+ current in rat magnocellular cholinergic basal forebrain neurones. *The Journal of Physiology*, *466*(1), 173–189. https://doi.org/10.1113/jphysiol.1993.sp019715

André, V., Marescaux, C., Nehlig, A., & Fritschy, J. M. (2001). Alterations of hippocampal GABAergic system contribute to development of spontaneous recurrent seizures in the rat lithium-pilocarpine model of temporal lobe epilepsy. *Hippocampus*, *11*(4), 452–468. https://doi.org/10.1002/hipo.1060

Aoyagi, K., Sugaya, T., Umeda, M., Yamamoto, S., Terakawa, S., & Takahashi, M. (2005). The activation of exocytotic sites by the formation of phosphatidylinositol 4,5-bisphosphate microdomains at syntaxin clusters. *Journal of Biological Chemistry*, *280*(17), 17346–17352. https://doi.org/10.1074/jbc.M413307200

Aung, K. T., Yoshioka, K., Aki, S., Ishimaru, K., Takuwa, N., & Takuwa, Y. (2019). The class II phosphoinositide 3-kinases PI3K-C2α and PI3K-C2β differentially regulate clathrin-dependent pinocytosis in human vascular endothelial cells. *Journal of Physiological Sciences*, *69*(2), 263–280. https://doi.org/10.1007/s12576-018-0644-2

Avinoam, O., Schorb, M., Beese, C. J., Briggs, J. A. G., & Kaksonen, M. (2015). Endocytic sites mature by continuous bending and remodeling of the clathrin coat. *Science*, *348*(6241), 1369–1372. https://doi.org/10.1126/science.aaa9555

Balla, T. (2013). Phosphoinositides: Tiny lipids with giant impact on cell regulation. *Physiological Reviews*, *93*(3), 1019–1137. https://doi.org/10.1152/physrev.00028.2012

Banaszynski, L. A., Liu, C. W., & Wandless, T. J. (2005). Characterization of the FKBP-rapamycin-FRB ternary complex. *Journal of the American Chemical Society*, *127*(13), 4715–4721. https://doi.org/10.1021/ja043277y

Baran, H., Kepplinger, B., Draxler, M., & Skofitsch, G. (2004). Choline acetyltransferase, glutamic acid decarboxylase and somatostatin in the kainic acid model for chronic temporal lobe epilepsy. *NeuroSignals*, *13*(6), 290–297. https://doi.org/10.1159/000081964

Barker, Kathy. (2005). At the Bench: A Laboratory Navigator. Updated. Seattle: The Institute for Systems Biology. Page: 279-312.

Bartley, A. F., & Dobrunz, L. E. (2015). Short-term plasticity regulates the excitation/inhibition ratio and the temporal window for spike integration in CA1 pyramidal cells. *European Journal of Neuroscience*, *41*(11), 1402–1415. https://doi.org/10.1111/ejn.12898

Bateup, H. S., Johnson, C. A., Denefrio, C. L., Saulnier, J. L., Kornacker, K., & Sabatini, B. L. (2013). Excitatory/Inhibitory Synaptic Imbalance Leads to Hippocampal Hyperexcitability in Mouse Models of Tuberous Sclerosis. *Neuron*, *78*(3), 510–522. https://doi.org/10.1016/j.neuron.2013.03.017

Baudry, M., Chou, M. M., & Bi, X. (2013). Targeting calpain in synaptic plasticity. *Expert Opinion on*

Therapeutic Targets, *17*(5), 579–592. https://doi.org/10.1517/14728222.2013.766169

Ben-Sahra, I., Howell, J. J., Asara, J. M., & Manning, B. D. (2013). Stimulation of de Novo Pyrimidine Synthesis by Growth Signaling Through mTOR and S6K1. *Science*, *339*(6125), 1323–1328. https://doi.org/10.1126/science.1228792

Berridge, M. J. (2006). Calcium microdomains: Organization and function. *Cell Calcium*, *40*(5–6), 405–412. https://doi.org/10.1016/j.ceca.2006.09.002

Betz, C., & Hall, M. N. (2013). Where is mTOR and what is it doing there? *Journal of Cell Biology*, *203*(4), 563–574. https://doi.org/10.1083/jcb.201306041

Bierer, B. E., Mattila, P. S., Standaert, R. F., Herzenberg, L. A., Burakoff, S. J., Crabtree, G., & Schreiber, S. L. (1990). Two distinct signal transmission pathways in T lymphocytes are inhibited by complexes formed between an immunophilin and either FK506 or rapamycin. *Proceedings of the National Academy of Sciences of the United States of America*, *87*(23), 9231–9235. https://doi.org/10.1073/pnas.87.23.9231

Bliss, T. V. P., & Gardner-Medwin, A. R. (1973). Long-lasting potentiation of synaptic transmission in the dentate area of the unanaesthetized rabbit following stimulation of the perforant path. *The Journal of Physiology*, *232*(2), 357–374. https://doi.org/10.1113/jphysiol.1973.sp010274

Borner, G. H. H., Harbour, M., Hester, S., Lilley, K. S., & Robinson, M. S. (2006). Comparative proteomics of clathrin-coated vesicles. *Journal of Cell Biology*, *175*(4), 571–578. https://doi.org/10.1083/jcb.200607164

Boukhalfa, A., Nascimbeni, A. C., Ramel, D., Dupont, N., Hirsch, E., Gayral, S., Laffargue, M., Codogno, P., & Morel, E. (2020). PI3KC2α-dependent and VPS34-independent generation of PI3P controls primary cilium-mediated autophagy in response to shear stress. *Nature Communications*, *11*(1), 1–9. https://doi.org/10.1038/s41467-019-14086-1

Brown, D. A. (2010). Muscarinic acetylcholine receptors (mAChRs) in the nervous system: Some functions and mechanisms. *Journal of Molecular Neuroscience*, *41*(3), 340–346. https://doi.org/10.1007/s12031-010-9377-2

Brown, D. A., Hughes, S. A., Marsh, S. J., & Tinker, A. (2007). Regulation of M(Kv7.2/7.3) channels in neurons by PIP2 and products of PIP2 hydrolysis: Significance for receptor-mediated inhibition. *Journal of Physiology*, *582*(3), 917–925. https://doi.org/10.1113/jphysiol.2007.132498

Buckmaster, P. S., Yamawaki, R., & Thind, K. (2016). More docked vesicles and larger active zones at basket cell-to-granule cell synapses in a rat model of temporal lobe epilepsy. *Journal of Neuroscience*, *36*(11), 3295–3308. https://doi.org/10.1523/JNEUROSCI.4049-15.2016

Burd, C. G., & Emr, S. D. (1998). Phosphatidylinositol(3)-phosphate signaling mediated by specific binding to RING FYVE domains. *Molecular Cell*, *2*(1), 157–162. https://doi.org/10.1016/S1097-2765(00)80125-2

Cafferkey, R., Young, P. R., McLaughlin, M. M., Bergsma, D. J., Koltin, Y., Sathe, G. M., Faucette, L., Eng, W. K., Johnson, R. K., & Livi, G. P. (1993). Dominant missense mutations in a novel yeast protein related to mammalian phosphatidylinositol 3-kinase and VPS34 abrogate rapamycin cytotoxicity. *Molecular and Cellular Biology*, *13*(10), 6012–6023. https://doi.org/10.1128/mcb.13.10.6012

Calne, R. Y., Lim, S., Samaan, A., Collier, D. S. J., Pollard, S. G., White, D. J. G., & Thiru, S. (1989). Rapamycin for Immunosuppression in Organ Allografting. *The Lancet*, *334*(8656), 227. https://doi.org/10.1016/S0140-6736(89)90417-0

Cammalleri, M., Lütjens, R., Berton, F., King, A. R., Simpson, C., Francesconi, W., & Sanna, P. P. (2003). Time-restricted role for dendritic activation of the mTOR-p70 S6K pathway in the induction of late-phase long-term potentiation in the CA1. *Proceedings of the National*

Academy of Sciences of the United States of America, *100*(SUPPL. 2), 14368–14373. https://doi.org/10.1073/pnas.2336098100

Campa, C. C., Margaria, J. P., Derle, A., Del Giudice, M., De Santis, M. C., Gozzelino, L., Copperi, F., Bosia, C., & Hirsch, E. (2018). Rab11 activity and PtdIns(3)P turnover removes recycling cargo from endosomes. *Nature Chemical Biology*, *14*(8), 801–810. https://doi.org/10.1038/s41589-018-0086-4

Campelo, F., McMahon, H. T., & Kozlov, M. M. (2008). The hydrophobic insertion mechanism of membrane curvature generation by proteins. *Biophysical Journal*, *95*(5), 2325–2339. https://doi.org/10.1529/biophysj.108.133173

Carlin, R. K., Grab, D. J., Cohen, R. S., & Siekevitz, P. (1980). Isolation and characterization of postsynaptic densities from various brain regions: Enrichment of different types of postsynaptic densities. *Journal of Cell Biology*, *86*(3), 831–843. https://doi.org/10.1083/jcb.86.3.831

Castillo, J. D., & Katz, B. . (1953). Statistical Nature of 'Facilitation' at a Single Nerve–Muscle Junction. *Nature*, *171*(4362), 1016–1017. https://doi.org/10.1038/1711016a0.

Caulfield, M. P., & Birdsall, N. J. M. (1998). International union of pharmacology. XVII. Classification of muscarinic acetylcholine receptors. *Pharmacological Reviews*, *50*(2), 279–290.

Chatzikonstantinou, A. (2014). Epilepsy and the hippocampus. *The Hippocampus in Clinical Neuroscience*, *34*, 121–142. https://doi.org/10.1159/000356435

Chen, C. Y., Chen, J., He, L., & Stiles, B. L. (2018). PTEN: Tumor suppressor and metabolic regulator. *Frontiers in Endocrinology*, *9*(JUL), 1–12. https://doi.org/10.3389/fendo.2018.00338

Chen, Y. J., Zhang, P., Egelman, E. H., & Hinshaw, J. E. (2004). The stalk region of dynamin drives the constriction of dynamin tubes. *Nature Structural and Molecular Biology*, *11*(6), 574–575. https://doi.org/10.1038/nsmb762

Cheng, S. Y., Wang, S. C., Lei, M., Wang, Z., & Xiong, K. (2018). Regulatory role of calpain in neuronal death. *Neural Regeneration Research*, *13*(3), 556–562. https://doi.org/10.4103/1673-5374.228762

Chéreau, R., Saraceno, G. E., Angibaud, J., Cattaert, D., & Nägerl, U. V. (2017). Superresolution imaging reveals activity-dependent plasticity of axon morphology linked to changes in action potential conduction velocity. *Proceedings of the National Academy of Sciences of the United States of America*, *114*(6), 1401–1406. https://doi.org/10.1073/pnas.1607541114

Chesler, M. (2003). Regulation and modulation of pH in the brain. *Physiological Reviews*, *83*(4), 1183–1221. https://doi.org/10.1152/physrev.00010.2003

Clements, J. D., Lester, R. A. J., Tong, G., Jahr, C. E., & Westbrook, G. L. (1992). The time course of glutamate in the synaptic cleft. *Science*, *258*(5087), 1498–1501. https://doi.org/10.1126/science.1359647

Cloëtta, D., Thomanetz, V., Baranek, C., Lustenberger, R. M., Lin, S., Oliveri, F., Atanasoski, S., & Rüegg, M. A. (2013). Inactivation of mTORC1 in the developing brain causes microcephaly and affects gliogenesis. *Journal of Neuroscience*, *33*(18), 7799–7810. https://doi.org/10.1523/JNEUROSCI.3294-12.2013

Cocucci, E., Aguet, F., Boulant, S., & Kirchhausen, T. (2012). The First Five Seconds in the Life of a Clathrin-Coated Pit. *Cell*, *150*(3), 495–507. https://doi.org/10.1016/j.cell.2012.05.047

Coombs, J. S., Eccles, J. C., & Fatt, P. (1955). The inhibitory suppression of reflex discharges from motoneurones. *The Journal of Physiology*, *130*(2), 396–413. https://doi.org/10.1113/jphysiol.1955.sp005414

Cossart, R., Dinocourt, C., Hirsch, J. C., Merchan-Perez, A., De Felipe, J., Ben-Ari, Y., Esclapez, M., & Bernard, C. (2001). Dendritic but not somatic GABAergic inhibition is decreased in experimental epilepsy. *Nature Neuroscience*, *4*(1), 52–62. https://doi.org/10.1038/82900

Cota, D., Proulx, K., Blake Smith, K. A., Kozma, S. C., Thomas, G., Woods, S. C., & Seeley, R. J. (2006). Hypothalamic mTOR signaling regulates food intake. *Science*, *312*(5775), 927–930. https://doi.org/10.1126/science.1124147

Coultrap, S. J., Freund, R. K., O'Leary, H., Sanderson, J. L., Roche, K. W., Dell'Acqua, M. L., & Bayer, K. U. (2014). Autonomous CaMKII Mediates Both LTP and LTD Using a Mechanism for Differential Substrate Site Selection. *Cell Reports*, *6*(3), 431–437. https://doi.org/10.1016/j.celrep.2014.01.005

Cullen, P. J. (2008). Endosomal sorting and signalling: an emerging role for sorting nexins. *Nature Reviews Molecular Cell Biology*, *9*(7), 574–582. https://doi.org/10.1038/nrm2427

Cunningham, J. T., Rodgers, J. T., Arlow, D. H., Vazquez, F., Mootha, V. K., & Puigserver, P. (2007). mTOR controls mitochondrial oxidative function through a YY1-PGC-1α transcriptional complex. *Nature*, *450*(7170), 736–740. https://doi.org/10.1038/nature06322

D'Andrea Meira, I., Romão, T. T., Do Prado, H. J. P., Krüger, L. T., Pires, M. E. P., & Da Conceição, P. O. (2019). Ketogenic diet and epilepsy: What we know so far. *Frontiers in Neuroscience*, *13*(JAN), 1–8. https://doi.org/10.3389/fnins.2019.00005

Dan, H. C., Ebbs, A., Pasparakis, M., Van Dyke, T., Basseres, D. S., & Baldwin, A. S. (2014). Akt-dependent activation of mTORC1 complex involves phosphorylation of mTOR (mammalian target of rapamycin) by IκB kinase α (IKKα). *Journal of Biological Chemistry*, *289*(36), 25227–25240. https://doi.org/10.1074/jbc.M114.554881

Darcy, K. J., Staras, K., Collinson, L. M., & Goda, Y. (2006). Constitutive sharing of recycling synaptic vesicles between presynaptic boutons. *Nature Neuroscience*, *9*(3), 315–321. https://doi.org/10.1038/nn1640

Davies, B., Kearns, I. R., Ure, J., Davies, C. H., & Lathe, R. (2001). Loss of hippocampal serine protease BSP1/neuropsin predisposes to global seizure activity. *Journal of Neuroscience*, *21*(18), 6993–7000. https://doi.org/10.1523/jneurosci.21-18-06993.2001

Davies, C. H., Davies, S. N., & Collingridge, G. L. (1990). Paired-pulse depression of monosynaptic GABA-mediated inhibitory postsynaptic responses in rat hippocampus. *The Journal of Physiology*, *424*(1), 513–531. https://doi.org/10.1113/jphysiol.1990.sp018080

Dayas, C. V., Smith, D. W., & Dunkley, P. R. (2012). An emerging role for the mammalian target of rapamycin in "pathological" protein translation: relevance to cocaine addiction. *Frontiers in Pharmacology*, *3 FEB*(February), 1–12. https://doi.org/10.3389/fphar.2012.00013

De Santis, M. C., Gulluni, F., Campa, C. C., Martini, M., & Hirsch, E. (2019). Targeting PI3K signaling in cancer: Challenges and advances. *Biochimica et Biophysica Acta - Reviews on Cancer*, *1871*(2), 361–366. https://doi.org/10.1016/j.bbcan.2019.03.003

Denker, A., Bethani, I., Kröhnert, K., Körber, C., Horstmann, H., Wilhelm, B. G., Barysch, S. V., Kuner, T., Neher, E., & Rizzoli, S. O. (2011). A small pool of vesicles maintains synaptic activity in vivo. *Proceedings of the National Academy of Sciences of the United States of America*, *108*(41), 17177–17182. https://doi.org/10.1073/pnas.1112688108

Denker, A., & Rizzoli, S. O. (2010). Synaptic vesicle pools: An update. *Frontiers in Synaptic Neuroscience*, *2*(OCT), 1–12. https://doi.org/10.3389/fnsyn.2010.00135

Dennis, S. H., Pasqui, F., Colvin, E. M., Sanger, H., Mogg, A. J., Felder, C. C., Broad, L. M., Fitzjohn, S. M., Isaac, J. T. R., & Mellor, J. R. (2016). Activation of Muscarinic M1 Acetylcholine Receptors Induces Long-Term Potentiation in the Hippocampus. *Cerebral Cortex*, *26*(1), 414–426. https://doi.org/10.1093/cercor/bhv227

Dhindsa, R. S., Bradrick, S. S., Yao, X., Heinzen, E. L., Petrovski, S., Krueger, B. J., Johnson, M. R., Frankel, W. N., Petrou, S., Boumil, R. M., & Goldstein, D. B. (2015). Epileptic encephalopathy-causing mutations in DNM1 impair synaptic vesicle endocytosis. *Neurology: Genetics*, *1*(1). https://doi.org/10.1212/01.NXG.0000464295.65736.da

Dibble, C. C., & Cantley, L. C. (2015). Regulation of mTORC1 by PI3K signaling. *Trends in Cell Biology*, *25*(9), 545–555. https://doi.org/10.1016/j.tcb.2015.06.002

Diering, G. H., & Huganir, R. L. (2018). The AMPA Receptor Code of Synaptic Plasticity. *Neuron*, *100*(2), 314–329. https://doi.org/10.1016/j.neuron.2018.10.018

Diril, M. K., Wienisch, M., Jung, N., Klingauf, J., & Haucke, V. (2006). Stonin 2 is an AP-2-dependent endocytic sorting adaptor for synaptotagmin internalization and recycling. *Developmental Cell*, *10*(2), 233–244. https://doi.org/10.1016/j.devcel.2005.12.011

Doyle, C. A., Cullen, W. K., Rowan, M. J., & Anwyl, R. (1997). Low-frequency stimulation induces homosynaptic depotentiation but not long-term depression of synaptic transmission in the adult anaesthetized and awake rat hippocampus in vivo. *Neuroscience*, *77*(1), 75–85. https://doi.org/10.1016/S0306-4522(96)00427-7

Dufner, A., & Thomas, G. (1999). Ribosomal S6 kinase signaling and the control of translation. *Experimental Cell Research*, *253*(1), 100–109. https://doi.org/10.1006/excr.1999.4683

Dulubova, I., Sugita, S., Hill, S., Hosaka, M., Fernandez, I., Südhof, T. C., & Rizo, J. (1999). A conformational switch in syntaxin during exocytosis: Role of munc18. *EMBO Journal*, *18*(16), 4372–4382. https://doi.org/10.1093/emboj/18.16.4372

Durrant, T. N., & Hers, I. (2020). PI3K inhibitors in thrombosis and cardiovascular disease. *Clinical and Translational Medicine*, *9*(1), 8. https://doi.org/10.1186/s40169-020-0261-6

Edmonds, B., Gibb, A. J., & Colquhoun, D. (1995). Mechanisms of Activation of Glutamate Receptors and the Time Course of Excitatory Synaptic Currents. *Annual Review of Physiology*, *57*(1), 495–519. https://doi.org/10.1146/annurev.ph.57.030195.002431

Edwards, R. H. (2007). The Neurotransmitter Cycle and Quantal Size. *Neuron*, *55*(6), 835–858. https://doi.org/10.1016/j.neuron.2007.09.001

Erdmann, K. S., Mao, Y., McCrea, H. J., Zoncu, R., Lee, S., Paradise, S., Modregger, J., Biemesderfer, D., Toomre, D., & De Camilli, P. (2007). A Role of the Lowe Syndrome Protein OCRL in Early Steps of the Endocytic Pathway. *Developmental Cell*, *13*(3), 377–390. https://doi.org/10.1016/j.devcel.2007.08.004

Falasca, M., Hughes, W. E., Dominguez, V., Sala, G., Fostira, F., Fang, M. Q., Cazzolli, R., Shepherd, P. R., James, D. E., & Maffucci, T. (2007). The role of phosphoinositide 3-kinase C2α in insulin signaling. *Journal of Biological Chemistry*, *282*(38), 28226–28236. https://doi.org/10.1074/jbc.M704357200

Farsi, Z., Jahn, R., & Woehler, A. (2017). Proton electrochemical gradient: Driving and regulating neurotransmitter uptake. *BioEssays*, *39*(5), 1–9. https://doi.org/10.1002/bies.201600240

Feng, Y., Backues, S. K., Baba, M., Heo, J. M., Harper, J. W., & Klionsky, D. J. (2016). Phosphorylation of Atg9 regulates movement to the phagophore assembly site and the rate of autophagosome formation. *Autophagy*, *12*(4), 648–658. https://doi.org/10.1080/15548627.2016.1157237

Feng, Y. C. A., Howrigan, D. P., Abbott, L. E., Tashman, K., Cerrato, F., Singh, T., Heyne, H., Byrnes, A., Churchhouse, C., Watts, N., Solomonson, M., Lal, D., Heinzen, E. L., Dhindsa, R. S., Stanley, K. E., Cavalleri, G. L., Hakonarson, H., Helbig, I., Krause, R., … Neale, B. M. (2019). Ultra-Rare Genetic Variation in the Epilepsies: A Whole-Exome Sequencing Study of 17,606 Individuals. *American Journal of Human Genetics*, *105*(2), 267–282. https://doi.org/10.1016/j.ajhg.2019.05.020

Fernández-Alfonso, T., Kwan, R., & Ryan, T. A. (2006). Synaptic Vesicles Interchange Their

Membrane Proteins with a Large Surface Reservoir during Recycling. *Neuron*, *51*(2), 179–186. https://doi.org/10.1016/j.neuron.2006.06.008

Fernández-Fernández, J. M., Abogadie, F. C., Milligan, G., Delmas, P., & Brown, D. A. (2001). Multiple pertussis toxin-sensitive G-proteins can couple receptors to GIRK channels in rat sympathetic neurons when expressed heterologously, but only native Gi-proteins do so in situ. *European Journal of Neuroscience*, *14*(2), 283–292. https://doi.org/10.1046/j.0953-816X.2001.01642.x

Ferrari, S., Bandi, H. R., Hofsteenge, J., Bussian, B. M., & Thomas, G. (1991). Mitogen-activated 70K S6 kinase. Identification of in vitro 40 S ribosomal S6 phosphorylation sites. *Journal of Biological Chemistry*, *266*(33), 22770–22775.

Fierro, L., & Llano, I. (1996). High endogenous calcium buffering in Purkinje cells from rat cerebellar slices. *Journal of Physiology*, *496*(3), 617–625. https://doi.org/10.1113/jphysiol.1996.sp021713

Franco, I., Gulluni, F., Campa, C. C., Costa, C., Margaria, J. P., Ciraolo, E., Martini, M., Monteyne, D., De Luca, E., Germena, G., Posor, Y., Maffucci, T., Marengo, S., Haucke, V., Falasca, M., Perez-Morga, D., Boletta, A., Merlo, G. R., & Hirsch, E. (2014). PI3K class II α controls spatially restricted endosomal PtdIns3P and Rab11 activation to promote primary cilium function. *Developmental Cell*, *28*(6), 647–658. https://doi.org/10.1016/j.devcel.2014.01.022

Franke, T. F. (2008). PI3K/Akt: Getting it right matters. *Oncogene*, *27*(50), 6473–6488. https://doi.org/10.1038/onc.2008.313

Freund, T. F. (2003). Interneuron Diversity series: Rhythm and mood in perisomatic inhibition. *Trends in Neurosciences*, *26*(9), 489–495. https://doi.org/10.1016/S0166-2236(03)00227-3

Fromer, M., Pocklington, A. J., Kavanagh, D. H., Williams, H. J., Dwyer, S., Gormley, P., Georgieva, L., Rees, E., Palta, P., Ruderfer, D. M., Carrera, N., Humphreys, I., Johnson, J. S., Roussos, P., Barker, D. D., Banks, E., Milanova, V., Grant, S. G., Hannon, E., … O'Donovan, M. C. (2014). De novo mutations in schizophrenia implicate synaptic networks. *Nature*, *506*(7487), 179–184. https://doi.org/10.1038/nature12929

Gaidarov, I., Smith, M. E. K., Domin, J., & Keen, J. H. (2001). The class II phosphoinositide 3-kinase C2α is activated by clathrin and regulates clathrin-mediated membrane trafficking. *Molecular Cell*, *7*(2), 443–449. https://doi.org/10.1016/S1097-2765(01)00191-5

Galanopoulou, A. S., Gorter, J. A., & Cepeda, C. (2012). Finding a better drug for epilepsy: The mTOR pathway as an antiepileptogenic target. *Epilepsia*, *53*(7), 1119–1130. https://doi.org/10.1111/j.1528-1167.2012.03506.x

Gamlin, C. R., Yu, W. Q., Wong, R. O. L., & Hoon, M. (2018). Assembly and maintenance of GABAergic and Glycinergic circuits in the mammalian nervous system. *Neural Development*, *13*(1), 1–17. https://doi.org/10.1186/s13064-018-0109-6

Gao, X. (2001). TSC1 and TSC2 tumor suppressors antagonize insulin signaling in cell growth. *Genes & Development*, *15*(11), 1383–1392. https://doi.org/10.1101/gad.901101

Garami, A., Zwartkruis, F. J. T., Nobukuni, T., Joaquin, M., Roccio, M., Stocker, H., Kozma, S. C., Hafen, E., Bos, J. L., & Thomas, G. (2003). Insulin activation of Rheb, a mediator of mTOR/S6K/4E-BP signaling, is inhibited by TSC1 and 2. *Molecular Cell*, *11*(6), 1457–1466. https://doi.org/10.1016/S1097-2765(03)00220-X

Gasnier, B. (2000). The loading of neurotransmitters into synaptic vesicles. *Biochimie*, *82*(4), 327–337. https://doi.org/10.1016/S0300-9084(00)00221-2

Ge, H., Tan, L., Wu, P., Yin, Y., Liu, X., Meng, H., Cui, G., Wu, N., Lin, J., Hu, R., & Feng, H. (2015). Poly-L-ornithine promotes preferred differentiation of neural stem/progenitor cells via ERK signalling pathway. *Scientific Reports*, *5*(October), 1–10. https://doi.org/10.1038/srep15535

Ghosh Mazumder, A., Shantaram Padwad, Y., & Singh, D. (2016). Anticancer Mammalian Target of Rapamycin (mTOR) Signaling Pathway Inhibitors: Current Status, Challenges and Future Prospects in Management of Epilepsy. *CNS & Neurological Disorders - Drug Targets*, *15*(8), 945–955. https://doi.org/10.2174/1871527315666160615022203

Giesemann, T., Schwarz, G., Nawrotzki, R., Berhörster, K., Rothkegel, M., Schlüter, K., Schrader, N., Schindelin, H., Mendel, R. R., Kirsch, J., & Jockusch, B. M. (2003). Complex formation between the postsynaptic scaffolding protein gephyrin, profilin, and Mena: A possible link to the microfilament system. *Journal of Neuroscience*, *23*(23), 8330–8339. https://doi.org/10.1523/jneurosci.23-23-08330.2003

Giorgi, F. S., Biagioni, F., Lenzi, P., Frati, A., & Fornai, F. (2015). The role of autophagy in epileptogenesis and in epilepsy-induced neuronal alterations. *Journal of Neural Transmission*, *122*(6), 849–862. https://doi.org/10.1007/s00702-014-1312-1

Glatigny, M., Moriceau, S., Rivagorda, M., Ramos-Brossier, M., Nascimbeni, A. C., Lante, F., Shanley, M. R., Boudarene, N., Rousseaud, A., Friedman, A. K., Settembre, C., Kuperwasser, N., Friedlander, G., Buisson, A., Morel, E., Codogno, P., & Oury, F. (2019). Autophagy Is Required for Memory Formation and Reverses Age-Related Memory Decline. *Current Biology*, *29*(3), 435-448.e8. https://doi.org/10.1016/j.cub.2018.12.021

Gray, B. E. G. (1959). Axo-somatic and axo-dendrtic synapses of the ceberal cortex: an electron microscope study. *J Anat.*, 420–433. https://pubmed.ncbi.nlm.nih.gov/13829103/

Greene, L. E., & Eisenberg, E. (1990). Dissociation of clathrin from coated vesicles by the uncoating ATPase. *Journal of Biological Chemistry*, *265*(12), 6682–6687.

Griffith, J. L., & Wong, M. (2018). The mTOR pathway in treatment of epilepsy: A clinical update. *Future Neurology*, *13*(2), 49–58. https://doi.org/10.2217/fnl-2018-0001

Gross, O. P., & von Gersdorff, H. (2016). Recycling at synapses. *ELife*, *5*(MAY2016), 3–5. https://doi.org/10.7554/eLife.17692

Gulluni, F., Martini, M., De Santis, M. C., Campa, C. C., Ghigo, A., Margaria, J. P., Ciraolo, E., Franco, I., Ala, U., Annaratone, L., Disalvatore, D., Bertalot, G., Viale, G., Noatynska, A., Compagno, M., Sigismund, S., Montemurro, F., Thelen, M., Fan, F., … Hirsch, E. (2017). Mitotic Spindle Assembly and Genomic Stability in Breast Cancer Require PI3K-C2α Scaffolding Function. *Cancer Cell*, *32*(4), 444-459.e7. https://doi.org/10.1016/j.ccell.2017.09.002

Gwinn, D. M., Shackelford, D. B., Egan, D. F., Mihaylova, M. M., Mery, A., Vasquez, D. S., Turk, B. E., & Shaw, R. J. (2008). AMPK Phosphorylation of Raptor Mediates a Metabolic Checkpoint. *Molecular Cell*, *30*(2), 214–226. https://doi.org/10.1016/j.molcel.2008.03.003

Haji, N., Riebe, I., Aguilar-Valles, A., Artinian, J., Laplante, I., & Lacaille, J. C. (2020). Tsc1 haploinsufficiency in Nkx2.1 cells upregulates hippocampal interneuron mTORC1 activity, impairs pyramidal cell synaptic inhibition, and alters contextual fear discrimination and spatial working memory in mice. *Molecular Autism*, *11*(1), 29. https://doi.org/10.1186/s13229-020-00340-7

Han, X., & Jackson, M. B. (2006). Structural transitions in the synaptic SNARE complex during Ca 2+-triggered exocytosis. *Journal of Cell Biology*, *172*(2), 281–293. https://doi.org/10.1083/jcb.200510012

Han, Z. J., Xue, W. W., Tao, L., & Zhu, F. (2018). Identification of novel immune-relevant drug target genes for Alzheimer's Disease by combining ontology inference with network analysis. *CNS Neuroscience and Therapeutics*, *24*(12), 1253–1263. https://doi.org/10.1111/cns.13051

Harada, K., Truong, A. B., Cai, T., & Khavari, P. A. (2005). The Class II Phosphoinositide 3-Kinase C2β Is Not Essential for Epidermal Differentiation. *Molecular and Cellular Biology*, *25*(24), 11122–11130. https://doi.org/10.1128/mcb.25.24.11122-11130.2005

Haucke, V., & Kozlov, M. M. (2018). Membrane remodeling in clathrin-mediated endocytosis. *Journal of Cell Science*, *131*(17), 1–10. https://doi.org/10.1242/jcs.216812

Hausch, F., Kozany, C., Theodoropoulou, M., & Fabian, A. K. (2013). FKBPs and the Akt/mTOR pathway. *Cell Cycle*, *12*(15), 2366–2370. https://doi.org/10.4161/cc.25508

Hayashi, M. K., Tang, C., Verpelli, C., Narayanan, R., Stearns, M. H., Xu, R., Li, H., Sala, C., & Hayashi, Y. (2009). The Postsynaptic Density Proteins Homer and Shank Form a Polymeric Network Structure. *Cell*, *137*(1), 159–171. https://doi.org/10.1016/j.cell.2009.01.050

Hayashi, S., & McMahon, A. P. (2002). Efficient recombination in diverse tissues by a tamoxifen-inducible form of Cre: A tool for temporally regulated gene activation/inactivation in the mouse. *Developmental Biology*, *244*(2), 305–318. https://doi.org/10.1006/dbio.2002.0597

He, K., Marsland III, R., Upadhyayula, S., Song, E., Dang, S., Capraro, B. R., Wang, W., Skillern, W., Gaudin, R., Ma, M., & Kirchhausen, T. (2017). Dynamics of phosphoinositide conversion in clathrin-mediated endocytic traffic. *Nature*, *552*(7685), 410–414. https://doi.org/10.1038/nature25146

He, R., Zhang, J., Yu, Y., Jizi, L., Wang, W., & Li, M. (2018). New Insights Into Interactions of Presynaptic Calcium Channel Subtypes and SNARE Proteins in Neurotransmitter Release. *Frontiers in Molecular Neuroscience*, *11*(July), 1–11. https://doi.org/10.3389/fnmol.2018.00213

Heckly, R. J., & Dimmick, R. L. (1978). Protection kinetics of additives on survival of lyophilized bacteria. In *Cryobiology* (Vol. 15, Issue 6).

Heim, R., Prashert, D. C., Tsien, R. Y., & Kandel, E. R. (1994). Wavelength mutations and posttranslational autoxidation of green fluorescent protein (Aequorea victoria/blue fluorescent protein/Escherichia coli/imidazolidinone). *Biochemistry*, *91*(December), 12501–12504.

Hell, J. W. (2014). CaMKII: Claiming Center Stage in Postsynaptic Function and Organization. *Neuron*, *81*(2), 249–265. https://doi.org/10.1016/j.neuron.2013.12.024

Hemmings, B. A., & Restuccia, D. F. (2015). The PI3k-PKB/Akt pathway. *Cold Spring Harbor Perspectives in Biology*, *7*(4), 3–5. https://doi.org/10.1101/cshperspect.a011189

Hentschke, M., Wiemann, M., Hentschke, S., Kurth, I., Hermans-Borgmeyer, I., Seidenbecher, T., Jentsch, T. J., Gal, A., & Hübner, C. A. (2006). Mice with a Targeted Disruption of the Cl–/HCO3– Exchanger AE3 Display a Reduced Seizure Threshold. *Molecular and Cellular Biology*, *26*(1), 182–191. https://doi.org/10.1128/mcb.26.1.182-191.2006

Hernandez, D., Torres, C. A., Setlik, W., Cebrián, C., Mosharov, E. V., Tang, G., Cheng, H.-C., Kholodilov, N., Yarygina, O., Burke, R. E., Gershon, M., & Sulzer, D. (2012). Regulation of Presynaptic Neurotransmission by Macroautophagy. *Neuron*, *74*(2), 277–284. https://doi.org/10.1016/j.neuron.2012.02.020

Heuser, J. E., & Reese, T. S. (1981). Structural changes after transmitter release at the frog neuromuscular junction. *Journal of Cell Biology*, *88*(3), 564–580. https://doi.org/10.1083/jcb.88.3.564

Hodgkin, A. L., & Huxley, A. F. (1952). A quantitative description of membrane current and its application to conduction and excitation in nerve. *The Journal of Physiology*, *117*(4), 500–544. https://doi.org/10.1113/jphysiol.1952.sp004764

Hoeffer, C. A., & Klann, E. (2010). mTOR signaling: At the crossroads of plasticity, memory and disease. *Trends in Neurosciences*, *33*(2), 67–75. https://doi.org/10.1016/j.tins.2009.11.003

Hoffmann, S., Orlando, M., Andrzejak, E., Bruns, C., Trimbuch, T., Rosenmund, C., Garner, C. C., & Ackermann, F. (2019). Light-activated ROS production induces synaptic autophagy. *Journal of Neuroscience*, *39*(12), 2163–2183. https://doi.org/10.1523/JNEUROSCI.1317-18.2019

Hokin, R.; Hokin, L. (1953). Enzyme Secretion and the Incorporation of P32 Into Phospholipides of Pancreas Slices. *J. Bio. Chem.*, *203*, 967–977.

Holz, M. K., & Blenis, J. (2005). Identification of S6 kinase 1 as a novel mammalian target of rapamycin (mTOR)-phosphorylating kinase. *Journal of Biological Chemistry*, *280*(28), 26089–26093. https://doi.org/10.1074/jbc.M504045200

Honigmann, A., van den Bogaart, G., Iraheta, E., Risselada, H. J., Milovanovic, D., Mueller, V., Müllar, S., Diederichsen, U., Fasshauer, D., Grubmüller, H., Hell, S. W., Eggeling, C., Kühnel, K., & Jahn, R. (2013). Phosphatidylinositol 4,5-bisphosphate clusters act as molecular beacons for vesicle recruitment. *Nature Structural & Molecular Biology*, *20*(6), 679–686. https://doi.org/10.1038/nsmb.2570

Höning, S., Ricotta, D., Krauss, M., Späte, K., Spolaore, B., Motley, A., Robinson, M., Robinson, C., Haucke, V., & Owen, D. J. (2005). Phosphatidylinositol-(4,5)-bisphosphate regulates sorting signal recognition by the clathrin-associated adaptor complex AP2. *Molecular Cell*, *18*(5), 519–531. https://doi.org/10.1016/j.molcel.2005.04.019

Horn, J. P., & Dodd, J. (1983). Inhibitory cholinergic synapses in autonomic ganglia. *Trends in Neurosciences*, *6*, 180–184. https://doi.org/10.1016/0166-2236(83)90082-6

Houchens, D. P., Ovejera, A. A., Riblet, S. M., & Slagel, D. E. (1983). Human brain tumor xenografts in nude mice as a chemotherapy model. *European Journal of Cancer and Clinical Oncology*, *19*(6), 799–805. https://doi.org/10.1016/0277-5379(83)90012-3

Huang, J., & Manning, B. D. (2009). A complex interplay between Akt, TSC2 and the two mTOR complexes. *Biochemical Society Transactions*, *37*(1), 217–222. https://doi.org/10.1042/BST0370217

Huang, X., Zhang, H., Yang, J., Wu, J., McMahon, J., Lin, Y., Cao, Z., Gruenthal, M., & Huang, Y. (2010). Pharmacological inhibition of the mammalian target of rapamycin pathway suppresses acquired epilepsy. *Neurobiology of Disease*, *40*(1), 193–199. https://doi.org/10.1016/j.nbd.2010.05.024

Huettner, J. E. (2003). Kainate receptors and synaptic transmission. *Progress in Neurobiology*, *70*(5), 387–407. https://doi.org/10.1016/S0301-0082(03)00122-9

Hulme, E. C., Birdsall, N. J. M., & Buckley, N. J. (1990). Muscarinic receptor subtypes. *Annual Review of Pharmacology and Toxicology*, *30*, 633–673. https://doi.org/10.1146/annurev.pa.30.040190.003221

Hunt, C. A., Schenker, L. J., & Kennedy, M. B. (1996). PSD-95 is associated with the postsynaptic density and not with the presynaptic membrane at forebrain synapses. *Journal of Neuroscience*, *16*(4), 1380–1388. https://doi.org/10.1523/jneurosci.16-04-01380.1996

Irvine, R. (2000). Nuclear Lipid Signaling. *Science Signaling*, *2000*(48), re1–re1. https://doi.org/10.1126/stke.2000.48.re1

Irvine, R. F. (2005). Inositide evolution - Towards turtle domination? *Journal of Physiology*, *566*(2), 295–300. https://doi.org/10.1113/jphysiol.2005.087387

Iwasato, T., Datwani, A., Wolf, A. M., Nishiyama, H., Taguchi, Y., Tonegawa, S., Knöpfel, T., Erzurumlu, R. S., & Itohara, S. (2000). Cortex-restricted disruption of NMDAR1 impairs neuronal patterns in the barrel cortex. *Nature*, *406*(6797), 726–731. https://doi.org/10.1038/35021059

Jaber, N., & Zong, W.-X. (2013). Class III PI3K Vps34: essential roles in autophagy, endocytosis, and heart and liver function. *Annals of the New York Academy of Sciences*, *1280*(1), 48–51. https://doi.org/10.1111/nyas.12026

Jackson, L. P., Kelly, B. T., McCoy, A. J., Gaffry, T., James, L. C., Collins, B. M., Höning, S., Evans, P. R., & Owen, D. J. (2010). A large-scale conformational change couples membrane recruitment

to cargo binding in the AP2 clathrin adaptor complex. *Cell*, *141*(7), 1220–1229. https://doi.org/10.1016/j.cell.2010.05.006

Jäpel, M., Gerth, F., Sakaba, T., Bacetic, J., Yao, L., Koo, S. J., Maritzen, T., Freund, C., & Haucke, V. (2020). Intersectin-Mediated Clearance of SNARE Complexes Is Required for Fast Neurotransmission. *Cell Reports*, *30*(2), 409-420.e6. https://doi.org/10.1016/j.celrep.2019.12.035

Jewell, J. L., Fu, V., Hong, A. W., Yu, F. X., Meng, D., Melick, C. H., Wang, H., Lam, W. L. M., Yuan, H. X., Taylor, S. S., & Guan, K. L. (2019). GPCR signaling inhibits mTORC1 via PKA phosphorylation of raptor. *ELife*, *8*, 1–26. https://doi.org/10.7554/eLife.43038

Ji, C., Fan, F., & Lou, X. (2017). Vesicle Docking Is a Key Target of Local PI(4,5)P 2 Metabolism in the Secretory Pathway of INS-1 Cells. *Cell Reports*, *20*(6), 1409–1421. https://doi.org/10.1016/j.celrep.2017.07.041

Jones, C., Watson, D., & Fone, K. (2011). Animal models of schizophrenia. *British Journal of Pharmacology*, *164*(4), 1162–1194. https://doi.org/10.1111/j.1476-5381.2011.01386.x

Jonkman, J., & Brown, C. M. (2015). Any way you slice it—A comparison of confocal microscopy techniques. *Journal of Biomolecular Techniques*, *26*(2), 54–65. https://doi.org/10.7171/jbt.15-2602-003

Jovanovic, J. N., Sihra, T. S., Nairn, A. C., Hemmings, H. C., Greengard, P., & Czernik, A. J. (2001). Opposing changes in phosphorylation of specific sites in synapsin I during Ca2+-dependent glutamate release in isolated nerve terminals. *Journal of Neuroscience*, *21*(20), 7944–7953. https://doi.org/10.1523/JNEUROSCI.21-20-07944.2001

Kaempf, N., Kochlamazashvili, G., Puchkov, D., Maritzen, T., Bajjalieh, S. M., Kononenko, N. L., & Haucke, V. (2015). Overlapping functions of stonin 2 and SV2 in sorting of the calcium sensor synaptotagmin 1 to synaptic vesicles. *Proceedings of the National Academy of Sciences of the United States of America*, *112*(23), 7297–7302. https://doi.org/10.1073/pnas.1501627112

Kaeser, P. S., Deng, L., Wang, Y., Dulubova, I., Liu, X., Rizo, J., & Südhof, T. C. (2011). RIM proteins tether Ca2+ channels to presynaptic active zones via a direct PDZ-domain interaction. *Cell*, *144*(2), 282–295. https://doi.org/10.1016/j.cell.2010.12.029

Kaeser, P. S., & Regehr, W. G. (2017). The readily releasable pool of synaptic vesicles. *Current Opinion in Neurobiology*, *43*(1), 63–70. https://doi.org/10.1016/j.conb.2016.12.012

Kanaseki, T., & Kadota, K. (1969). The "vesicle in a basket". A morphological study of the coated vesicle isolated from the nerve endings of the guinea pig brain, with special reference to the mechanism of membrane movements. *The Journal of Cell Biology*, *42*(1), 202–220. https://doi.org/10.1083/jcb.42.1.202

Kelly, B. T., Graham, S. C., Liska, N., Dannhauser, P. N., Höning, S., Ungewickell, E. J., & Owen, D. J. (2014). AP2 controls clathrin polymerization with a membrane-activated switch. *Science*, *345*(6195), 459–463. https://doi.org/10.1126/science.1254836

Kennedy, M. J., & Ehlers, M. D. (2006). Organelles and Trafficking Machinery for Postsynaptic Plasticity. *Annual Review of Neuroscience*, *29*(1), 325–362. https://doi.org/10.1146/annurev.neuro.29.051605.112808

Kim, C., Lv, G., Lee, J. S., Jung, B. C., Masuda-Suzukake, M., Hong, C. S., Valera, E., Lee, H. J., Paik, S. R., Hasegawa, M., Masliah, E., Eliezer, D., & Lee, S. J. (2016). Exposure to bacterial endotoxin generates a distinct strain of α-synuclein fibril. *Scientific Reports*, *6*, 1–12. https://doi.org/10.1038/srep30891

Kim, E, & Sheng, M. (2009). Quick guide The postsynaptic density. *Current Biology*, *19*(17), 723–724. https://doi.org/10.1016/j.cub.2009.07.047

Kim, Eunjoon, & Sheng, M. (2004). PDZ domain proteins of synapses. *Nature Reviews Neuroscience*,

5(10), 771–781. https://doi.org/10.1038/nrn1517

Kim, H., Mansi, T., & Bernasconi, N. (2013). Disentangling hippocampal shape anomalies in epilepsy. *Frontiers in Neurology*, *4 SEP*(September), 1–7. https://doi.org/10.3389/fneur.2013.00131

Kim, J. K., & Lee, J. H. (2019). Mechanistic target of rapamycin pathway in epileptic disorders. *Journal of Korean Neurosurgical Society*, *62*(3), 272–287. https://doi.org/10.3340/jkns.2019.0027

Kim, Joungmok, Kundu, M., Viollet, B., & Guan, K.-L. (2011). AMPK and mTOR regulate autophagy through direct phosphorylation of Ulk1. *Nature Cell Biology*, *13*(2), 132–141. https://doi.org/10.1038/ncb2152

Kim, Juyoung, Jung, K. H., Yoo, J., Park, J. H., Yan, H. H., Fang, Z., Lim, J. H., Kwon, S. R., Kim, M. K., Park, H. J., & Hong, S. S. (2020). PBT-6, a novel PI3KC2Γ inhibitor in rheumatoid arthritis. *Biomolecules and Therapeutics*, *28*(2), 172–183. https://doi.org/10.4062/biomolther.2019.153

Kirchhausen, T. (2009). Imaging endocytic clathrin structures in living cells. *Trends in Cell Biology*, *19*(11), 596–605. https://doi.org/10.1016/j.tcb.2009.09.002

Knight, Z. A., Tan, K., Birsoy, K., Schmidt, S., Garrison, J. L., Wysocki, R. W., Emiliano, A., Ekstrand, M. I., & Friedman, J. M. (2012). Molecular Profiling of Activated Neurons by Phosphorylated Ribosome Capture. *Cell*, *151*(5), 1126–1137. https://doi.org/10.1016/j.cell.2012.10.039

Kok, K., Geering, B., & Vanhaesebroeck, B. (2009). Regulation of phosphoinositide 3-kinase expression in health and disease. *Trends in Biochemical Sciences*, *34*(3), 115–127. https://doi.org/10.1016/j.tibs.2009.01.003

Kong, A. M., Speed, C. J., O'Malley, C. J., Layton, M. J., Meehan, T., Loveland, K. L., Cheema, S., Ooms, L. M., & Mitchell, C. A. (2000). Cloning and characterization of a 72-kDa inositol-polyphosphate 5-phosphatase localized to the Golgi network. *Journal of Biological Chemistry*, *275*(31), 24052–24064. https://doi.org/10.1074/jbc.M000874200

Kononenko, N. L., Puchkov, D., Classen, G. A., Walter, A. M., Pechstein, A., Sawade, L., Kaempf, N., Trimbuch, T., Lorenz, D., Rosenmund, C., Maritzen, T., & Haucke, V. (2014). Clathrin/AP-2 mediate synaptic vesicle reformation from endosome-like vacuoles but are not essential for membrane retrieval at central synapses. *Neuron*, *82*(5), 981–988. https://doi.org/10.1016/j.neuron.2014.05.007

Koo, S. J., Kochlamazashvili, G., Rost, B., Puchkov, D., Gimber, N., Lehmann, M., Tadeus, G., Schmoranzer, J., Rosenmund, C., Haucke, V., & Maritzen, T. (2015). Vesicular Synaptobrevin/VAMP2 Levels Guarded by AP180 Control Efficient Neurotransmission. *Neuron*, *88*(2), 330–344. https://doi.org/10.1016/j.neuron.2015.08.034

Koo, S. J., Markovic, S., Puchkov, D., Mahrenholz, C. C., Beceren-Braun, F., Maritzen, T., Dernedde, J., Volkmer, R., Oschkinat, H., & Haucke, V. (2011). SNARE motif-mediated sorting of synaptobrevin by the endocytic adaptors clathrin assembly lymphoid myeloid leukemia (CALM) and AP180 at synapses. *Proceedings of the National Academy of Sciences of the United States of America*, *108*(33), 13540–13545. https://doi.org/10.1073/pnas.1107067108

Krauss, M., Kukhtina, V., Pechstein, A., & Haucke, V. (2006). Stimulation of phosphatidylinositol kinase type I-mediated phosphatidylinositol (4,5)-bisphosphate synthesis by AP-2μ-cargo complexes. *Proceedings of the National Academy of Sciences of the United States of America*, *103*(32), 11934–11939. https://doi.org/10.1073/pnas.0510306103

Krishtal, O. A., Osipchuk, Y. V., Shelest, T. N., & Smirnoff, S. V. (1987). Rapid extracellular pH transients related to synaptic transmission in rat hippocampal slices. *Brain Research*, *436*(2), 352–356. https://doi.org/10.1016/0006-8993(87)91678-7

Kunz, J., Henriquez, R., Schneider, U., Deuter-Reinhard, M., Movva, N. R., & Hall, M. N. (1993).

Target of rapamycin in yeast, TOR2, is an essential phosphatidylinositol kinase homolog required for G1 progression. *Cell*, *73*(3), 585–596. https://doi.org/10.1016/0092-8674(93)90144-F

Kwiatkowski, D. J., & Manning, B. D. (2005). Tuberous sclerosis: A GAP at the crossroads of multiple signaling pathways. *Human Molecular Genetics*, *14*(SUPPL. 2). https://doi.org/10.1093/hmg/ddi260

Kwon, S. E., & Chapman, E. R. (2011). Synaptophysin Regulates the Kinetics of Synaptic Vesicle Endocytosis in Central Neurons. *Neuron*, *70*(5), 847–854. https://doi.org/10.1016/j.neuron.2011.04.001

Kyung, J. W., Kim, J. M., Lee, W., Ha, T. Y., Cha, S. H., Chung, K. H., Choi, D. J., Jou, I., Song, W. K., Joe, E. H., Kim, S. H., & Park, S. M. (2018). DJ-1 deficiency impairs synaptic vesicle endocytosis and reavailability at nerve terminals. *Proceedings of the National Academy of Sciences of the United States of America*, *115*(7), 1629–1634. https://doi.org/10.1073/pnas.1708754115

Lai, Y., Diao, J., Liu, Y., Ishitsuka, Y., Su, Z., Schulten, K., Ha, T., & Shin, Y. K. (2013). Fusion pore formation and expansion induced by Ca2+ and synaptotagmin. *Proceedings of the National Academy of Sciences of the United States of America*, *110*(4), 1333–1338. https://doi.org/10.1073/pnas.1218818110

Lam, P. M., & González, M. I. (2019). Calpain activation and neuronal death during early epileptogenesis. *Neurobiology of Disease*, *124*(1), 141–151. https://doi.org/10.1016/j.nbd.2018.11.005

Larson, J., & Lynch, G. (1988). Role of N-methyl-D-aspartate receptors in the induction of synaptic potentiation by burst stimulation patterned after the hippocampal θ-rhythm. *Brain Research*, *441*(1–2), 111–118. https://doi.org/10.1016/0006-8993(88)91388-1

Larson, J., Wong, D., & Lynch, G. (1986). Patterned stimulation at the theta frequency is optimal for the induction of hippocampal long-term potentiation. *Brain Research*, *368*(2), 347–350. https://doi.org/10.1016/0006-8993(86)90579-2

Leach, J. P., Mohanraj, R., & Borland, W. (2012). Alcohol and drugs in epilepsy: Pathophysiology, presentation, possibilities, and prevention. *Epilepsia*, *53*(SUPPL. 4), 48–57. https://doi.org/10.1111/j.1528-1167.2012.03613.x

Lee, S. E., Jeong, S., Lee, U., & Chang, S. (2019). SGIP1α functions as a selective endocytic adaptor for the internalization of synaptotagmin 1 at synapses. *Molecular Brain*, *12*(1), 1–11. https://doi.org/10.1186/s13041-019-0464-1

Leevers, S. J., Vanhaesebroeck, B., & Waterfield, M. D. (1999). Signalling through phosphoinositide 3-kinases: The lipids take centre stage. *Current Opinion in Cell Biology*, *11*(2), 219–225. https://doi.org/10.1016/S0955-0674(99)80029-5

Legendre, P. (2001). The glycinergic inhibitory synapse. *Cellular and Molecular Life Sciences*, *58*(5–6), 760–793. https://doi.org/10.1007/PL00000899

Lemmon, M. A., & Schlessinger, J. (2010). Cell Signaling by Receptor Tyrosine Kinases. *Cell*, *141*(7), 1117–1134. https://doi.org/10.1016/j.cell.2010.06.011

Lévi, S., Logan, S. M., Tovar, K. R., & Craig, A. M. (2004). Gephyrin Is Critical for Glycine Receptor Clustering but Not for the Formation of Functional GABAergic Synapses in Hippocampal Neurons. *Journal of Neuroscience*, *24*(1), 207–217. https://doi.org/10.1523/JNEUROSCI.1661-03.2004

Liang, Q., Luo, Z., Zeng, J., Chen, W., Foo, S. S., Lee, S. A., Ge, J., Wang, S., Goldman, S. A., Zlokovic, B. V., Zhao, Z., & Jung, J. U. (2016). Zika Virus NS4A and NS4B Proteins Deregulate Akt-mTOR Signaling in Human Fetal Neural Stem Cells to Inhibit Neurogenesis and Induce Autophagy. *Cell Stem Cell*, *19*(5), 663–671. https://doi.org/10.1016/j.stem.2016.07.019

Liaw, J. S., & Berger, T. W. (1996). Dynamic synapse: A new concept of neural representation and computation. *Hippocampus*, *6*(6), 591–600. https://doi.org/10.1002/(SICI)1098-1063(1996)6:6<591::AID-HIPO4>3.0.CO;2-K

LiCausi, F., & Hartman, N. (2018). Role of mTOR Complexes in Neurogenesis. *International Journal of Molecular Sciences*, *19*(5), 1544. https://doi.org/10.3390/ijms19051544

Lieberman, O. J., & Sulzer, D. (2020). The Synaptic Autophagy Cycle. *Journal of Molecular Biology*, *432*(8), 2589–2604. https://doi.org/10.1016/j.jmb.2019.12.028

Lo, W. T., Vujičić Žagar, A., Gerth, F., Lehmann, M., Puchkov, D., Krylova, O., Freund, C., Scapozza, L., Vadas, O., & Haucke, V. (2017). A Coincidence Detection Mechanism Controls PX-BAR Domain-Mediated Endocytic Membrane Remodeling via an Allosteric Structural Switch. *Developmental Cell*, *43*(4), 522-529.e4. https://doi.org/10.1016/j.devcel.2017.10.019

Lømo, T. (2003). The discovery of long-term potentiation. *Philosophical Transactions of the Royal Society B: Biological Sciences*, *358*(1432), 617–620. https://doi.org/10.1098/rstb.2002.1226

Lopes, M. W., Soares, F. M. S., De Mello, N., Nunes, J. C., Cajado, A. G., De Brito, D., De Cordova, F. M., Da Cunha, R. M. S., Walz, R., & Leal, R. B. (2013). Time-dependent modulation of AMPA receptor phosphorylation and mRNA expression of NMDA receptors and glial glutamate transporters in the rat hippocampus and cerebral cortex in a pilocarpine model of epilepsy. *Experimental Brain Research*, *226*(2), 153–163. https://doi.org/10.1007/s00221-013-3421-8

Lou, X. (2018). Sensing exocytosis and triggering endocytosis at synapses: Synaptic vesicle exocytosis–endocytosis coupling. *Frontiers in Cellular Neuroscience*, *12*(March). https://doi.org/10.3389/fncel.2018.00066

Lu, B., Su, Y., Das, S., Wang, H., Wang, Y., Liu, J., & Ren, D. (2009). Peptide neurotransmitters activate a cation channel complex of NALCN and UNC-80. *Nature*, *457*(7230), 741–744. https://doi.org/10.1038/nature07579

Lu, R., Drubin, D. G., & Sun, Y. (2016). Clathrin-mediated endocytosis in budding yeast at a glance. *Journal of Cell Science*, *129*(8), 1531–1536. https://doi.org/10.1242/jcs.182303

Lundmark, R., & Carlsson, S. R. (2009). SNX9 - A prelude to vesicle release. *Journal of Cell Science*, *122*(1), 5–11. https://doi.org/10.1242/jcs.037135

Maccaferri, G. (2005). Stratum oriens horizontal interneurone diversity and hippocampal network dynamics. *Journal of Physiology*, *562*(1), 73–80. https://doi.org/10.1113/jphysiol.2004.077081

MacDermott, A. B., Role, L. W., & Siegelbaum, S. A. (1999). Presynaptic Ionotropic Receptors and the Control of Transmitter Release. *Annual Review of Neuroscience*, *22*(1), 443–485. https://doi.org/10.1146/annurev.neuro.22.1.443

Man, H. Y., Wang, Q., Lu, W. Y., Ju, W., Ahmadian, G., Liu, L., D'Souza, S., Wong, T. P., Taghibiglou, C., Lu, J., Becker, L. E., Pei, L., Liu, F., Wymann, M. P., MacDonald, J. F., & Wang, Y. T. (2003). Activation of PI3-kinase is required for AMPA receptor insertion during LTP of mEPSCs in cultured hippocampal neurons. *Neuron*, *38*(4), 611–624. https://doi.org/10.1016/S0896-6273(03)00228-9

Marat, A. L., Wallroth, A., Lo, W. T., Müller, R., Norata, G. D., Falasca, M., Schultz, C., & Haucke, V. (2017). mTORC1 activity repression by late endosomal phosphatidylinositol 3,4-bisphosphate. *Science*, *356*(6341), 968–972. https://doi.org/10.1126/science.aaf8310

Marra, V., Burden, J. J., Thorpe, J. R., Smith, I. T., Smith, S. L., Häusser, M., Branco, T., & Staras, K. (2012). A Preferentially Segregated Recycling Vesicle Pool of Limited Size Supports Neurotransmission in Native Central Synapses. *Neuron*, *76*(3), 579–589. https://doi.org/10.1016/j.neuron.2012.08.042

Martelli, A. M., Evangelisti, C., Chiarini, F., & McCubrey, J. A. (2010). The phosphatidylinositol 3-kinase/Akt/mTOR signaling network as a therapeutic target in acute myelogenous leukemia

patients. *Oncotarget*, *1*(2), 89–103. https://doi.org/10.18632/oncotarget.114

Matteis, M. A. De, & Godi, A. (2004). PI-loting membrane traffic. *Nature Cell Biology*, *6*(6), 487–492. https://doi.org/10.1038/ncb0604-487

Mattoon, D. R., Lamothe, B., Lax, I., & Schlessinger, J. (2004). The docking protein Gab1 is the primary mediator of EGF-stimulated activation of the PI-3K/Akt cell survival pathway. *BMC Biology*, *2*, 1–12. https://doi.org/10.1186/1741-7007-2-24

Mayer, M. L., Westbrook, G. L., & Guthrie, P. B. (1984). Voltage-dependent block by Mg2+ of NMDA responses in spinal cord neurones. *Nature*, *309*(5965), 261–263. https://doi.org/10.1038/309261a0

McMahon, J., Huang, X., Yang, J., Komatsu, M., Yue, Z., Qian, J., Zhu, X., & Huang, Y. (2012). Impaired autophagy in neurons after disinhibition of mammalian target of rapamycin and its contribution to epileptogenesis. *Journal of Neuroscience*, *32*(45), 15704–15714. https://doi.org/10.1523/JNEUROSCI.2392-12.2012

Medeiros, A., Bubacco, L., & Morgan, J. (2018). Impacts of increased α-synuclein on clathrin-mediated endocytosis at synapses: Implications for neurodegenerative diseases. *Neural Regeneration Research*, *13*(4), 647–648. https://doi.org/10.4103/1673-5374.230289

Meikle, L., Talos, D. M., Onda, H., Pollizzi, K., Rotenberg, A., Sahin, M., Jensen, F. E., & Kwiatkowski, D. J. (2007). A mouse model of tuberous sclerosis: Neuronal loss of Tsc1 causes dysplastic and ectopic neurons, reduced myelination, seizure activity, and limited survival. *Journal of Neuroscience*, *27*(21), 5546–5558. https://doi.org/10.1523/JNEUROSCI.5540-06.2007

Memmott, R. M., & Dennis, P. A. (2010). The role of the Akt/mTOR pathway in tobacco carcinogen-induced lung tumorigenesis. *Clinical Cancer Research*, *16*(1), 4–10. https://doi.org/10.1158/1078-0432.CCR-09-0234

Menon, S., Dibble, C. C., Talbott, G., Hoxhaj, G., Valvezan, A. J., Takahashi, H., Cantley, L. C., & Manning, B. D. (2014). Spatial Control of the TSC Complex Integrates Insulin and Nutrient Regulation of mTORC1 at the Lysosome. *Cell*, *156*(4), 771–785. https://doi.org/10.1016/j.cell.2013.11.049

Merrill, N. M., Schipper, J. L., Karnes, J. B., Kauffman, A. L., Martin, K. R., & MacKeigan, J. P. (2017). PI3K-C2α knockdown decreases autophagy and maturation of endocytic vesicles. *PLoS ONE*, *12*(9), 1–23. https://doi.org/10.1371/journal.pone.0184909

Metzger, D., & Chambon, P. (2001). Site- and time-specific gene targeting in the mouse. *Methods*, *24*(1), 71–80. https://doi.org/10.1006/meth.2001.1159

Miesenböck, G., De Angelis, D. A., & Rothman, J. E. (1998). Visualizing secretion and synaptic transmission with pH-sensitive green fluorescent proteins. *Nature*, *394*(6689), 192–195. https://doi.org/10.1038/28190

Milosevic, I. (2018). Revisiting the role of clathrin-mediated endoytosis in synaptic vesicle recycling. *Frontiers in Cellular Neuroscience*, *12*(February), 1–13. https://doi.org/10.3389/fncel.2018.00027

Mittelstaedt, T., Alvaréz-Baron, E., & Schoch, S. (2010). RIM proteins and their role in synapse function. *Biological Chemistry*, *391*(6), 599–606. https://doi.org/10.1515/BC.2010.064

Morel, E., Chamoun, Z., Lasiecka, Z. M., Chan, R. B., Williamson, R. L., Vetanovetz, C., Dall'Armi, C., Simoes, S., Point Du Jour, K. S., McCabe, B. D., Small, S. A., & Di Paolo, G. (2013). Phosphatidylinositol-3-phosphate regulates sorting and processing of amyloid precursor protein through the endosomal system. *Nature Communications*, *4*. https://doi.org/10.1038/ncomms3250

Muller, D., Guo, C. H., Amiel, S., Jones, P. M., & Persaud, S. J. (2006). Identification of insulin

signaling elements in human β-cells: Autocrine regulation of insulin gene expression. *Diabetes*, *55*(10), 2835–2842. https://doi.org/10.2337/db06-0532

Mutch, S. A., Kensel-Hammes, P., Gadd, J. C., Fujimoto, B. S., Allen, R. W., Schiro, P. G., Lorenz, R. M., Kuyper, C. L., Kuo, J. S., Bajjalieh, S. M., & Chiu, D. T. (2011). Protein quantification at the single vesicle level reveals that a subset of synaptic vesicle proteins are trafficked with high precision. *Journal of Neuroscience*, *31*(4), 1461–1470. https://doi.org/10.1523/JNEUROSCI.3805-10.2011

Naisbitt, S., Eunjoon, K., Tu, J. C., Xiao, B., Sala, C., Valtschanoff, J., Weinberg, R. J., Worley, P. F., & Sheng, M. (1999). Shank, a novel family of postsynaptic density proteins that binds to the NMDA receptor/PSD-95/GKAP complex and cortactin. *Neuron*, *23*(3), 569–582. https://doi.org/10.1016/S0896-6273(00)80809-0

Nakatsu, F., Perera, R. M., Lucast, L., Zoncu, R., Domin, J., Gertler, F. B., Toomre, D., & De Camilli, P. (2010). The inositol 5-phosphatase SHIP2 regulates endocytic clathrin-coated pit dynamics. *Journal of Cell Biology*, *190*(3), 307–315. https://doi.org/10.1083/jcb.201005018

Napolitano, G., Esposito, A., Choi, H., Matarese, M., Benedetti, V., Di Malta, C., Monfregola, J., Medina, D. L., Lippincott-Schwartz, J., & Ballabio, A. (2018). mTOR-dependent phosphorylation controls TFEB nuclear export. *Nature Communications*, *9*(1). https://doi.org/10.1038/s41467-018-05862-6

Nathanson, A. J., Davies, P. A., & Moss, S. J. (2019). Inhibitory Synapse Formation at the Axon Initial Segment. *Frontiers in Molecular Neuroscience*, *12*(November), 1–7. https://doi.org/10.3389/fnmol.2019.00266

Neasta, J., Hamida, S. Ben, Yowell, Q., Camicella, S., & Ron, D. (2010). Role for mammalian target of rapamycin complex 1 signaling in neuroadaptations underlying alcohol-related disorders. *Proceedings of the National Academy of Sciences of the United States of America*, *107*(46), 20093–20098. https://doi.org/10.1073/pnas.1005554107

Neher, E., & Augustine, G. J. (1992). Calcium gradients and buffers in bovine chromaffin cells. *The Journal of Physiology*, *450*(1), 273–301. https://doi.org/10.1113/jphysiol.1992.sp019127

Neher, Erwin. (2010). What is rate-limiting during sustained synaptic activity: Vesicle supply or the availability of release sites. *Frontiers in Synaptic Neuroscience*, *2*(SEP), 1–6. https://doi.org/10.3389/fnsyn.2010.00144

New, D. C., & Wong, Y. H. (2007). Molecular mechanisms mediating the G protein-coupled receptor regulation of cell cycle progression. *Journal of Molecular Signaling*, *2*, 1–15. https://doi.org/10.1186/1750-2187-2-2

New, D. C., Wu, K., Kwok, A. W. S., & Wong, Y. H. (2007). G protein-coupled receptor-induced Akt activity in cellular proliferation and apoptosis. *FEBS Journal*, *274*(23), 6025–6036. https://doi.org/10.1111/j.1742-4658.2007.06116.x

Nicholls, John G., A. Robert Martin, Paul A. Fuchs, David A. Brown, Mathew E. Diamond, and David A. Weisblat. (2012). From Neuron to Brain. 5. Sunderland, Massachusetts: Sinauer Associates, Inc. Page: 183-243.

Niere, F., & Raab-Graham, K. F. (2017). mTORC1 is a local, postsynaptic voltage sensor regulated by positive and negative feedback pathways. *Frontiers in Cellular Neuroscience*, *11*(May), 1–15. https://doi.org/10.3389/fncel.2017.00152

Nikoletopoulou, V., Sidiropoulou, K., Kallergi, E., Dalezios, Y., & Tavernarakis, N. (2017). Modulation of Autophagy by BDNF Underlies Synaptic Plasticity. *Cell Metabolism*, *26*(1), 230-242.e5. https://doi.org/10.1016/j.cmet.2017.06.005

Nojima, H., Tokunaga, C., Eguchi, S., Oshiro, N., Hidayat, S., Yoshino, K. I., Hara, K., Tanaka, N., Avruch, J., & Yonezawa, K. (2003). The mammalian target of rapamycin (mTOR) partner,

raptor, binds the mTOR substrates p70 S6 kinase and 4E-BP1 through their TOR signaling (TOS) motif. *Journal of Biological Chemistry*, *278*(18), 15461–15464. https://doi.org/10.1074/jbc.C200665200

Nowak, L., Bregestovski, P., Ascher, P., Herbet, A., & Prochiantz, A. (1984). Magnesium gates glutamate-activated channels in mouse central neurones. *Nature*, *307*(5950), 462–465. https://doi.org/10.1038/307462a0

O'Dell, T. J., & Kandel, E. R. (1994). Low-frequency stimulation erases LTP through an NMDA receptor-mediated activation of protein phosphatases. *Learning Memory*, *1*(2), 129–139. https://doi.org/10.1101/lm.1.2.129

Odgerel, Z., Sonti, S., Hernandez, N., Park, J., Ottman, R., Louis, E. D., & Clark, L. N. (2019). Whole genome sequencing and rare variant analysis in essential tremor families. *PLoS ONE*, *14*(8), 1–28. https://doi.org/10.1371/journal.pone.0220512

Ohno-Shosaku, T., Hashimotodani, Y., Maejima, T., & Kano, M. (2005). Calcium signaling and synaptic modulation: Regulation of endocannabinoid-mediated synaptic modulation by calcium. *Cell Calcium*, *38*(3-4 SPEC. ISS.), 369–374. https://doi.org/10.1016/j.ceca.2005.06.014

Ohno-Shosaku, T., Matsui, M., Fukudome, Y., Shosaku, J., Tsubokawa, H., Taketo, M. M., Manabe, T., & Kano, M. (2003). Postsynaptic M1 and M3 receptors are responsible for the muscarinic enhancement of retrograde endocannabinoid signalling in the hippocampus. *European Journal of Neuroscience*, *18*(1), 109–116. https://doi.org/10.1046/j.1460-9568.2003.02732.x

Onda, H., Crino, P. B., Zhang, H., Murphey, R. D., Rastelli, L., Rothberg, B. E. G., & Kwiatkowski, D. J. (2002). Tsc2 null murine neuroepithelial cells are a model for human tuber giant cells, and show activation of an mTOR pathway. *Molecular and Cellular Neuroscience*, *21*(4), 561–574. https://doi.org/10.1006/mcne.2002.1184

Ostendorf, A. P., & Wong, M. (2015). mTOR Inhibition in Epilepsy: Rationale and Clinical Perspectives. *CNS Drugs*, *29*(2), 91–99. https://doi.org/10.1007/s40263-014-0223-x

Park, J., Kim, Y., Lee, S., Park, J. J., Park, Z. Y., Sun, W., Kim, H., & Chang, S. (2010). SNX18 shares a redundant role with SNX9 and modulates endocytic trafficking at the plasma membrane. *Journal of Cell Science*, *123*(10), 1742–1750. https://doi.org/10.1242/jcs.064170

Park, M. (2018). AMPA receptor trafficking for postsynaptic potentiation. *Frontiers in Cellular Neuroscience*, *12*(October), 1–10. https://doi.org/10.3389/fncel.2018.00361

Perera, R. M., Zoncu, R., Lucast, L., De Camilli, P., & Toomre, D. (2006). Two synaptojanin 1 isoforms are recruited to clathrin-coated pits at different stages. *Proceedings of the National Academy of Sciences of the United States of America*, *103*(51), 19332–19337. https://doi.org/10.1073/pnas.0609795104

Perez, Y. (1996). Axonal sprouting of CA1 pyramidal cells in hyperexcitable hippocampal slices of kainate-treated rats. *European Journal of Neuroscience*, *8*(4), 736–748. https://doi.org/10.1111/j.1460-9568.1996.tb01259.x

Perucca, P. (2018). Genetics of focal epilepsies: What do we know and where are we heading? *Epilepsy Currents*, *18*(6), 356–362. https://doi.org/10.5698/1535-7597.18.6.356

Porstmann, T., Santos, C. R., Griffiths, B., Cully, M., Wu, M., Leevers, S., Griffiths, J. R., Chung, Y. L., & Schulze, A. (2008). SREBP Activity Is Regulated by mTORC1 and Contributes to Akt-Dependent Cell Growth. *Cell Metabolism*, *8*(3), 224–236. https://doi.org/10.1016/j.cmet.2008.07.007

Posor, Y., Eichhorn-Gruenig, M., Puchkov, D., Schöneberg, J., Ullrich, A., Lampe, A., Müller, R., Zarbakhsh, S., Gulluni, F., Hirsch, E., Krauss, M., Schultz, C., Schmoranzer, J., Noé, F., & Haucke, V. (2013). Spatiotemporal control of endocytosis by phosphatidylinositol-3,4-

bisphosphate. *Nature*, *499*, 233–237. https://doi.org/10.1038/nature12360

Praefcke, G. J. K., Ford, M. G. J., Schmid, E. M., Olesen, L. E., Gallop, J. L., Peak-Chew, S. Y., Vallis, Y., Babu, M. M., Mills, I. G., & McMahon, H. T. (2004). Evolving nature of the AP2 α-appendage hub during clathrin-coated vesicle endocytosis. *EMBO Journal*, *23*(22), 4371–4383. https://doi.org/10.1038/sj.emboj.7600445

Praefcke, G. J. K., & McMahon, H. T. (2004). The dynamin superfamily: Universal membrane tubulation and fission molecules? *Nature Reviews Molecular Cell Biology*, *5*(2), 133–147. https://doi.org/10.1038/nrm1313

Price, D., Grove, Calvo, V., Avruch, J., & Bierer, B. (1992). Rapamycin-induced inhibition of the 70-kilodalton S6 protein kinase. *Science*, *257*(5072), 973–977. https://doi.org/10.1126/science.1380182

Prior, P., Schmitt, B., Grenningloh, G., Pribilla, I., Multhaup, G., Beyreuther, K., Maulet, Y., Werner, P., Langosch, D., Kirsch, J., & Betz, H. (1992). Primary structure and alternative splice variants of gephyrin, a putative glycine receptor-tubulin linker protein. *Neuron*, *8*(6), 1161–1170. https://doi.org/10.1016/0896-6273(92)90136-2

Purcell, S. M., Moran, J. L., Fromer, M., Ruderfer, D., Solovieff, N., Roussos, P., O'Dushlaine, C., Chambert, K., Bergen, S. E., Kähler, A., Duncan, L., Stahl, E., Genovese, G., Fernández, E., Collins, M. O., Komiyama, N. H., Choudhary, J. S., Magnusson, P. K. E., Banks, E., … Sklar, P. (2014). A polygenic burden of rare disruptive mutations in schizophrenia. *Nature*, *506*(7487), 185–190. https://doi.org/10.1038/nature12975

Qualmann, B., Boeckers, T. M., Jeromin, M., Gundelfinger, E. D., & Kessels, M. M. (2004). Linkage of the Actin Cytoskeleton to the Postsynaptic Density via Direct Interactions of Abp1 with the ProSAP/Shank Family. *Journal of Neuroscience*, *24*(10), 2481–2495. https://doi.org/10.1523/JNEUROSCI.5479-03.2004

Raimondi, A., Ferguson, S. M., Lou, X., Armbruster, M., Paradise, S., Giovedi, S., Messa, M., Kono, N., Takasaki, J., Cappello, V., O'Toole, E., Ryan, T. A., & De Camilli, P. (2011). Overlapping Role of Dynamin Isoforms in Synaptic Vesicle Endocytosis. *Neuron*, *70*(6), 1100–1114. https://doi.org/10.1016/j.neuron.2011.04.031

Ramakrishnan, N. A., Drescher, M. J., & Drescher, D. G. (2012). The SNARE complex in neuronal and sensory cells. *Molecular and Cellular Neuroscience*, *50*(1), 58–69. https://doi.org/10.1016/j.mcn.2012.03.009

Riban, V., Bouilleret, V., Pham-Lê, B. T., Fritschy, J. M., Marescaux, C., & Depaulis, A. (2002). Evolution of hippocampal epileptic activity during the development of hippocampal sclerosis in a mouse model of temporal lobe epilepsy. *Neuroscience*, *112*(1), 101–111. https://doi.org/10.1016/S0306-4522(02)00064-7

Richards, D. A., Guatimosim, C., Rizzoli, S. O., & Betz, W. J. (2003). Synaptic vesicle pools at the frog neuromuscular junction. *Neuron*, *39*(3), 529–541. https://doi.org/10.1016/S0896-6273(03)00405-7

Ridler, K., Suckling, J., Higgins, N., Bolton, P., & Bullmore, E. (2004). Standardized whole brain mapping of tubers and subependymal nodules in tuberous sclerosis complex. *Journal of Child Neurology*, *19*(9), 658–665. https://doi.org/10.1177/08830738040190090501

Rizzoli, S. O., & Betz, W. J. (2005). Synaptic vesicle pools. *Nature Reviews Neuroscience*, *6*(1), 57–69. https://doi.org/10.1038/nrn1583

Rizzoli, S. O., & Jahn, R. (2007). Kiss-and-run, collapse and "readily retrievable" vesicles. *Traffic*, *8*(9), 1137–1144. https://doi.org/10.1111/j.1600-0854.2007.00614.x

Rohde, G., Wenzel, D., & Haucke, V. (2002). A phosphatidylinositol (4,5)-bisphosphate binding site within μ-adaptin regulates clathrin-mediated endocytosis. *Journal of Cell Biology*, *158*(2),

209–214. https://doi.org/10.1083/jcb.200203103

Roos, A., & Boron, W. F. (1981). Intracellular pH. *Physiological Reviews*, *61*(2), 296–434. https://doi.org/10.1152/physrev.1981.61.2.296

Rosner, M., Schipany, K., & Hengstschläger, M. (2012). P70 S6K1 nuclear localization depends on its mTOR-mediated phosphorylation at T389, but not on its kinase activity towards S6. *Amino Acids*, *42*(6), 2251–2256. https://doi.org/10.1007/s00726-011-0965-4

Rothnie, A., Clarke, A. R., Kuzmic, P., Cameron, A., & Smith, C. J. (2011). A sequential mechanism for clathrin cage disassembly by 70-kDa heat-shock cognate protein (Hsc70) and auxilin. *Proceedings of the National Academy of Sciences of the United States of America*, *108*(17), 6927–6932. https://doi.org/10.1073/pnas.1018845108

Russell, R. C., Tian, Y., Yuan, H., Park, H. W., Chang, Y., Kim, J., Kim, H., Neufeld, T. P., Dillin, A., & Guan, K. (2013). ULK1 induces autophagy by phosphorylating Beclin-1 and activating VPS34 lipid kinase. *Nature Cell Biology*, *15*(7), 741–750. https://doi.org/10.1038/ncb2757

Ryskalin, L., Limanaqi, F., Frati, A., Busceti, C. L., & Fornai, F. (2018). mTOR-related brain dysfunctions in neuropsychiatric disorders. *International Journal of Molecular Sciences*, *19*(8), 11–13. https://doi.org/10.3390/ijms19082226

Sabatini, D. M., Erdjument-Bromage, H., Lui, M., Tempst, P., & Snyder, S. H. (1994). RAFT1: A mammalian protein that binds to FKBP12 in a rapamycin-dependent fashion and is homologous to yeast TORs. *Cell*, *78*(1), 35–43. https://doi.org/10.1016/0092-8674(94)90570-3

Sabers, C. J., Martin, M. M., Brunn, G. J., Williams, J. M., Dumont, F. J., Wiederrecht, G., & Abraham, R. T. (1995). Isolation of a Protein Target of the FKBP12-Rapamycin Complex in Mammalian Cells. *Journal of Biological Chemistry*, *270*(2), 815–822. https://doi.org/10.1074/jbc.270.2.815

Saheki, Y., & De Camilli, P. (2012). Synaptic Vesicle Endocytosis. *Cold Spring Harbor Perspectives in Biology*, *4*(9), a005645–a005645. https://doi.org/10.1101/cshperspect.a005645

Sancak, Y., Thoreen, C. C., Peterson, T. R., Lindquist, R. A., Kang, S. A., Spooner, E., Carr, S. A., & Sabatini, D. M. (2007). PRAS40 Is an Insulin-Regulated Inhibitor of the mTORC1 Protein Kinase. *Molecular Cell*, *25*(6), 903–915. https://doi.org/10.1016/j.molcel.2007.03.003

Sanderson, T. M. (2012). Molecular Mechanisms Involved in Depotentiation and Their Relevance to Schizophrenia. *Chonnam Medical Journal*, *48*(1), 1. https://doi.org/10.4068/cmj.2012.48.1.1

Sankaranarayanan, S., De Angelis, D., Rothman, J. E., & Ryan, T. A. (2000). The Use of pHluorins for Optical Measurements of Presynaptic Activity. *Biophysical Journal*, *79*(4), 2199–2208. https://doi.org/10.1016/S0006-3495(00)76468-X

Sato, T., Nakashima, A., Guo, L., & Tamanoi, F. (2009). Specific activation of mTORC1 by Rheb G-protein in vitro involves enhanced recruitment of its substrate protein. *Journal of Biological Chemistry*, *284*(19), 12783–12791. https://doi.org/10.1074/jbc.M809207200

Savtchenko, L. P., & Rusakov, D. A. (2007). The optimal height of the synaptic cleft. *Proceedings of the National Academy of Sciences of the United States of America*, *104*(6), 1823–1828. https://doi.org/10.1073/pnas.0606636104

Schikorski, T., & Stevens, C. F. (1997). Quantitative Ultrastructural Analysis of Hippocampal. *J. Neurosci.*, *17*(15), 5858–5867. https://pdfs.semanticscholar.org/6317/17f04ca52a47f6c909b5e614a4a2afa6c141.pdf

Schmid, S. L., & Mettlen, M. (2013). Lipid switches and traffic control. *Nature*, *499*(7457), 161–162. https://doi.org/10.1038/nature12408

Schöneberg, J., Lehmann, M., Ullrich, A., Posor, Y., Lo, W. T., Lichtner, G., Schmoranzer, J., Haucke, V., & Noé, F. (2017). Lipid-mediated PX-BAR domain recruitment couples local membrane

constriction to endocytic vesicle fission. *Nature Communications*, *8*(May). https://doi.org/10.1038/ncomms15873

Schuldiner, O., & Yaron, A. (2015). Mechanisms of developmental neurite pruning. *Cellular and Molecular Life Sciences*, *72*(1), 101–119. https://doi.org/10.1007/s00018-014-1729-6

Seet, L. F., & Hong, W. (2006). The Phox (PX) domain proteins and membrane traffic. *Biochimica et Biophysica Acta - Molecular and Cell Biology of Lipids*, *1761*(8), 878–896. https://doi.org/10.1016/j.bbalip.2006.04.011

Shao, S., & Hegde, R. S. (2011). Membrane Protein Insertion at the Endoplasmic Reticulum. *Annual Review of Cell and Developmental Biology*, *27*(1), 25–56. https://doi.org/10.1146/annurev-cellbio-092910-154125

Shehata, M., Matsumura, H., Okubo-Suzuki, R., Ohkawa, N., & Inokuchi, K. (2012). Neuronal stimulation induces autophagy in hippocampal neurons that is involved in AMPA receptor degradation after chemical long-term depression. *Journal of Neuroscience*, *32*(30), 10413–10422. https://doi.org/10.1523/JNEUROSCI.4533-11.2012

Shih, W., Gallusser, A., & Kirchhausen, T. (1995). A clathrin-binding site in the hinge of the β2 chain of mammalian AP-2 complexes. *Journal of Biological Chemistry*, *270*(52), 31083–31090. https://doi.org/10.1074/jbc.270.52.31083

Shin, O. H., Xu, J., Rizo, J., & Südhof, T. C. (2009). Differential but convergent functions of Ca2+ binding to synaptotagmin-1 C2 domains mediate neurotransmitter release. *Proceedings of the National Academy of Sciences of the United States of America*, *106*(38), 16469–16474. https://doi.org/10.1073/pnas.0908798106

Siksou, L., Rostaing, P., Lechaire, J. P., Boudier, T., Ohtsuka, T., Fejtová, A., Kao, H. T., Greengard, P., Gundelfinger, E. D., Triller, A., & Marty, S. (2007). Three-dimensional architecture of presynaptic terminal cytomatrix. *Journal of Neuroscience*, *27*(26), 6868–6877. https://doi.org/10.1523/JNEUROSCI.1773-07.2007

Slack, B. E., & Blusztajn, J. K. (2008). Differential regulation of mTOR-dependent S6 phosphorylation by muscarinic acetylcholine receptor subtypes. *Journal of Cellular Biochemistry*, *104*(5), 1818–1831. https://doi.org/10.1002/jcb.21745

Smith, S. M., Baker, M., Halebian, M., & Smith, C. J. (2017). Weak molecular interactions in clathrin-mediated endocytosis. *Frontiers in Molecular Biosciences*, *4*(NOV). https://doi.org/10.3389/fmolb.2017.00072

Sonenberg, N., & Hinnebusch, A. G. (2009). Regulation of Translation Initiation in Eukaryotes: Mechanisms and Biological Targets. *Cell*, *136*(4), 731–745. https://doi.org/10.1016/j.cell.2009.01.042

Soykan, T., Kaempf, N., Sakaba, T., Vollweiter, D., Goerdeler, F., Puchkov, D., Kononenko, N. L., & Haucke, V. (2017). Synaptic Vesicle Endocytosis Occurs on Multiple Timescales and Is Mediated by Formin-Dependent Actin Assembly. *Neuron*, *93*(4), 854-866.e4. https://doi.org/10.1016/j.neuron.2017.02.011

Stafstrom, C. E. (2004). Dietary Approaches to Epilepsy Treatment: Old and New Options on the Menu. *Epilepsy Currents*, *4*(6), 215–222. https://doi.org/10.1111/j.1535-7597.2004.46001.x

Stambolic, V., Suzuki, A., De la Pompa, J. L., Brothers, G. M., Mirtsos, C., Sasaki, T., Ruland, J., Penninger, J. M., Siderovski, D. P., & Mak, T. W. (1998). Negative regulation of PKB/Akt-dependent cell survival by the tumor suppressor PTEN. *Cell*, *95*(1), 29–39. https://doi.org/10.1016/S0092-8674(00)81780-8

Staubli, U., & Lynch, G. (1990). Stable depression of potentiated synaptic responses in the hippocampus with 1-5 Hz stimulation. *Brain Research*, *513*(1), 113–118. https://doi.org/10.1016/0006-8993(90)91096-Y

Stenmark, H., Aasland, R., Toh, B. H., & D'Arrigo, A. (1996). Endosomal localization of the autoantigen EEA1 is mediated by a zinc- binding FYVE finger. *Journal of Biological Chemistry*, *271*(39), 24048–24054. https://doi.org/10.1074/jbc.271.39.24048

Stoica, L., Zhu, P. J., Huang, W., Zhou, H., Kozma, S. C., & Costa-Mattioli, M. (2011). Selective pharmacogenetic inhibition of mammalian target of Rapamycin complex I (mTORC1) blocks long-term synaptic plasticity and memory storage. *Proceedings of the National Academy of Sciences of the United States of America*, *108*(9), 3791–3796. https://doi.org/10.1073/pnas.1014715108

Südhof, T. C. (2004). THE SYNAPTIC VESICLE CYCLE. *Annual Review of Neuroscience*, *27*(1), 509–547. https://doi.org/10.1146/annurev.neuro.26.041002.131412

Südhof, T. C. (2018). Towards an Understanding of Synapse Formation. *Neuron*, *100*(2), 276–293. https://doi.org/10.1016/j.neuron.2018.09.040

Sun, Y. V., Sung, Y. J., Tintle, N., & Ziegler, A. (2011). Identification of genetic association of multiple rare variants using collapsing methods. *Genetic Epidemiology*, *35*(SUPPL. 1), 1–11. https://doi.org/10.1002/gepi.20658

Takamori, S. (2016). Presynaptic Molecular Determinants of Quantal Size. *Frontiers in Synaptic Neuroscience*, *8*(February), 1–9. https://doi.org/10.3389/fnsyn.2016.00002

Takamori, S., Holt, M., Stenius, K., Lemke, E. A., Grønborg, M., Riedel, D., Urlaub, H., Schenck, S., Brügger, B., Ringler, P., Müller, S. A., Rammner, B., Gräter, F., Hub, J. S., De Groot, B. L., Mieskes, G., Moriyama, Y., Klingauf, J., Grubmüller, H., … Jahn, R. (2006). Molecular Anatomy of a Trafficking Organelle. *Cell*, *127*(4), 831–846. https://doi.org/10.1016/j.cell.2006.10.030

Takei, N., & Nawa, H. (2014). mTOR signaling and its roles in normal and abnormal brain development. *Frontiers in Molecular Neuroscience*, *7*(1 APR), 1–12. https://doi.org/10.3389/fnmol.2014.00028

ter Haar, E., Musacchio, A., Harrison, S. C., & Kirchhausen, T. (1998). Atomic Structure of Clathrin. *Cell*, *95*(4), 563–573. https://doi.org/10.1016/S0092-8674(00)81623-2

Thomas, R. C. (1972). Electrogenic sodium pump in nerve and muscle cells. *Physiological Reviews*, *52*(3), 563–594. https://doi.org/10.1152/physrev.1972.52.3.563

Thompson, S. M., & Gahwiler, B. H. (1989). Activity-dependent disinhibition. I. Repetitive stimulation reduces IPSP driving force and conductance in the hippocampus in vitro. *Journal of Neurophysiology*, *61*(3), 501–511. https://doi.org/10.1152/jn.1989.61.3.501

Tiosano, D., Baris, H. N., Chen, A., Hitzert, M. M., Schueler, M., Gulluni, F., Wiesener, A., Bergua, A., Mory, A., Copeland, B., Gleeson, J. G., Rump, P., van Meer, H., Sival, D. A., Haucke, V., Kriwinsky, J., Knaup, K. X., Reis, A., Hauer, N. N., … Buchner, D. A. (2019). Mutations in PIK3C2A cause syndromic short stature, skeletal abnormalities, and cataracts associated with ciliary dysfunction. *PLoS Genetics*, *15*(4), 1–21. https://doi.org/10.1371/journal.pgen.1008088

Traub, L. M., Downs, M. A., Westrich, J. L., & Fremont, D. H. (1999). Crystal structure of the α appendage of AP-2 reveals a recruitment platform for clathrin-coat assembly. *Proceedings of the National Academy of Sciences of the United States of America*, *96*(16), 8907–8912. https://doi.org/10.1073/pnas.96.16.8907

Tremblay, R., Lee, S., & Rudy, B. (2016). GABAergic Interneurons in the Neocortex: From Cellular Properties to Circuits. *Neuron*, *91*(2), 260–292. https://doi.org/10.1016/j.neuron.2016.06.033

Tsokas, P., Grace, E. A., Chan, P. M., Ma, T., Sealfon, S. C., Iyengar, R., Landau, E. M., & Blitzer, R. D. (2005). Local protein synthesis mediates a rapid increase in dendritic elongation factor 1A after induction of late long-term potentiation. *Journal of Neuroscience*, *25*(24), 5833–5843. https://doi.org/10.1523/JNEUROSCI.0599-05.2005

Umpierre, A. D., Bennett, I. V., Nebeker, L. D., Newell, T. G., Tian, B. B., Thomson, K. E., White, H.

S., White, J. A., & Wilcox, K. S. (2016). Repeated low-dose kainate administration in C57BL/6J mice produces temporal lobe epilepsy pathology but infrequent spontaneous seizures. *Experimental Neurology*, *279*(1), 116–126. https://doi.org/10.1016/j.expneurol.2016.02.014

Vanhaesebroeck, B., Guillermet-Guibert, J., Graupera, M., & Bilanges, B. (2010). The emerging mechanisms of isoform-specific PI3K signalling. *Nature Reviews Molecular Cell Biology*, *11*(5), 329–341. https://doi.org/10.1038/nrm2882

Vasileva, M., Horstmann, H., Geumann, C., Gitler, D., & Kuner, T. (2012). Synapsin-dependent reserveo pool of synaptic vesicles supports replenishment of the readily releasable pool under intense synaptic transmission. *European Journal of Neuroscience*, *36*(8), 3005–3020. https://doi.org/10.1111/j.1460-9568.2012.08225.x

Veroux, M., Tallarita, T., Corona, D., D'Assoro, A., & Veroux, P. (2013). Exploring new frontiers: Sirolimus as a pharmacokinetic modulator in advanced cancer patients. *Expert Review of Anticancer Therapy*, *13*(1), 17–20. https://doi.org/10.1586/era.12.151

Vosler, P. S., Brennan, C. S., & Chen, J. (2008). Calpain-Mediated Signaling Mechanisms in Neuronal Injury and Neurodegeneration. *Molecular Neurobiology*, *38*(1), 78–100. https://doi.org/10.1007/s12035-008-8036-x

Vukoja, A., Rey, U., Petzoldt, A. G., Ott, C., Vollweiter, D., Quentin, C., Puchkov, D., Reynolds, E., Lehmann, M., Hohensee, S., Rosa, S., Lipowsky, R., Sigrist, S. J., & Haucke, V. (2018). Presynaptic Biogenesis Requires Axonal Transport of Lysosome-Related Vesicles. *Neuron*, *99*(6), 1216-1232.e7. https://doi.org/10.1016/j.neuron.2018.08.004

Wallroth, A., & Haucke, V. (2018). Phosphoinositide conversion in endocytosis and the endolysosomal system. *Journal of Biological Chemistry*, *293*(5), 1526–1535. https://doi.org/10.1074/jbc.R117.000629

Wallroth, A., Koch, P. A., Marat, A. L., Krause, E., & Haucke, V. (2019). Protein kinase N controls a lysosomal lipid switch to facilitate nutrient signalling via mTORC1. *Nature Cell Biology*, *21*(9), 1093–1101. https://doi.org/10.1038/s41556-019-0377-3

Wang, L., Harris, T. E., & Lawrence, J. C. (2008). Regulation of proline-rich akt substrate of 40 kDa (PRAS40) function by mammalian target of rapamycin complex 1 (mTORC1)-mediated phosphorylation. *Journal of Biological Chemistry*, *283*(23), 15619–15627. https://doi.org/10.1074/jbc.M800723200

Wang, Y., Okamoto, M., Schmitz, F., Hofmann, K., & Südhof, T. C. (1997). Rim is a putative rab3 effector in regulating synaptic-vesicle fusion. *Nature*, *388*(6642), 593–598. https://doi.org/10.1038/41580

Wee, P., & Wang, Z. (2017). Epidermal growth factor receptor cell proliferation signaling pathways. *Cancers*, *9*(5), 1–45. https://doi.org/10.3390/cancers9050052

Wheeler, M., & Domin, J. (2006). The N-terminus of phosphoinositide 3-kinase-C2β regulates lipid kinase activity and binding to clathrin. *Journal of Cellular Physiology*, *206*(3), 586–593. https://doi.org/10.1002/jcp.20507

Wickman, K., & Clapham, D. E. (1995). Ion channel regulation by G proteins. *Physiological Reviews*, *75*(4), 865–885. https://doi.org/10.1152/physrev.1995.75.4.865

Wilson, N. R., Kang, J., Hueske, E. V., Leung, T., Varoqui, H., Murnick, J. G., Erickson, J. D., & Liu, G. (2005). Presynaptic regulation of quantal size by the vesicular glutamate transporter VGLUT1. *Journal of Neuroscience*, *25*(26), 6221–6234. https://doi.org/10.1523/JNEUROSCI.3003-04.2005

Wong, M., & Crino, P. B. (2012). Tuberous sclerosis and epilepsy: Role of astrocytes. *Glia*, *60*(8), 1244–1250. https://doi.org/10.1002/glia.22326

Wu, L.-G., Hamid, E., Shin, W., & Chiang, H.-C. (2014). Exocytosis and Endocytosis: Modes,

Functions, and Coupling Mechanisms. *Annual Review of Physiology*, *76*(1), 301–331. https://doi.org/10.1146/annurev-physiol-021113-170305

Wu, X. S., Xue, L., Mohan, R., Paradiso, K., Gillis, K. D., & Wu, L. G. (2007). The origin of quantal size variation: Vesicular glutamate concentration plays a significant role. *Journal of Neuroscience*, *27*(11), 3046–3052. https://doi.org/10.1523/JNEUROSCI.4415-06.2007

Xu, Jia, Ji, J., & Yan, X. H. (2012). Cross-Talk between AMPK and mTOR in Regulating Energy Balance. *Critical Reviews in Food Science and Nutrition*, *52*(5), 373–381. https://doi.org/10.1080/10408398.2010.500245

Xu, Jianhua, He, L., & Wu, L. G. (2007). Role of Ca2+ channels in short-term synaptic plasticity. *Current Opinion in Neurobiology*, *17*(3), 352–359. https://doi.org/10.1016/j.conb.2007.04.005

Xu, Junjie, Brewer, K. D., Perez-Castillejos, R., & Rizo, J. (2013). Subtle interplay between synaptotagmin and complexin binding to the SNARE complex. *Journal of Molecular Biology*, *425*(18), 3461–3475. https://doi.org/10.1016/j.jmb.2013.07.001

Yamawaki, R., Thind, K., & Buckmaster, P. S. (2015). Blockade of excitatory synaptogenesis with proximal dendrites of dentate granule cells following rapamycin treatment in a mouse model of temporal lobe epilepsy. *Journal of Comparative Neurology*, *523*(2), 281–297. https://doi.org/10.1002/cne.23681

Yang, Y., Lee, M., & Fairn, G. D. (2018). Phospholipid subcellular localization and dynamics. *Journal of Biological Chemistry*, *293*(17), 6230–6240. https://doi.org/10.1074/jbc.R117.000582

Yang, Y., Park, M., Maekawa, M., & Fairn, G. D. (2019). Enforced expression of phosphatidylinositol 4-phosphate 5-kinase homolog alters PtdIns(4,5)P2 distribution and the localization of small G-proteins. *Scientific Reports*, *9*(1), 1–15. https://doi.org/10.1038/s41598-019-51272-z

Yim, Y. I., Sun, T., Wu, L. G., Raimondi, A., De Camilli, P., Eisenberg, E., & Greene, L. E. (2010). Endocytosis and clathrin-uncoating defects at synapses of auxilin knockout mice. *Proceedings of the National Academy of Sciences of the United States of America*, *107*(9), 4412–4417. https://doi.org/10.1073/pnas.1000738107

Yoshioka, K., Yoshida, K., Cui, H., Wakayama, T., Takuwa, N., Okamoto, Y., Du, W., Qi, X., Asanuma, K., Sugihara, K., Aki, S., Miyazawa, H., Biswas, K., Nagakura, C., Ueno, M., Iseki, S., Schwartz, R. J., Okamoto, H., Sasaki, T., … Takuwa, Y. (2012). Endothelial PI3K-C2α, a class II PI3K, has an essential role in angiogenesis and vascular barrier function. *Nature Medicine*, *18*(10), 1560–1569. https://doi.org/10.1038/nm.2928

Yun, C. W., & Lee, S. H. (2018). The roles of autophagy in cancer. *International Journal of Molecular Sciences*, *19*(11), 1–18. https://doi.org/10.3390/ijms19113466

Zachari, M., & Ganley, I. G. (2017). The mammalian ULK1 complex and autophagy initiation. *Essays in Biochemistry*, *61*(6), 585–596. https://doi.org/10.1042/EBC20170021

Zeng, L. H., Rensing, N. R., Zhang, B., Gutmann, D. H., Gambello, M. J., & Wong, M. (2011). Tsc2 gene inactivation causes a more severe epilepsy phenotype than Tsc1 inactivation in a mouse model of Tuberous Sclerosis Complex. *Human Molecular Genetics*, *20*(3), 445–454. https://doi.org/10.1093/hmg/ddq491

Zhao, L. X., Ge, Y. H., Li, J. B., Xiong, C. H., Law, P. Y., Xu, J. R., Qiu, Y., & Chen, H. Z. (2019). M1 muscarinic receptors regulate the phosphorylation of AMPA receptor subunit GluA1 via a signaling pathway linking cAMP-PKA and PI3K-Akt. *FASEB Journal*, *33*(5), 6622–6631. https://doi.org/10.1096/fj.201802351R

Zhou, Q., Zhou, P., Wang, A. L., Wu, D., Zhao, M., Südhof, T. C., & Brunger, A. T. (2017). The primed SNARE–complexin–synaptotagmin complex for neuronal exocytosis. *Nature*, *548*(7668), 420–425. https://doi.org/10.1038/nature23484

Zilly, F. E., Sørensen, J. B., Jahn, R., & Lang, T. (2006). Munc18-bound syntaxin readily forms SNARE

complexes with synaptobrevin in native plasma membranes. *PLoS Biology*, *4*(10), 1789–1797. https://doi.org/10.1371/journal.pbio.0040330

Zoncu, R., Perera, R. M., Sebastian, R., Nakatsu, F., Chen, H., Balla, T., Ayala, G., Toomre, D., & De Camilli, P. V. (2007). Loss of endocytic clathrin-coated pits upon acute depletion of phosphatidylinositol 4,5-bisphosphate. *Proceedings of the National Academy of Sciences of the United States of America*, *104*(10), 3793–3798. https://doi.org/10.1073/pnas.0611733104

7 Appendix

7.1 List of Abbreviations

4E-BPs	Eukaryotic initiation factor binding proteins
ACSF	Artificial cerebrospinal fluid
AMPA	α-amino-3-hydroxy-5-methyl-4-isoxazolepropionic acid
AP	Action potential
AP180	Monomeric adaptor protein 180
AP-2	Adaptor protein 2
APV	(2R)-amino-5-phosphonovaleric acid
AraC	β-D-arabinofuranoside
BAR	Bin-amphiphysin-rvs
CALM	Clathrin assembly lymphoid myeloid leukemia protein
CaMKII	Calmodulin-dependent protein kinase-II
CBD	Clathrin binding domain
CCP	Clathrin coated pit
CME	Clathrin mediated endocytosis
CNQX	6-cyano-7-nitroquinoxaline-2,3-dione
DIV	Days in vitro
DMSO	Dimethyl sulfoxide
E/I	Excitatory/Inhibitory
EF	Endotoxin free
eIF4E	Eukaryotic translation initiation factor 4E
EM	Electron microscopy
ER	Endoplasmic reticulum
FCS	Foetal calf serum
fEPSPs	Field excitatory postsynaptic potentials
FV	Fibre volley
GABA	Gamma-aminobutyric acid
GDP	Guanosine diphosphate
GPCRs	G Protein-Coupled Receptors
GTP	Guanosine triphosphate
HBSS	Hank's Balanced Salt Solution
HEK	Human embryonic kidney
HET	Heterozygous
Hippo	Hippocampus
IP	Intraperitoneal
KO	Knockout
LTP	Long-term potentiation

mTORC1	Mammalian target of rapamycin complex 1
Munc	Mammalian uncoordinated
NBA	Neurobasal A
NGS	Normal goat serum
NH_4Cl	Ammonium chloride
NLS	Nuclear location sequence
NMDA	N-methyl-D-aspartate
PBS	Phosphate-buffered saline
PCR	Polymerase chain reaction
PFA	Paraformaldehyde
PH	Pleckstrin homology
PI	Phosphatidylinositol
$PI(3,4)P_2$	Phosphatidylinositol-3,4-bisphosphate
$PI(3,4,5)P_3$	Phosphatidylinositol-3,4,5-trisphosphate
$PI(4,5)P_2$	Phosphatidylinositol-4,5-bisphosphate
PI3KC2α	Class II PI3K alpha
PI3KC2β	Class II PI3K beta
PI3Ks	Phosphoinositide 3-kinases
PI3P	Phosphatidylinositol-3-phosphate
PI4P	Phosphatidylinositol-4-phosphate
PI5P	Phosphatidylinositol-5-phosphate
PIC	Protease inhibitor cocktail
PIP5Ks	Phosphoinositide 5-kinases
PIPs	Phosphoinositides
PKN	PKC-related serine/threonine-protein kinase N
PS	Population spike
PSD	Postsynaptic density
PTZ	Pentylenetetrazol
PX	Phox homolog
RIM	Regulating synaptic membrane exocytosis protein
ROIs	Regions of interest
RRP	Readily releasable pool
RTKs	Receptor Tyrosine Kinases
S6	Ribosomal protein S6
S6K	Ribosomal protein S6 kinase beta-1
SDS-PAGE	Sodium dodecyl sulfate–polyacrylamide gel electrophoresis
SH3	Terminal SRC Homology 3
SNAREs	Soluble N-ethylmaleimide-sensitive fusion protein attachment protein receptors
SNPs	Small nucleotide polymorphisms
Syp	Synaptophysin1

Syp-pH	Synaptophysin1-pHluorin
Syt1	Synaptotamin1
Syt1-pH	Synaptotamin1-pHluorin
TAE	Tris-Acetate-EDTA buffer
TBE	Tris-Borate-EDTA buffer
TBS	Tris-buffered saline
TBS	Theta-burst stimulation
TSC	Tuberous sclerosis complex
t-SNARE	Target-SNARE
ULK1	Unc-51 like autophagy activating kinase 1
V-ATPase	Vacuolar-type H^+-ATPase
v-SNARE	Vesicle-SNARE
WT	Wild type

7.2 Macro Scripts

Text files of Macro scripts can be provided on request, please contact albert@mackintosh.family. Script may require modification for Z-stack size and Microscope used.

7.2.1 Z-slice projection

```
imagenumber = nImages
dir = getDirectory("choose where to save");
for (j = 0; j < imagenumber; j++) {
name = getTitle;
sum = "SUM_" + name;
selectWindow(name);
run("Z Project...", "projection=[Sum Slices]");
selectWindow(sum);
saveAs(".tif", dir + sum);
close(name);
name = getTitle;
close(name);
}
```

7.2.2 Z-slice separation

```
imagenumber = nImages
zplane= "3";
dir = getDirectory("choose where to save");
for (j = 0; j < imagenumber; j++) {
name = getTitle;
selectWindow(name);
run("Stack Slicer", "split_z");
for (z = 0; z < zplane; z++) {
zno = name + " - Z=" + z;
selectWindow(zno);
saveAs(".tif", dir + zno);
close(zno + ".tif");
}
}
```

7.2.3 Glial coverage estimates

```
imagenumber = nImages
run("Set Measurements...", "area mean standard min integrated display redirect=None decimal=3");
for (j = 0; j < imagenumber; j++) {
name = getTitle;
selectWindow(name);
        dotIndex = indexOf(name, ".");
        title = substring(name, 0, dotIndex);
run("Stack to Images");
selectWindow(title + "-0002");
run("Duplicate...", " ");
rename(title + "Measurement");
close(title + "-0003");
close(title + "-0004");
selectWindow(title + "-0001");
setTool("polygon");
roiManager("reset");
waitForUser("select roi");
roiManager("add");
roiManager("deselect");
close(title + "-0001");
roiManager("Select", 0);
selectWindow(title + "-0002");
run("Subtract Background...", "rolling=50 slice");
run("8-bit");
run("Auto Threshold", "method=Triangle white");
roiManager("Select", 0);
run("Analyze Particles...", "summarize slice");
close(title + "Measurement");
close(title + "-0002");
}
```

7.2.4 Histogram plotter

```
nBins = 250;
histMin = 0;
histMax = 500;
imagenumber = 100

for (j = 0; j < imagenumber; j++) {
run("Clear Results");
row = 0;
name = getTitle;
resultname = "Histogram_summary_of_" + name;
selectWindow(name);
setTool("polygon");
roiManager("reset")
Stack.setChannel(2);
waitForUser("select roi");
roiManager("add")
roiManager("Show All");
roiManager("Select", 0);
Stack.setChannel(3);
getHistogram(values, counts, nBins, histMin, histMax);
for (i=0; i<nBins; i++) {
    setResult("Value", row, values[i]);
    setResult("Count", row, counts[i]);
    row++;
}
updateResults();
IJ.renameResults(resultname)
dir = getDirectory("choose where to save");
saveAs("results", dir + resultname + ".csv");
close(resultname +".csv");
selectWindow(name);
close(name);
}
```

7.2.5 Simple intensity macro

```
imagenumber = nImages
run("Set Measurements...", "area mean standard min integrated display redirect=None decimal=3");
for (j = 0; j < imagenumber; j++) {
name = getTitle;
selectWindow(name);
        dotIndex = indexOf(name, ".");
        title = substring(name, 0, dotIndex);
run("Stack to Images");
selectWindow(title + "-0003");
run("Duplicate...", " ");
rename(title + "Measurement");
close(title + "-0002");
close(title + "-0004");
selectWindow(title + "-0001");
setTool("polygon");
roiManager("reset");
waitForUser("select roi");
roiManager("add");
roiManager("deselect");
close(title + "-0001");
roiManager("Select", 0);
run("Measure");
close(title + "Measurement");
close(title + "-0003");
}
```

7.2.6 Synapse density estimate

```
imagenumber = nImages;
run("Set Measurements...", "area mean integrated display redirect=None decimal=3");
dir = getDirectory("choose where to save");
for (j = 0; j < imagenumber; j++) {
synapse = "synapse";
roiManager("reset");
name = getTitle;
selectWindow(name);
        dotIndex = indexOf(name, ".");
        title = substring(name, 0, dotIndex);
name2 = title + "_" + synapse + "_" + j ;
run("Stack to Images");
selectWindow("Ch1-T1");
close();
selectWindow("Ch1-T3");
run("Duplicate...", "title=" + title + "Measure");
selectWindow("Ch1-T2");
run("Median...", "radius=1");
run("Subtract Background...", "rolling=5");
selectWindow("Ch1-T3");
run("Median...", "radius=1");
run("Subtract Background...", "rolling=5");
selectWindow("Ch1-T2");
run("8-bit");
run("Auto Threshold", "method=Triangle white");
setOption("BlackBackground", true);
run("Analyze Particles...", "size=1-Infinity pixel add slice");
count=roiManager("count");
array=newArray(count);
for(i=0; i<count;i++) {
      array[i] = i;
}
selectWindow(title + "Measure");
roiManager("Select", array);
roiManager("combine");
roiManager("save", dir + "ROISET" + title + ".zip");
run("Measure");
close("Ch1-T2");
close("Ch1-T3");
close(title + "Measure");
}
```